SOLVENT FREE EMULSIFICATION IN A TWIN-SCREW EXTRUDER

SOLVENT FREE EMULSIFICATION IN A TWIN-SCREW EXTRUDER

By David J.W. Lawton, B.Eng (ChemEng)

A Thesis submitted to the School of Graduate Studies in Partial Fulfillment of the Requirements for the Degree of Master of Applied Science

Master of Applied Science (2013) McMaster University

(Chemical Engineering) Hamilton, Ontario

Title: SOLVENT FREE EMULSIFICATION IN A TWIN-SCREW EXTRUDER

Author: David J.W. Lawton, B.Eng

Supervisor: Dr. Michael Thompson (McMaster University)

Number of Pages: xvi, 141

ABSTRACT

The production of latex in a solvent-free process within a twin screw extruder is of great industrial interest given the associated reduction in environmental impact when compared to conventional solvent-based emulsification techniques. The ability to produce latex continuously is also advantageous, compared to batch-wise solvent-based processes.

The process of solvent-free emulsification in a twin screw extruder is studied. An inline fiber optic spectroscopic system was installed in the extruder to study the residence time distribution profile of resin through the emulsification process. A design of experiment study was performed analyzing the response of latex particle size from screw speed and feed rate factors. Finally, scanning electron microscopy was used to determine the morphology of the poorly-emulsified and pre-emulsified resin.

Experimental results demonstrate that the residence time distribution of the polymer within the extruder is largely invariant of screw speed; the system also demonstrated a very low degree of axial mixing – which was not expected but can be attributed to high degree-of-fill within the screw. The results of the design of experiments study show that the final latex particle size is more influenced by the feed rate of the polymer than the screw speed of the extruder. These results were found to be consistent with the literature based on both batch-phase inversion emulsification as well as continuous polymer blending of

immiscible phases. Finally, results from a study on morphology provided evidence of water domains within the pre-inverted polymer domains, analogous to a ‘water-in-oil-in water’ dispersion. Evidence of a bicontinuous network of polymer and water was also found to exist. The summation of these experimental results leads to the hypothesis that the solvent-free emulsification process is a phase inversion-type emulsification mechanism as opposed to a direct emulsification mechanism.

ACKNOWLEDGMENTS

This Master's thesis would not be possible without the guidance and insight from my supervisor Dr. Michael Thompson – thank you for showing me how to be a more critical thinker every day. I'd also like to thank Dr. Santiago Faucher for giving me an opportunity to work on this project as well as my first job in engineering – I would not be where I am today without his help. I would like to thank Dr. Hwee Ng for taking me under his supervision and overall just being a great guy – thanks for all the help, motivation, mentorship and everything you've taught me about life. I'd like to thank both Dr. Chieh-Min Cheng and Dr. Marko Saban for the motivation and encouragement they gave me throughout the writing of this thesis. I'd like to thank David Borbely and Steven Qiu for all their support throughout this project and always being willing to help. I'd also like to thank Nels Grauman Neader for the friendship and advice during my graduate studies. Most importantly, I'd like to thank all my family and friends whose patience and support made this possible.

TABLE OF CONTENTS

LIST OF FIGURES

LIST OF TABLES

CHAPTER 1: INTRODUCTION

1.0 Solvent Free Emulsification

Synthetic latexes are used in coating and adhesive industries, these latexes are generally produced by emulsion or dispersion polymerization from monomers... There are many polymers however, such as olefins and polyester, which cannot be polymerized in the presence of water. Their production often involves the use of large amounts of organic solvents to facilitate their production. For these polymers, phase inversion processes are currently practiced where a sub-micron particle size is desired. These phase inversion processes typically involve first dissolving a polymer in a solvent, optionally in the presence of surfactant, before water is added to carry out the inversion to yield discrete polymer particles in a continuous aqueous phase.

A novel process to create latexes is through solvent-free emulsification (SFE); this new process uses surfactants to facilitate the contact between aqueous and polymer phases. This process is significantly more environmentally friendly than most current latex production processes. There is also a large benefit to worker safety as it eliminates the risks involved with handling solvents and monomers during latex production. Moreover, the capital cost of production is significantly lower as solvent-recovery operations are not required.

1.1 Research Objectives and Purpose:

In this thesis, the process of solvent-free emulsification (SFE) of a polyester resin with a twin screw extruder is studied. The determination of the mechanism of SFE is of specific interest as well as the process response to variations in operating conditions. A literature review will also be presented in order to draw upon understanding from similar fields of research as continuous SFE with an extruder has not been presented in literature to the best of the author's knowledge.

A review of direct emulsification as well as phase inversion emulsification is detailed in **Chapter 2**. Batch phase-inversion solvent free emulsification processes are also provided as continuous processes have not been described yet in literature. Relevant work in the field of blending immiscible polymer-polymer systems is also detailed as high viscosity systems are seldom studied in aqueous phase inversion processes.

A method to determine the time scales of the SFE process with a twin screw extruder is presented in **Chapter 3**. Through the use of an inline fiber optic probe and fluorescent tracer, the residence time distribution was determined for some select operating conditions. These were chosen to determine the influence of screw speed as well as water content within the dispersion zone of the extruder.

The response of latex particle size was analyzed in **Chapter 4** as a function of process operating conditions. A design of experiments is presented to determine the response of emulsion particle size with the factors of feed rate and screw speed varied through several levels. When possible, analogies to the batch phase inversion process were described to draw upon the understanding detailed in the literature.

The physical morphology of poorly or pre-dispersed latex is studied by scanning electron microscopy (SEM) in **Chapter 5**. First, poorly-dispersed resin particles are analyzed which were extruded at high and low failure-mode temperatures, as well as at a somewhat reduced surfactant concentration. These were analyzed through a range of resin-to-water rations in the dispersion zone of the extruder. Failure mode materials are of specific interest as they yield insight to the physical mechanism of phase inversion since successful emulsifications only yield latex particles. Second, the morphology of pre-dispersed material (i.e. undiluted, non-emulsified) was analyzed. This material was prepared without dilution as to analyze the morphology of the material within the dispersion zone of the extruder.

Finally, the research within this thesis in summarized in **Chapter 6**. The significance of the research is also given as are the recommendations for future work.

CHAPTER 2: LITERATURE REVIEW

2.1 Direct Emulsification

The emulsification of light oils and low molecular weight polymers is a common practice and is the subject of extensive scientific literature. These processes of creating oil-in-water (O/W) emulsions can be classified in two categories, direct emulsification and phase inversion. Direct emulsification methods involve directly dispersing the oil into a continuous water phase to create the O/W emulsion. This generally involves the input of high amounts of mechanical energy into the system to shear the oil phase into subsequently smaller domains. The volume fraction of the dispersed phase also tends to be much lower in direct emulsification due to agglomeration [1]. The size of the domains – oil droplets – is a function of both the amount of energy inputted into the system as well as the interfacial energy between the oil and water phases. High levels of energy can be directed into the system by means of high-shear mechanical devices, such as rotor-stator homogenizers. The shear forces exerted on the oil droplets causes them to elongate themselves along the axis of the shearing field. The magnitude of the shearing force exerted upon the droplet to initiate breakup is inversely proportional to the size of the droplet. The force required to break a droplet into a smaller domains therefore increases as the droplet size decreases. Thus, there exists a limiting size of droplet (often in the

order of one micron) based on the foreseeable level of shear reasonably imposed in direct emulsification methods.

Droplets, such as oil in an oil-in-water (O/W) emulsion resist deformation based on two mechanisms, interfacial tension and viscosity. The interfacial tension between the two phases causes a driving force in the droplet to minimize its surface area in order to achieve its' lowest energy state. The energy required to initiate breakup in a droplet is based on the interfacial energy between the dispersed and continuous phases. Interfacial energy, γ, is defined by the rate of change in Gibb's free energy, δG, divided by the rate of change in interfacial area, $\delta \mathrm{A}$. Surface tension can be described as the energy required to create a unit of surface area; the work required to create this surface is reversible and is written as $\gamma = (\delta \mathrm{G}/\delta \mathrm{A})_{\mathrm{T,P,n}}$ [2]. The work required to increase the area of the interface by δA, is then a function of the interfacial energy, $W = \gamma \delta A$ [3]. This interfacial energy is a function of the cohesive forces between molecules in each of the phases. Contact between two similar molecules requires less free energy, per unit area, than the contact between two dissimilar molecules. The breakup of droplets into smaller domains thusly increases the free energy of the system as the interfacial area is increased, initiating more contact between the two phases. The lowest energy state of a droplet is therefore a sphere as it minimizes the degree of curvature at the interface, and hence the contact between the two phases. This minimization of interfacial area is what counteracts the shear and extension forces applied to the droplet which seeks to increase the size of the

interface. These forces must exceed the interfacial tension in order to elongate the droplet and subsequently break it into smaller domains.

For the case of simple shear, such as Couette flow, the viscose forces inside droplets act to resist the deformation of imposed shearing flows during emulsification. The shearing force exerted on the droplet is dependent on the viscosity of the continuous phase. This shearing force occurs parallel to the interface of a droplet in an O/W emulsion as well as along the axis of flow. The force, F, acting on an interfacial area, A, of a discrete droplet in a continuous phase is equal to the shear stress by $\tau = F/A$. The magnitude of this shear stress is dependent on the velocity gradient, $\Delta u/\Delta y$, of the water moving past the droplet – or strain rate, $\dot{\epsilon}$, at its' surface, $y = 0$. In this way, shearing forces are diffused through the continuous phase by the introduction of large velocity gradients in the aqueous phase. The shearing force, or shear stress, acting upon the droplets' surface is related to the viscosity, μ, of the aqueous phase by $\tau = \mu * \dot{\epsilon}$. Therefore the shear stress exerted by the aqueous phase onto the droplet's surface is directly related to the aqueous phase viscosity. The deformation rate, or strain rate, of the droplet is dependent on its' own viscosity and the shear stress exerted by the water at the interface. The viscosity ratio, p, between the dispersed, μ_d, and continuous phases, μ_c, therefore describes the ratio of relative strain rates experience in a simple shear environment. A large viscosity ratio between phases in an O/W emulsion means that very high velocity gradients (high shearing) must be imposed on the aqueous phase in order to

create sufficient strain in the droplet to overcome the viscose forces and initiate breakup.

Taylor [4] pioneered the study of droplet deformation mechanics while studying the “mechanics of stirring processes” for the mixing of immiscible fluids. Taylor divided his work into two classes of flow regime: simple shear, and elongational flow. Figure 1 shows the two flow apparatus Taylor used to study both simple shear and elongation. The most significant contribution of this work was the defining a relationship between the viscous or external forces upon the droplet and the interfacial forces within the droplet.

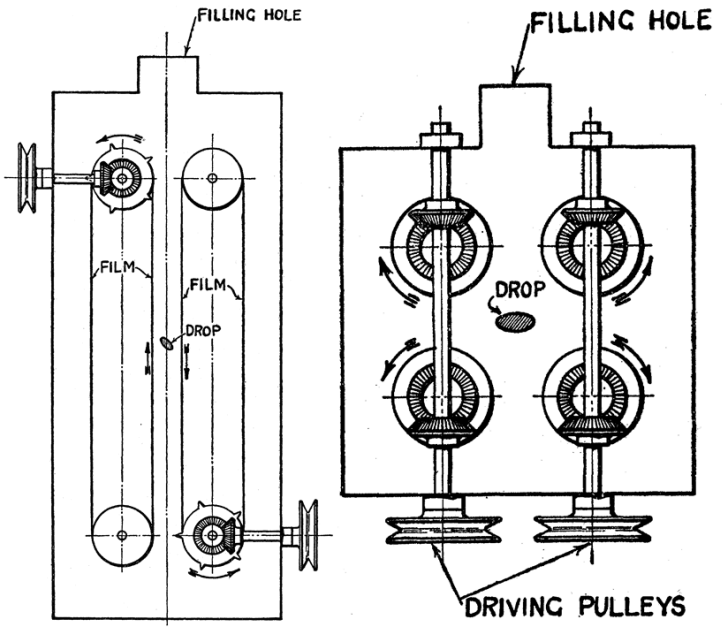

Figure 1 - Flow apparatus utilized by Taylor to study the droplet deformation in simple shear (left) and planar elongational (right) [4].

Grace [5] famously expanded upon Taylor’s work in quantifying the influence of interfacial tension viscosity ratio on the breakup of discrete droplets

in a continuous medium for liquid-liquid dispersions. The relationship between the viscosity ratio and the critical shear capillary number yielded the so-called Grace-plot, shown below, in Figure 2. The local capillary number represents the relative balance of viscous forces against interfacial forces during deformation:

$$Ca = \frac{\eta_m \dot{\gamma} B}{2\sigma} \tag{3.1}$$

Where, η_m, is the viscosity of the matrix; $\dot{\gamma}$, the shear rate; B, the characteristic size of the deformed dispersed phase; and σ, the interfacial tension. The Grace-plot describes the values of critical capillary number for which droplet breakup occurs under simple shear and elongational shear.

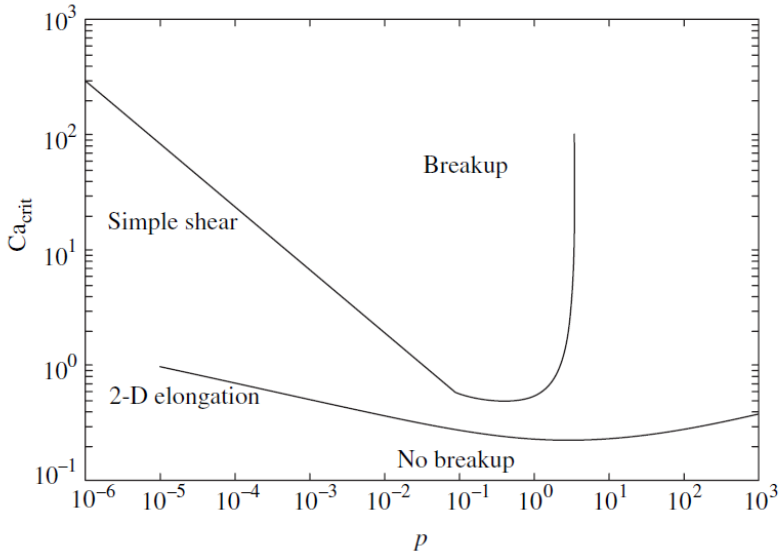

Figure 2 - Critical capillarity number for drop breakup in shear and extensional flow [6].

2.2 Phase Inversion Emulsification

2.2.1 Introduction

Phase inversion processes differ from direct emulsification in that the final continuous phase is first dispersed as a discrete phase throughout the initially continuous phase. This feature allows phase inversion emulsions to be produced at much higher loadings of the dispersed phase. Most importantly however, phase inversion allows for the emulsification of materials with a viscosity much greater than water. This is impossible with direct emulsification under simple shear flow, as shown by Grace [5], when the viscosity ration between the dispersed and continuous phase exceeds 4.

There exist two types of phase inversion routes in producing O/W emulsions from a preliminary W/O emulsion. These routes are referred to as the *transitional phase inversion* (TPI) route and the *catastrophic phase inversion* route (CPI). A good way of describing these routes is by defining a locus of phase inversion based on the balance of hydrophilic or lipophilic affinity of a surfactant and the overall water volume fraction [7]. A schematic illustration of this locus of phase inversion can be seen in Figure 3. The phase inversion locus represents the case where the net curvature at the interface between water and oil phases is zero. Physically, this manifests itself as bicontinuous morphology between the phases where the localized interface curvature may be non-zero yet the bulk average curvature is zero [8]. Catastrophic phase inversion is seen as a kinetic

response whereas transitional phase inversion represents a thermodynamic response [9]. This means that phase inversion by CPI is achieved by gradual addition of one component into the other at a rate specific to the system chemistry whereas by TPI the rate of addition is irrelevant. In theory neither mechanism requires mechanical force to produce the final emulsion; however, the timescale for this may be in the order of minutes to years based on the system viscosity and so agitation is invariably involved.

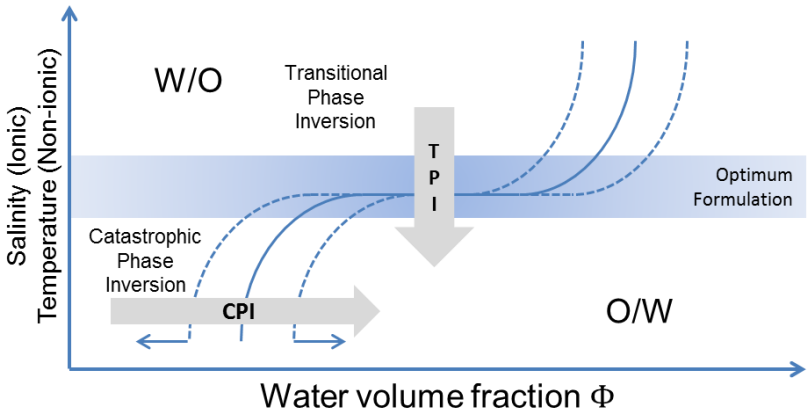

Figure 3 – Schematic illustration of the locus of phase inversion depicting two possible routes of inverting a W/O emulsion to an O/W emulsion. The solid line represents the phase inversion locus while the dashed lines represent the hysteresis zone. Adapted from Fernandez et al. [7]

2.2.2 Transitional Phase Inversion

Solvent-free phase inversion can be induced by quenching through the Phase Inversion Temperature (PIT) method. This behavior is driven by a change in the spontaneous curvature of the surfactant at the interface. The curvature of the surfactant layer at the interface is influenced by the relative solubility of the surfactant in either the water or oil phase. This relationship is described by

Bancroft's rule which says that the continuous phase is generally that which the surfactant is more soluble [10]. The change in curvature with non-ionic surfactants can be related to the dependency of their *hydrophilic-lipophilic balance* (HLB) on temperature. Higher temperatures lead to increased solubilisation of the hydrophobic portion of these surfactants in the oil phase; increased temperatures also reduce the hydration of the hydrophilic portion of these surfactant chains. This behavior was first described by Shinoda and Saito in their work with polyethoxylated non-ionic surfactants [11]. Figure 4 shows the schematic transition of curvature and change in relative strength of the hydrophilic/lipophilic portions of a surfactant chain as temperature is changed.

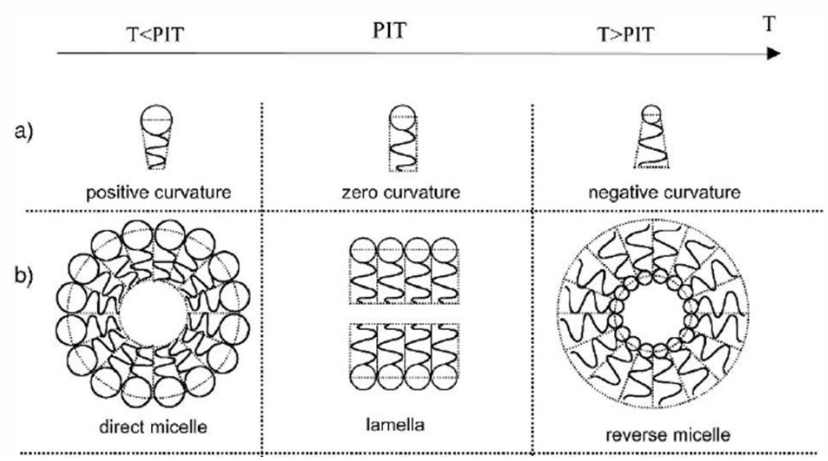

Figure 4 – (a) Schematic representation of the change in curvature of the surfactant layer at the interface. (b) Transition from hydrophobic-centred micelle (oil-in-water emulsion) through lamella (bi-continuous phase) to hydrophilic-centred micelle (water-in-oil emulsion) as temperature is increased [12].

2.2.3 Catastrophic Phase Inversion

The term catastrophic phase inversion was introduced by Salager [13] to refer to emulsion inversion which were brought about by a change in the oil-to-

water ratio, as opposed to the surfactant affinity of the phases as in TPI. In O/W emulsions created through catastrophic phase inversion, water is added to the oil phase under shearing to produce discrete droplets of water within the oil phase, or a water-in-oil emulsion, W/O. Since the viscosity of the oil phase is usually much higher than the water phase, simple shearing alone is sufficient to produce a fine dispersion of water droplets within the oil phase. As the number of droplets increase to a critical value, they begin to coalesce. This coalescence is the onset of the bicontinuous phase morphology in which both the oil phase and water phase extend throughout the matrix [14]. Once fully coalesced, the water phase 'traps' the oil phase into discrete regions, giving way to an O/W emulsion [9].

2.2.4 Solvent Free Emulsification – Related Work

This section relates to the phase inversion emulsification of very high viscosity materials into a continuous aqueous phase. Many studies have been done on microemulsions involving low viscosity materials but much less have been presented on high viscosity ones. Due to the difficulty in dispersing high viscosity materials directly into water because of the high viscosity ratio (10^2 to 10^5), the phase inversion route presents a very interesting alternative. It is also noted that phase inversion emulsification has been known to produce much smaller emulsion particle sizes, those typically only achievable through direct emulsion polymerization.

Akay [15] studied flow-induced phase inversion (FIPI) emulsification of high viscosity polymeric epoxide resins in water using a multiple expansion-contraction static mixer (MECSM). The MECSM induces a orthogonal superimposition of shear flows and extensional flows, which Akay claims to promote more efficient droplet breakup [16]. The mean particle size for the emulsified epoxide resins were on the order of 1-5µm with some experiments reaching as low at 0.7µm. The preparation of the emulsion first included the pre-dispersion of water into the epoxide resin/surfactant mixture using a simple anchor blade impeller to form a W/O dispersion. This W/O dispersion was then phase inverted by passing through the MECSM to create an O/W dispersion. Akay found higher extension rates (flow-rate through MECSM) and a greater number of MECSM elements decreased the resulting particle size of the O/W emulsion. The critical extension rate required to induce phase inversion was found to decrease with increasing anionic surfactant concentration. The onset of phase inversion also occurred at lower water volume fractions when the fraction of anionic surfactant was increased. Mechanistically, Akay proposed a mechanism for FIPI wherein the water domains are extended into cylindrical threads and then compressed into hemispherical shells and discs. These discs then begin to aggregate and coalesce, gradually encapsulating oil domains.

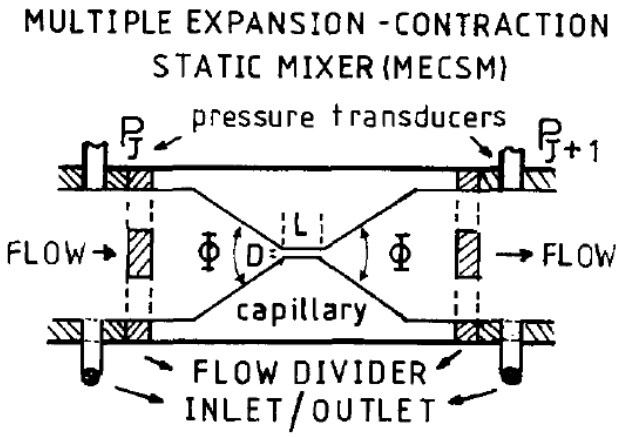

Figure 5 - Geometry of the multiple expansion-contraction static mixer utilized by Akay for the phase inversion emulsification of polymeric epoxide resins [15].

Akay and Tong [1] studied the FIPI of low-density polyethylene (LDPE) (M_n = 40,000) into water for the creation of a colloidal latex. The authors utilized a HAAKE Rheomix 3000 batch mixer fitted with a reflux condenser to carry out the emulsification. Hydrophobically-modified water soluble polymers (HMWSP) were used as emulsifiers; these were acrylic acid/lauryl methacrylate sodium salts with a mole ratio of 25:1. Other emulsifiers utilized were found to be ineffective in emulsification, these included: sodium polyacrylates as well as molecular surfactants of ethoxylated alcohols and esters. Briefly, the procedure was to premix the LDPE with a 25-33% aqueous solution of HMWSP, heat the mixer to 120°C, feed the LDPE/HMWSP mixture in and allow the aqueous phase to evaporate until the torque reached a maximum value. The condenser cooled with chilled water was then fitted to the mixer and room temperature distilled water was metered into the mixer. The phase inversion point was indicated by a slight increase in torque measured by the mixer following a steady decline of torque

upon the addition of the aqueous phase; this is shown in Figure 6. The D50 particle sizes generated in this study varied from about 0.9-4.2µm using the HMWSPs; higher emulsifier concentrations were found to lead to smaller particle sizes and distributions. Of the two HMWSP studied, the HMWSP which was more hydrophilic resulted in a lower particle size. It is interesting to note that the authors could not emulsify the LDPE with the addition of an anionic molecular surfactant (Aerosol OT); upon addition of the water, lubrication took over and insufficient stress was available to disperse the water into the polymer melt. The critical water volume fraction to induce phase inversion with the HMWSPs was found to be approximately 20wt%, the authors claimed this was consistent with their previous study which described the limit as the viscosity of the oil phase becomes very large (i.e. viscosity ratio very small). Upon cooling the phase inverted mixtures and further mixing, subsequent phase inversions were also observed to yield exotic multiple-emulsion morphology including double emulsions (W/O/W) as well as micro-porous polymer lattices.

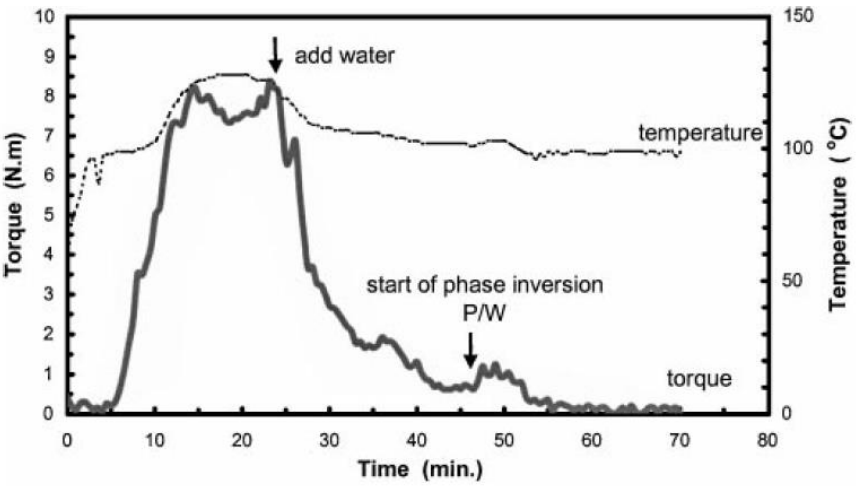

Figure 6 - Phase inversion emulsification history of LDPE/ HMWSP in a HAAKE Rheomixer 3000 indicating the increase in toque during phase inversion [1].

Akay et al. [17] replicated their earlier work with HMWSPs and LDPE now using ethylene-vinyl acetate (EVA) (28% vinyl acetate content, M_n = 19,000) and the same HMWSP emulsifiers. In contrast to the LDPE study discussed above, the EVA study found that smaller particle sizes were obtained when using the more hydrophobic of the two HMWSPs. Moreover, there was nearly a ten-fold difference in particle size between the two HMWSPs – much larger than observed with the LDPE. The critical water volume fraction at the phase inversion point (PIP) was again found to be approximately 20wt%. The particle sizes obtained with EVA was 1.5µm with the more hydrophobic HMWSP and about 26µm with the more hydrophilic HMWSP. The particle size difference was mainly attributed to the difference in viscosity of the polymer. With the LDPE being more viscous, it was believe that higher stresses would be able to be transferred to the aqueous domains.

Urigen et al. [18] studied the phase-inversion emulsification in a batch reactor of an ethylene-1-octene (EO) copolymer and anhydride grafted polypropylene (PP-g-MA) using non-ionic surfactants in order to evaluate the homogenous nucleation of polymers. The PP-g-MA emulsions had much lower particle sizes than the EO copolymer emulsions. This was attributed to the maleic anhydride functionality of the polypropylene which was susceptible to ring-opening reactions upon the addition of potassium hydroxide (KOH) to yield carboxylic groups. This functionality yielded particle sizes below the measurement threshold of their particle size device which was 40nm, at least under certain formulation conditions. Reduction in the KOH and polyethylene oxide surfactants led to multimodal particle size distributions with peaks ranging from 1-100µm. The EO dispersions had a minimum peak particle size of approximately 1µm with the development of some bi/tri-modal distributions upon the lowering of surfactant concentration. It would then appear that the presence of functional groups within the polymer chain is required for the production of sub-micron dispersions of polymers. This result is consistent with Akay's work with non-functionalized polymers [1, 15, 19].

Yang et al. [20, 21] carried out a two-part study on the preparation of waterborne sub-micron dispersions of epoxy resin through phase inversion emulsification in a batch reactor. The bisphenol-A (BPA) epoxy resin was emulsified using a polymeric emulsifier which was a multiblock copolymer consisting of 10% BPA epoxy and 90% polyethylene glycol (PEG). The phase

inversion was carried out in a similar manner to the studies previously described. Briefly, the BPA epoxy and emulsifier were melted and mixed in a reactor for a set amount of time such that the mixture became homogenous, then water was metered in slowly and the phase inversion point was marked by a sudden decrease in the impedance of the mixture as measured by a high frequency multimeter. Interestingly, the phase inversion point also corresponded to a critical water phase volume fraction of about 20% as reported previously by Akay et al. [1, 19]. A graph depicting the Amplitude of impedance versus the water content (wt%) from Yang et al. [20] is shown below in Figure 7. The authors also showed a very interesting pseudoplastic rheological response after the PIP of shear thinning using a dynamic stress rheometer. This was attributed to the strong interaction among the waterborne particles due to hydrogen bonding between the PEG portion of the emulsifier and the aqueous phase. Two typical viscosity curves from this study are presented in Figure 8 illustrating the increase in viscosity at low shear stress with increased emulsifier concentrations due to the increased degree of hydrogen bonding. The viscosity then decreases at higher shear stresses as the hydrogen bond interaction decreases indicating pseudoplasticity. A significant increase in the elasticity of the matrix beyond the PIP was also observable, marked by an increase in the storage modulus. Investigation of the evolution in morphology as a function of water content indicated regions of localized phase inversion when the bulk water fraction approached the PIP. The authors attributed this to fluctuations in temperature

and water content throughout the system. The effect of temperature upon the PIP was also investigated by the authors. High emulsification temperatures lead to the development of complex W/O/W emulsions whereas lower temperatures lead to the development of O/W dispersions following phase inversion. The authors concluded that there were two methods to promote the development of O/W dispersions over complex W/O/W: (1) higher emulsifier concentrations and (2) lower temperatures.

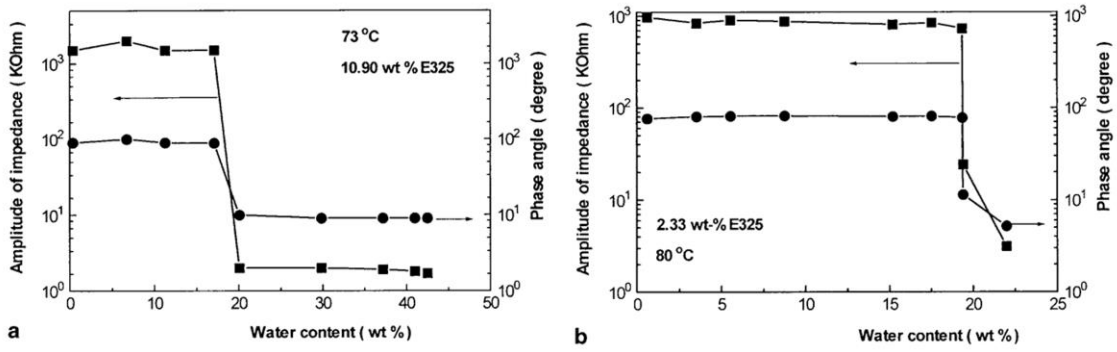

Figure 7 - Phase inversion point of BPA epoxy resins as indicated by the sudden decrease in the amplitude of impedance and phase angle upon reaching the critical water phase volume fraction [20].

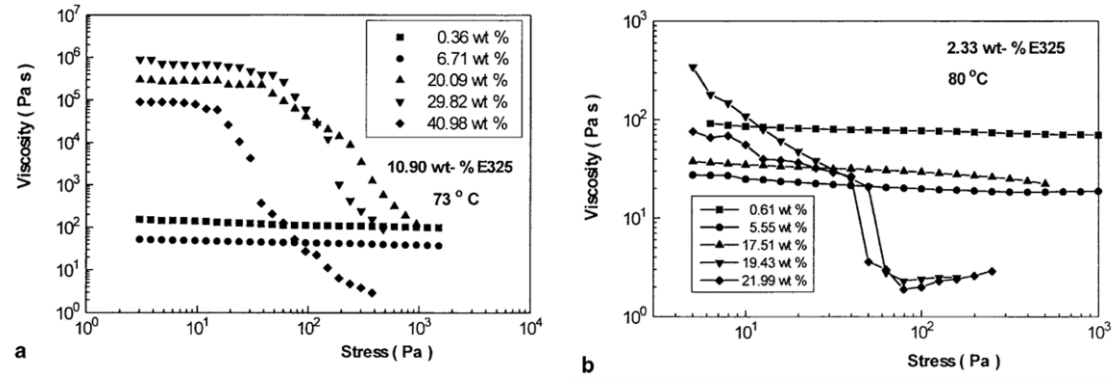

Figure 8 - Viscosity curves as a function of shear stress and water volume fraction within the BPA epoxy/emulsifier blends with a significant shear-thinning behaviour prevalent beyond the PIP corresponding to a water content of >20% [20].

The second portion of the study by Yang et al. [21] dealt with the theoretical considerations of the phase inversion process. The authors proposed a physical model of phase inversion wherein the critical PIP is reached when a small change in control variables (water content or temperature, for example) will create an abrupt increase in the attraction between dispersed water particles. That is to say that prior to the PIP the dispersed water domains are stable up to the point of phase inversion (attraction = repulsion) and highly unstable after the PIP (attraction >> repulsion). This is depicted in Figure 9 (left) where (1-2) a uniform size distribution of water domains stems from reversible collisions of water droplets exchanging matter to equilibrate the size distribution of the aqueous domains; the coalescence of discrete water droplets (3) or strings of water domains (4) coalesce and surround polymer domains leading to inversion. The authors also put forth a physical model for the generation of complete W/O/W dispersions which stems from the coalescence of a multimodal size distribution of water domains due to irreversible collisions between water droplets prior to inversion. The coalescence of these multimodal size water droplets at the PIP leads to the encapsulation of both polymer domains as well as smaller water domains, as depicted by the authors in Figure 9 (right). The authors put forth a theoretical model to describe the ratio of diameters between the dispersed water phase and resulting polymer particles after the PIP. This model was based on the assumption that due to the nature of the packing required for coalescence of water droplets with a phase inversion unit-cell, the number of discrete water

domains prior to the PIP was equal to the number of discrete polymer domains following the PIP. If the domains of both phases are assumed to be spherical (an assumption which is likely not the case due to shear deformation) a relationship between water content and diameter ratio can be developed. This relationship is shown in Figure 10 where D_p is the polymer diameter, D_w is the water diameter, and R is the water content (weight fraction) [21].

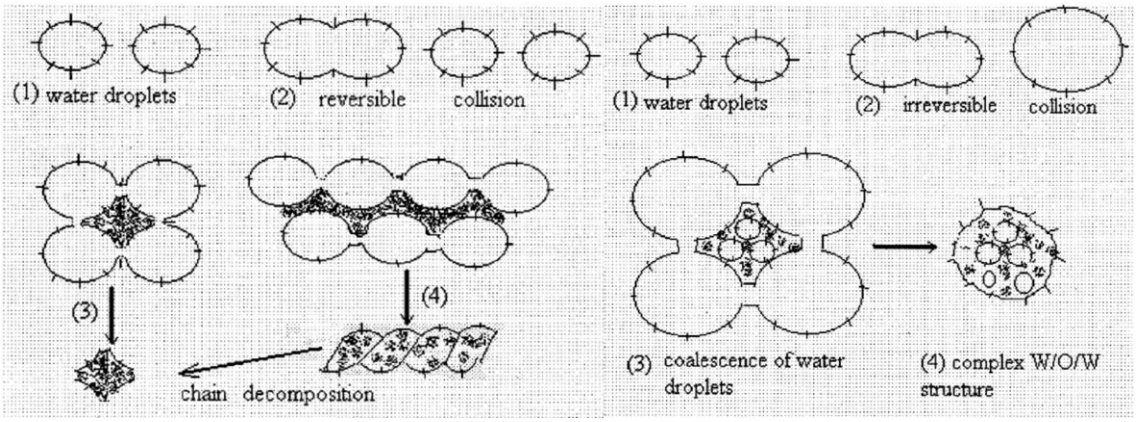

Figure 9 - Physical model of phase inversion process put forth by Yang et al.; (left) depicts complete phase inversion originating from a uniform size distribution of water domains and (right) depicts incomplete phase inversion from a multimodal particle size distribution of water domains, prior to the PIP [21].

$$D_p = \left(\frac{1-R}{R}\right)^{\frac{1}{3}} D_w$$

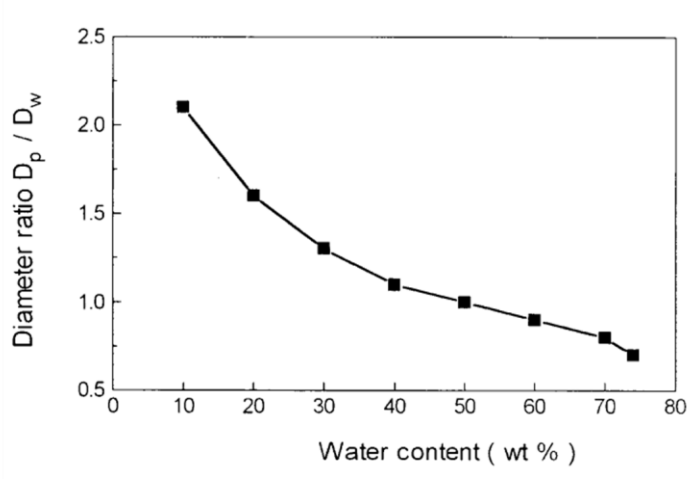

Figure 10 - Theoretical prediction of the diameter ratio between the dispersed water phase prior to the PIP and the resulting discrete polymer particles based on the model described by Yang et al. [21]

Song et al. [22] studied catastrophic phase inversion emulsification for the batch production of tackifier emulsions made from a rosin ester and a partially hydrogenated wood rosin acid emulsifier. In this system, the emulsifier was formed in-situ by neutralizing the terminal carboxylic groups in the rosin acid with potassium hydroxide (KOH). This study was based on the effects of changes in operating conditions during the preparation of the emulsion by investigating jacket temperature, mixing speed, and rate of water addition. The authors used an instrumented reaction vessel detailed in a previous paper (Song et al. [23]) which measured conductivity and torque throughout the phase inversion process. The onset of phase inversion was marked by a maximum viscosity value (as indicated by torque) and a sharp increase in conductivity. The authors found that lower jacket temperatures led to smaller particle sizes in the final emulsion. This was attributed to an increased matrix viscosity during the initial dispersion of

water into the rosin. This increased viscosity promoted increased droplet breakup of the aqueous phase prior to inversion. There was also a slight decrease in the critical water fraction required for inversion as the temperature was decreased. The rate of water addition had a more pronounced effect on the time to reach the PIP, mixture viscosity, and the resulting particle size. The first result is to be expected in a batch system as the rate of water addition coincides with the time it takes to reach the critical water volume fraction for the PIP. This delay in the onset of the PIP can be seen in Figure 11 (a). Interestingly, the authors also observed a depression in the critical water volume fraction as the rate of water addition was decreased; this can be seen in Figure 11 (b). An increase in viscosity was also observed as the flow rate was decreased. Although the phase inversion process was more rapid as higher water flow rates, the authors noted a bimodal particle size distribution (sub-micron and micron size) developed with increasing water flow rate at low agitation speeds. Upon increasing the agitation rate, both the bimodality and particle size decreased. This signifies the importance in incorporation of the aqueous phase in a homogenous manner.

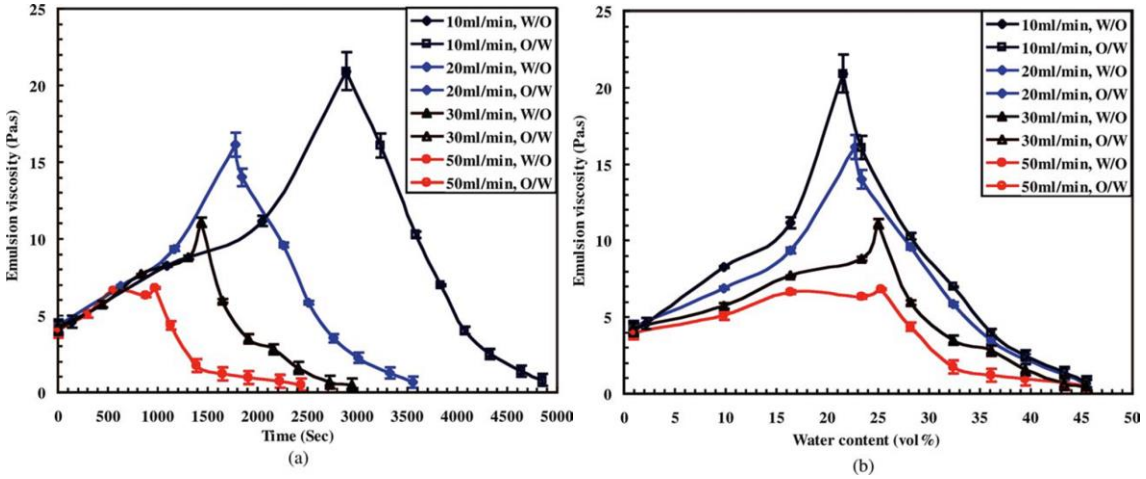

Figure 11 - (a) Emulsion viscosity vs. time at different water flow rates and (b) onset of PIP for different water flowrates for the study by Song et al. [22].

In another study by Song et al. [24], the authors studied the influence of the degree of neutralization of the rosin acid ([COO-/K+] concentration) upon the phase inversion of the same tackifier emulsion system. Not surprisingly, the authors found that decreasing the KOH ratio led to an increase in mean particle size as well as the development of bimodal particle size distributions. Interestingly, the viscosity of the mixture through the PIP increased as a function of the effective surfactant concentration which was based on the degree of neutralization of the wood rosin acid emulsifier. This increase in viscosity is then correlated with the decrease in particle size of the final emulsion This effect also present in the previously mentioned study by Song et al. [22] where the viscosity increased as a result of decreased jacket temperature and reduced water flowrate, both of which ultimately led to a decrease in particle size observed in the final emulsion. This effect is most likely due to the increased hydrogen bonding at the interface which increases the W/O matrix viscosity prior to the PIP.

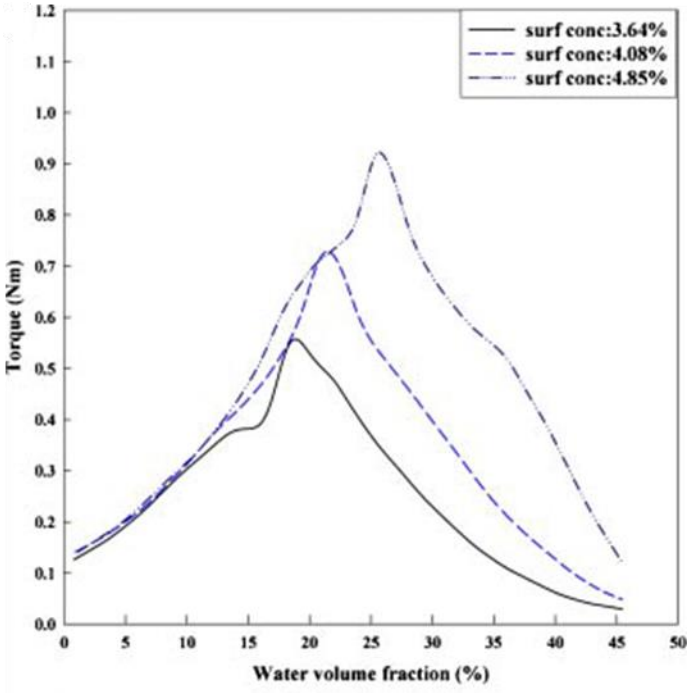

Figure 12 - Increase in emulsion viscosity as a function of effective surfactant concentration based on the degree of neutralization of a wood rosin acid emulsifier as studied by Song et al. [24].

2.3 Patent Literature Review

2.3.1 Continuous Solvent-free Emulsification

Typically, latex production has been a batch-wise process – regardless of the previously mentioned routes taken. From a production standpoint, it is generally preferred to implement continuous production processes for a multitude of reasons not discussed here. Recently, a novel way to continuously produce solvent-free latexes has been explored using a twin-screw extruder (TSE); none of the cited literature studies were carried out in this type of machine. The method allows for polymer resins to be fed directly to the TSE, which directly outputs

latex at the die-face of the machine. The scalable nature of the TSE also allows for a myriad of production rates, based on the size of the machine. Moreover, a single TSE can produce latex at a variety of die-flow rates; this allows the latex production is to be scaled in real-time. The TSE is particularly well suited to the plasticating and mixing of high viscosity polymers and is also continuous which is desirable from the manufacturing standpoint.

Continuous SFE processes involve the continuous extrusion of a polymer resin with injections of aqueous components along the length of the extruder. The transition from a single-phase polymer to bi-continuous water and polymer phase is accompanied by an inversion of the continuous polymer phase to that of a water-continuous latex material. This inversion is carried out through the gradual increase in water-volume fraction within the material. The intimate mixing of the polymer and water phases is thus of paramount importance in terms of both distributive and dispersive mixing. Due to the immiscibility of the two phases, surfactant is used to promote contact between the two phases. Moreover, the structure of the material is such that acid-end groups may be neutralized by a base in order to create surface-active functionality in the end groups – further enhancing the water-miscibility of the polymer.

Warner et al. [25] were the first, in 1978, to report the continuous production of a solvent-free polymer emulsion. The inventors used a concentric cylinder rotating within a heated barrel to provide purely laminar mixing in which polymer pumped through and water injected along its' length. Two steps are

noted in the preparation of the emulsion: (1) a heterogeneous dispersion of aqueous phase in a continuous polymer phase and (2) converting the composition to a water continuous heterogeneous dispersion of discrete polymer particles. The range of particle sizes the authors obtained were from 0.55-12.84 µm. The smallest particles were obtained by pumping a bisphenol-A-based epoxy resin with a softening point around 72°C from a heated pot by a gear pump to the variable shear mixer shown in Figure 13. The mixer was operated at a speed of 1055 revolutions per minute, or a shear rate of 550 s^{-1}, and heated to a temperature of 80°. The emulsifying agent used was an aqueous polyvinyl alcohol solution of 16.7% which was metered into the mixer at ports 6 and 8, shown in Figure 13, to yield a final concentration of 6% polyvinyl alcohol based on the weight of bisphenol-A. Interestingly, the process utilized a recycle stream which re-injected the resulting emulsion back into the mixer in port 10, shown in Figure 13, with dilution water injected at port 14.

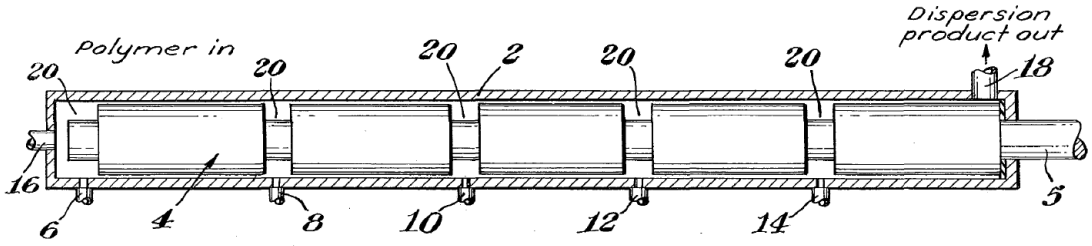

Figure 13 - Variable shear laminar mixer utilized in patent 4,123,403 [25]

Abe, et al. [26], were the first to utilize a twin screw extruder to carry out the continuous emulsification of a polymer resin. It is also important to note that the authors dispersed an olefinic resin, the first solvent-free sub-micron emulsion

of this class of polymers. The authors utilized a three-lobed twin-screw extruder with a length-to-diameter (L/D) ratio of 17, shown below in Figure 14. Several materials were dispersed including ethylene vinyl acetate, maleic anhydride-grafter ethylene vinyl acetate, ethylene-propylene copolymer, and low density polyethylene. Partially saponified polyvinyl alcohol, with a various degrees of saponification were utilized as emulsifiers. The particle size obtained was in the range of 0.5-5µm.

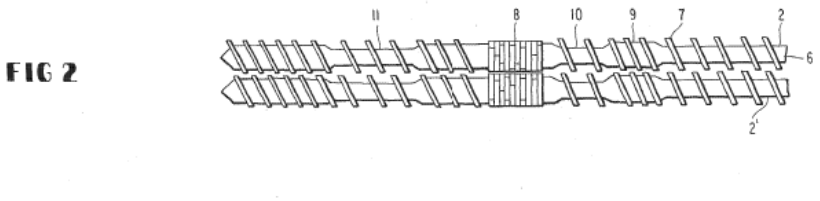

Figure 14 – Screw design utilized in US patent 4,320,041 for the production of aqueous dispersions of polyolefin resins using a twin screw extruder.

There have been a variety of patents filled and granted subsequent to the Abe, et al. [26] patent. The material sets in the patent literature have largely been either olefins or polyesters as these materials cannot be emulsified directly into an aqueous dispersion as in emulsion polymerization. Though there is little technical content upon which to review in the patent literature, the sheer number of applications– increasing in the last decade – indicates the great interest in this field. The lack of academic publications also perhaps indicates a lack of fundamental understanding of this process.

2.5 Conclusion

The field of phase inversion emulsification is extensive throughout literature though most systems deal with low viscosity, Newtonian materials. The solvent-free emulsification of highly viscous materials is less prevalent in the literature. Typically, these viscous systems require the use of solvents to lower the viscosity in order to facilitate emulsification. The solvent-free emulsification process is generally very similar to the phase inversion processes utilizing solvents, with the obvious alleviation of the need to handle and distill solvents. The removal of solvents from the emulsification process presents both economic and environmental benefits.

Direct emulsification has several limitations including particle size and the ability to emulsify highly viscous dispersed phase based on the limits of Taylor dispersion. Phase inversion processes present a means to produce sub-micron emulsions of viscose materials in aqueous (or non-aqueous) mediums without the use of solvents. The smallest particle sizes are obtainable when a surfactant in utilized in conjunction with a polymer containing some polar functionality, such as carboxylic acid or maleic anhydride groups. From a high level, the steps required for the phase inversion of these materials under agitation are as follows: melting the polymeric material; reacting the functional groups within the polymer chain to increase polarity, usually through neutralization with a strong base; adding surfactant to the system, either molecular or polymeric; and finally,

introducing water into the system and transitioning through the phase inversion point.

Many batch systems have been studied in academic literature; many more continuous processes utilizing extruders have been presented in the patent literature. The development of continuous production methods through process intensification represents a very attractive route to improving both the economics and quality of material manufacturing. The porting of the understanding of phase inversion emulsification from batch systems to continuous ones represents a field with a great potential value. The use of continuous processes also introduces new methods of studying the mechanics of phase inversion as the timescales of emulsification are an order of magnitude less than those found in batch systems.

CHAPTER 3 – RESIDENCE TIME DISTRIBUTION

3.1 Objective and Scope

The purpose of this chapter was to develop a method for inline residence time distribution monitoring of the resin phase in the extruder during solvent-free emulsification. The frequency of sampling the extrudate for offline measurement of tracer concentration is directly related to the overall resolution of the resulting residence time distribution. Analyzing samples individually – utilizing offline equipment – is a cumbersome method and introduces more operator error into the measurement as samples need to be handled and prepared. Moreover, the workload associated with evaluating a single residence time distribution scales linearly with increasing temporal resolution of the distribution. A new method was required to address the sampling time limitations of off-line tracer concentration determination. Inline measurement was desired to increase the sampling frequency of the extrudate in order to provide a higher-resolution residence time distribution when compared to offline methods.

The determination of the residence time distribution of the polymeric resin within the extruder during solvent free emulsification is also important in establishing the order of magnitude of the time scales associated with the SFE mechanism. The evaluation of the time scale of the dispersion mechanism will allow for comparison against different mechanisms presented in literature, which will be discussed.

The effect of screw speed and resin-to-water ratio was investigated with respect to latex particle size and residence time distribution. These variables were chosen to determine the relative impact of mechanical energy or shear rate, which is critical in a droplet deformation dispersion process, and residence time, which is critical to the kinetics of thermodynamically-driven phase inversion processes. Screw speed was varied through 3-levels while the resin-to-water ratio was varied through 2-levels; a full design of experiments was completed for these factors and levels. The particle size was measured for each of the experiments. The goal of these experiments was to determine the impact of screw speed on the particle size of the emulsified resin and relate any differences in the particle size to different flow paths through the extruder during SFE.

The real concentration of a tracer exiting a reactor as a function of time is a continuous function, this function must be discretized; however, when observed digitally. Fluorescence was chosen as the method of tracking tracer concentration within the extruder due to the high sampling resolution of mini-spectrometers utilizing fiber optic probes.

The method for determining the residence time distribution with an inline fiber optic backscattering probe and fluorescently-tagged polyester tracer was first validated against offline fluorometer spectroscopic measurements of samples taken at discrete intervals. The fluorescently-tagged tracer was then used to measure the residence time distribution of resin by mounting the fiber-optic probe

inline at the die-face of the extruder and recording fluorescent emission of the tracer as a function of time.

3.2 Introduction to Monitoring of Residence Time Distribution

The exit-age residence time in a reactor is the measure of the length of time it takes for a feed material to exit a reactor. In an ideal plug-flow reactor, all molecules of a feed material spend an equal amount of time traveling through the reactor. In an ideal batch reactor, the same is true in that all material spends the same amount of time in the reactor before exiting. These reactor types are the only ones in which it can be said that there is only a single residence time; for non-ideal reactors, there instead exists a distribution of residence times corresponding to the different lengths of time material takes to exit. The residence time distribution (RTD) reflects the flow path, i.e. mixing, which occurs within the reactor. Typically this relates to convective transport, though diffusion can be an important aspect of that transport in some systems.

The residence time distribution can be determined experimentally by carrying out a pulse tracer experiment to yield the exit-age distribution function, *E(t)*, directly [27]:

$$E(t) = \frac{C(t)}{\int_0^\infty C(t)dt} \tag{3.1}$$

where *C(t)* is the tracer concentration as a function of time and the denominator integral is equal to the total concentration of tracer. The integral of *E(t)* from t_1 to t_2 can then be describe as the fraction of material in the reactor which has taken between t_1 to t_2 to flow through, the reactor, or the exit-age.

In the pulse technique, a tracer is injected in a sufficiently short timeframe to approximate an instantaneous Dirac delta function [27]. The alternative to the pulse tracer approach is the step tracer method which yields the cumulative distribution function, *F(t)*, directly [27]:

$$F(t) = \int_0^t E(t)dt \qquad (3.2)$$

where *F(t)* corresponds to the cumulative fraction of material spending less than time, *t*, in the reactor before exiting.

The step tracer method introduces the tracer as a step input, generally a positive step-change. This technique can be a more accurate method than the pulse input method since the pulse method is sensitive to deviations from the ideal Dirac delta assumption and does not account for tracer diffusion in the feed section prior to injection [27]. Moreover, the step tracer method does not require knowledge of the total tracer amount, though in practice the total tracer amount can be estimated by integration of the tracer concentration as a function of time in a pulse experiment. There are significant drawbacks to the step tracer method, however, which may be difficult to overcome. The two biggest drawbacks are the

difficulty in maintaining constant tracer injection rates, which is increasingly difficult with smaller reactor volumes or very concentrated tracers; and the high cost of specialized tracers as a step input, either positive or negative, require much larger tracer volumes than pulse inputs.

Mean residence time (MRT), t_m, is taken as the first moment of *E(t)* [27]:

$$t_m = \int_0^\infty E(t)dt \tag{3.3}$$

The MRT corresponds to the average time the material takes to exit the reactor. This MRT is the most widely used moment of the exit-age distribution and is useful in bulk determination of mixing time scales. There are also higher moments of the *E(t)* function which also bear useful information about the distribution.

The second moment about the mean is described as the variance of the distribution, σ_t^2, or square of the standard deviation of the distribution, and is given as [27]:

$$\sigma_t^2 = \int_0^\infty (t - t_m)^2 E(t)dt \tag{3.4}$$

The magnitude of the variance is a measure of the spread of the distribution about the mean, with units of time-squared; large σ_t^2 values correspond to wider distributions. The variance may also be expressed in a dimensionless form which

is independent of the magnitude of t_m [28]. This dimensionless variance, σ^2 , is given as [27]:

$$\sigma^2 = \frac{\sigma_t^2}{t_m^2} \tag{3.5}$$

For ideal piston flow, $\sigma_{PFR}^2 = 0$; for perfectly mixed tank reactors, $\sigma_{CSTR}^2 = 1$ [28, 29]. The entire distribution is typically presented in normalized form as well by defining a dimensionless parameter, Θ, and is given as [27]:

$$\Theta = \frac{t}{t_m} \tag{3.6}$$

The dimensionless, normalized exit-age distribution is then defined [27]:

$$E(\Theta) = t_m E(t) \tag{3.7}$$

This normalization allows for comparison of the exit-age distribution function amongst reactors of different volumes, for example, as the mean residence time is removed as a variable [30]. For all perfectly CSTRs, numerically the $E(\Theta)$function is the same; for all normalized $E(\Theta)$ functions, the mean residence time corresponds to a value of $\Theta = 1$ [27].

3.3 Inline Fiber Optic Probe Monitoring of an Extruder

The nature of the extruder makes it very difficult to ‘observe’ what is happening between the feeding port and the die-face. Often, observations related

to the state of the material within the extruder need to be inferred as direct observation is not typically possible due to high internal pressures and a need to very high levels of heat to keep the polymer molten. For this reason, the extruder can be viewed as a sort of ‘black-box’ where certain things go in and others come out.

Bur and Gallant [31] were the first to report the use of a fiber optic probe to monitor the concentration of a fluorescent analyte within a twin screw extruder; this reference is important to the current thesis as it was the adopted method of process monitoring during emulsification. The system they studied was a polybutadiene and calcium carbonate compounding process. The fluorescent dye, coumarin 30, was used to determine the residence time distribution, the quality of mixing between the polymer and particulate phases and the mix concentrations as a function of processing conditions. The setup from their original paper, shown below in Figure 15, used a photomultiplier tube (PMT) to record the amount of emitted light from the fluorescent probe into a measurable voltage, which is then recorded as a function of time. The system worked by utilizing a bifurcated optical probe which relayed the excitation light from the laser light source, along the fibre to material within the extruder. The light was absorbed by the fluorescent tracer and the emitted light was collected by a separate strand of fibres which fed into the PMT. Bandpass filters were used in front of the PMT to filter out light which was above or below the wavelengths of emission for the tracer. This filtering removed the specular and diffuse reflectance

of the light source from the surface of the polymer melt – this is important as the intensity of emitted light was much lower than the excitation light fed to the system.

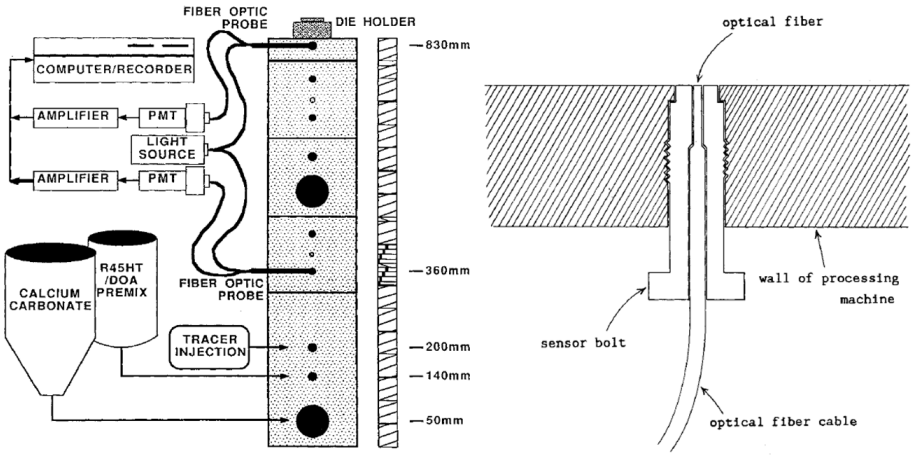

Figure 15 - Schematic diagram of the fluorescence monitoring setup used by A.J. Bur and F.M. Gallant [31].

Hu, et al. [32] studied the residence time distribution of several anthracene based tracers which were copolymerized into polystyrene and polymethylmethacrylate chains. The authors used a similar setup to Bur and Gallant, using a bifurcated optical probe and a photomultiplier tube. The key difference is the direct polymerization of the tracer into the polymer backbone. This was done to ensure similar flow properties between the tracer and polymer system being studied. The authors created two polystyrene-based tracers having molecular weights of 68 kg/mol and 180 kg/mol. The authors compared the two tracers to a masterbatch created by mixing the bulk polystyrene and the 68 kg/mol polystyrene-tracer; no significant differences were seen, as shown in Figure 16. This is an important finding which validates the accuracy of

polymerizing a fluorescent tracer directly into a lower molecular weight polymer, which bears similar chemical structure to the polymer being processed.

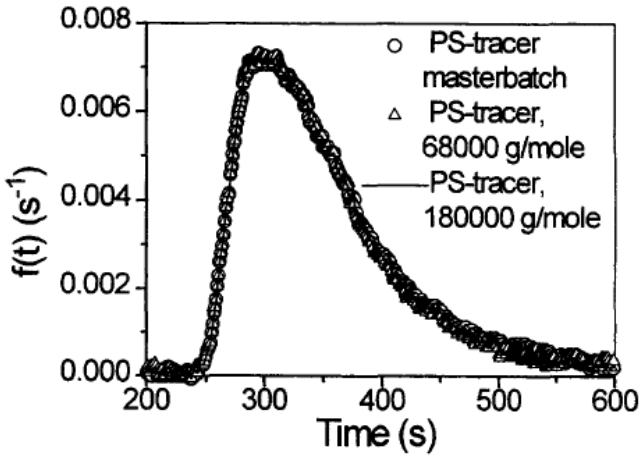

Figure 16 - Comparison of the measured RTD curves of three tracers showing little difference in flow patterns for tracers of different molecular weights but having similar chemical compositions [32].

Carnerio, et al. [33] went further to study the local residence times in a kneading section within a twin-screw extruder. The authors also did extensive comparison of in-line to off-line measurements to confirm the accuracy of the method, good agreement was found. Their measurement setup consisted of an avalanche photo-diode (APD) connected to the extruder with a similar bifurcated setup as reported by Bur, et al. and Hu, et al. In a similar manner, RTD curves were constructed as a function of the voltage of the APD which was correlated to the concentration of a fluorescent probe within the extruder. The key distinction in their paper was the use of a modified sampling port which was fitted at various distances along the screw length; the setup is shown in Figure 17. The authors also investigated how the orientation of an optical probe mounted in a rectangular

slit die on a single-screw extruder (SSE) would affect the recorded RTD. The goal was to determine how the parabolic shape of the flow field in the slit die would affect measurement if observed in a horizontal position, slowest polymer velocity; or vertical position, highest polymer velocity. It was found that the horizontally mount probe showed much larger variance in the observed RTD at lower screw speeds. This is presumably due to the stagnation of the polymer melt at the wall of the slit die due to the low velocity gradient created at low flow rates (low screw speeds in SSE).

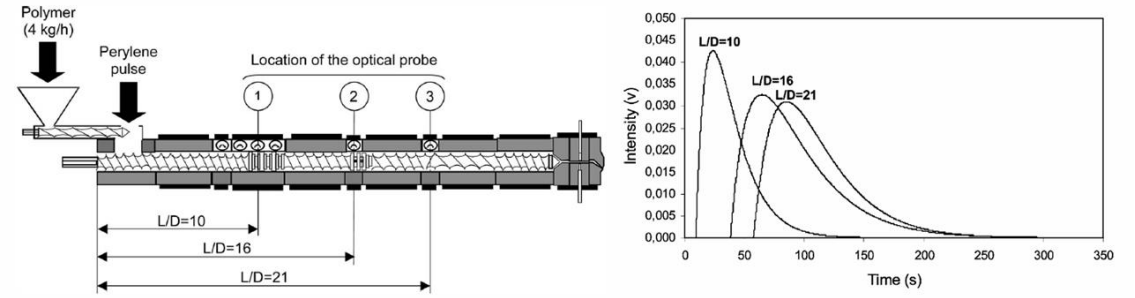

Figure 17 - Experimental setup used by Carneiro, et al. in the determination of local residence time distribution at different L/D ratios along the length of the extruder [33].

3.3 Experimental Determination of Residence Time Distribution

3.3.1 Experimental Setup

A co-rotating, twin screw extruder was used in this study (Leistritz Micro 18, 40 L/D; American Leistritz Corp., Sommerville, NJ) having a cooled feeding zone (*Z0*), 7 heated zones (*Z1-Z7*) as well as a heated die (*Z8*). The extruder was equipped with a gravimetric feeder for solids metering (K-Tron KT20 Twin

Screw Gravimetric Feeder, K-Tron Soder, Niederlenz, Switzerland). Liquid injection feeds were metered by a high-pressure syringe pump (ISCO model 500D and 1000D, Teledyne ISCO, Lincoln, NE) and a high pressure piston pump (Eldex Optos Model 3, Eldex Laboratories Inc., Napa, CA). A schematic layout of the locations of solids feed (*Z0*), and deionized water injection (*Z2*, *Z6*) is given, below, in Figure 18. The zone 2 DIW injection stream was first past through heated bath using a stainless steel coil for heat transfer before flowing into the injection nozzle mounted on the extruder. The bath temperature was set at 140°C.

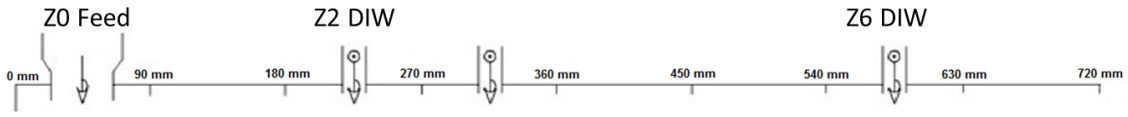

Figure 18 - Schematic layout of injection ports for screw speed, R:W vs. RTD experiment set.

3.3.2 Materials

An amorphous polyester resin was chosen as the basis of this study on solvent-free emulsification and is used throughout this body of work. The polyester is supplied in powdered form and is used directly without any modification. A table of properties for the polyester resin is listed below, in Table 1. Sodium dodecylbenzenesulfonate (SDBS) having a molecular weight of 348.48 g/mol was purchased from Sigma-Aldrich (Catalog number: 289957, Sigma-Aldrich Canada, Ltd, Mississauga, Ontario, Canada) and was specified as technical grade. Sodium hydroxide (NaOH) was also purchased from Sigma-

Aldrich Canada, Ltd (pellet-form). The NaOH was then ground from pellets into a fine powder using an analytical grinding mill (IKA A11 basic; IKA-Werke GmbH, Staufen, Germany) to be incorporated with the powdered resin during dry-blending. Deionized water (DIW) having an average resistivity of 18 M-Ohm.cm, and no less than 15 M-Ohm.cm, was used for injection into the extruder and it should be assumed that whenever water is mentioned in the discussion, it refers to deionized water.

Table 1 - Properties of the polyester resin utilized in this study.

Property	Value	Units
Onset Tg	60	*°C*
Tm	107	*°C*
Acid Value	12	*mg KOH/g resin*
Mn	4,000	*Datlons*
Mp	13,000	*Daltons*
Mw	18,000	*Daltons*

3.3.3 Offline Spectrofluorometer

A Horiba Scientific *FluoroMax-4* was used to determine fluorescent emission from latex samples taken from the extruder to calculate the fluorescent tracer concentration. The Fluoromax-4 was configured with a 150-W xenon lamp with a continuous output. The grating has 1200-grooves/mm, the excitation gratings were blazed at 330 nm (220-600 nm optical range) and the emission at 500 nm (290-850 nm optical range). Latex samples were measured in a cuvette without dilution. The excitation source slit width was fixed at 5nm centered about a bandpass wavelength of 475nm. Emission was recorded at a bandpass

wavelength of 525nm with a slit width of 1nm. The total integration time was 1 second.

3.3.4 Fiber Optic Mini-Spectrometer

An Ocean Optics SD2000 dual-channel fiber optic mini-spectrometer was used to record the fluorescent emission of the latex. The ‘master’ channel had 600 lines blazed at 300 nm with a bandwidth of 200-850 nm and a 10 µm slit. The ‘slave’ channel had 600 lines blazed at 750 nm with a bandwidth of 500-1150 nm and a 10 µm slit. Only the master channel was used during the course of this study as it was optimized for UV-VIS spectra. An Ocean Optics ADC1000-USB analog-to-digital converter was used to connect the spectrometer to a computer. Ocean Optics *Spectrasuite* software was used to configure the spectrometer and capture data from the attached probe. The probe was a bifuricated backscattering/reflectance probe manufactured by Ocean Optics. The probe consists of 14 fibers having a diameter of 200µm; 6 UV-VIS illumination fibers, 6 VIS-NIR illumination fibers, one UV-VIS emission fiber, and one VIS-NIR emission fiber. The master channel of the SD2000 was the only channel used in this study as it is optimized for the UV-VIS readings. An image of the probe tip, depicting the arrangement of the fibers, is shown below in Figure 19. The illumination fibers of the bifuricated probe were connected to an Ocean Optics LS-450 Blue LED light source with a wavelength of maximum emission at 470nm, shown below in Figure 20. The emission fibers of the bifuricated probe were connected to the mini-spectrometer. The setup is shown below, in Figure 21.

Figure 19 - Surface of bifurcated probe face showing the arrangement of the 14 fibers; 12 illumination fibers are arranged around two central emission fibers [34].

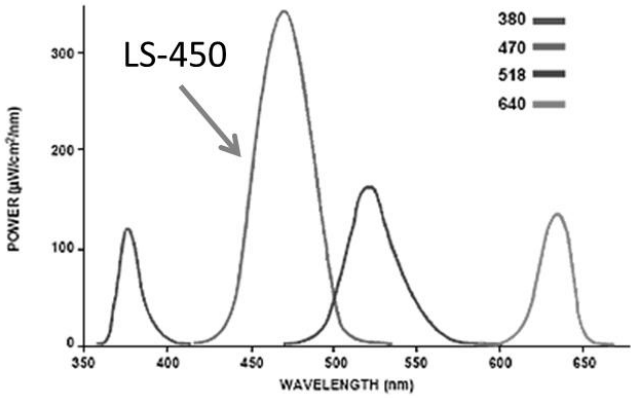

Figure 20 - Spectral output of the Ocean Optics LS-450. Figured adapted from [35]

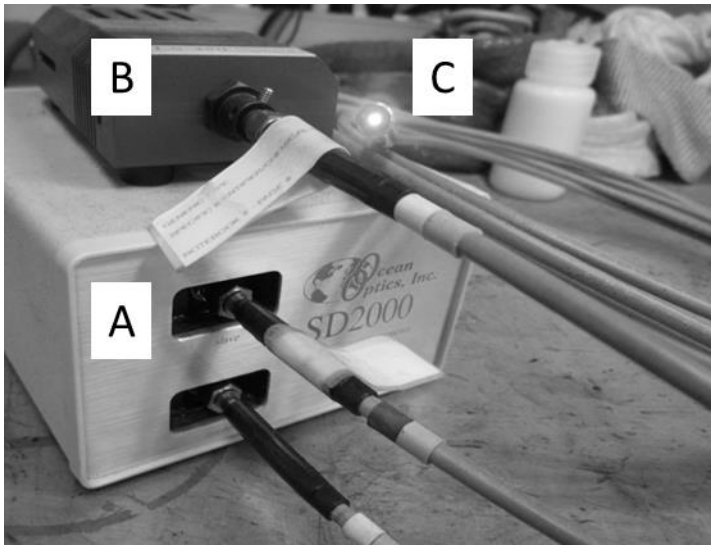

Figure 21 - Ocean Optics SD2000 mini-spectrometer (A) and LS-450 LED light source (B) attached to a bifuricated backscattering/reflectance probe (C).

The SD2000 was configured using the Spectrasuite software provided by ocean optics. The emission was recorded at either 515 nm or 525 nm using a bandwidth value of 1nm. The integration time was fixed at 1000 ms for both single measurements as well as continuous measurements. To validate the use of the fiber optic mini-spectrometer, a set of samples taken during a tracer experiment were analyzed for tracer concentration using both the fluorometer as well as the fiber optic probe system – both offline. The normalized fluorescence intensity was compared for both methods by taking the absolute reading by both instruments, in counts-per-second (cps), and dividing through by the integral of the total concentration of tracer used to account for differences in sensitivity between the two methods. The results are shown below, in Figure 22.

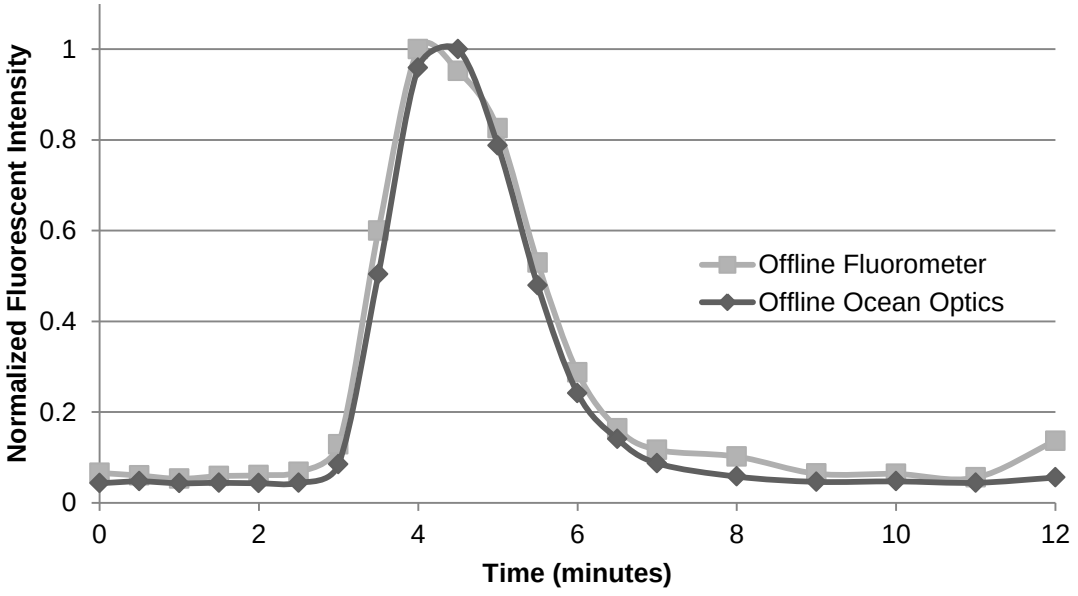

Figure 22 – Offline Validation of Fiber Optic Probe Against Fluorometer for Discrete Sampling.

3.3.5 Inline Fiber Optic Probe Monitoring System

The inline determination of fluorescence emission was carried out by mounting the tip of the bifurcated fiber optic backscattering/reflectance probe to the die at the end of the extruder. This was accomplished by fixing a bored-through ¼'' Swagelok fitting, at a 90°C angle to the extrudate stream. The probe was inserted into the fitting using PTFE ferrule sets to allow for removal of the probe from the die but also to allow the ferrules to be removed from the probe. The probe was mounted at a depth in the fitting to allow the probe face to sit flush with the internal cavity in the die. A schematic of the entire inline fiber optic probe monitoring system is shown below, in Figure 23.

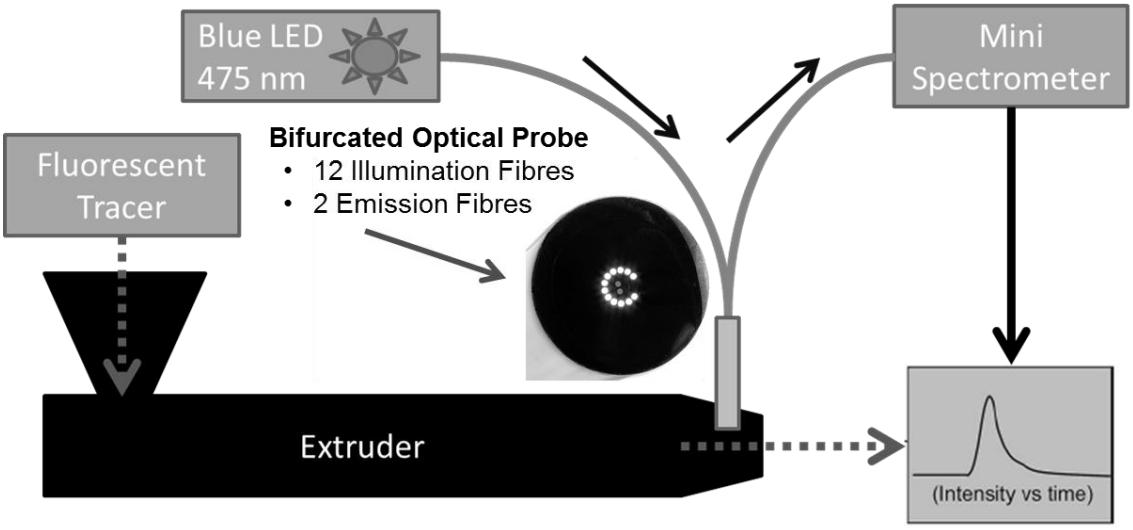

Figure 23 - Schematic of Inline Fiber Optic Probe Setup for Measuring Fluorescent Tracer Concentration.

3.3.6 Fluorescently-Tagged Polyester as a Tracer

A fluorescently-tagged crystalline polyester was used as a fluorescent tracer, or fluorophore, in these studies due to the high compatibility of the tracer with the polymer system in the extruder. It is advantageous to choose a tracer which is non-reactive and has good miscibility with the material so that the tracer flow is representative of the matrix and its total concentration remains constant. The details of the tracer can be found in US patent application 20120065359 A1. The structure of the fluorophore is shown below, in Figure 24.

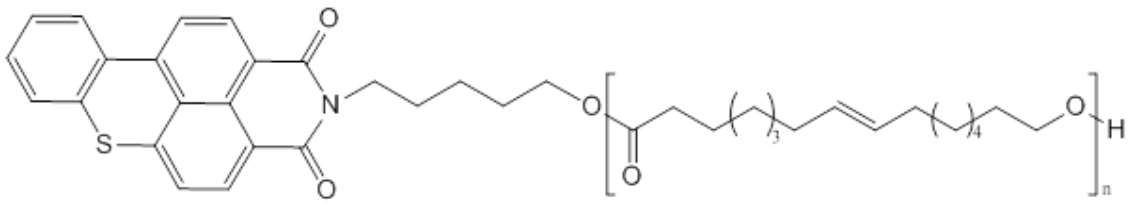

Figure 24 - Fluorophore comprising covalently bonded polyester to a fluorescent Hostasol dye.

The frequency of maximum excitation and emission from the fluorophore in the latex system was 475nm and 525nm, respectively, and this is shown in Figure 25. The peak excitation and emission was measured by taking a sample near the peak residence time, or maximum instantaneous fluorophore concentration, and measuring emission offline using both the fluorometer and fiber optic probe. It is interesting to note that when measuring the fluorescent emission with the fiber optic probe mounted inline at the die-face the maximum emission shifted down to 515nm. That is to say that the fluorescent tracer showed a shift in wavelength of maximum emission to 515nm when measured at

the die-face compared to 525nm, when measured offline using the same fiber optic probe. A comparison between the recorded emission captured by the inline probe at wavelengths of 525nm and 515nm, is shown in Figure 26; the excitation source was a blue LED lamp centered at 470nm. The main difference between the measurement of the latex inline and offline was that the temperature of the latex was higher when measuring inline as the offline samples were allowed to cool to room temperature before measurement. This change in temperature from the die-face, ~85°C-95°C, to room temperature also passes through the glass transition temperature of the polymer which is 60°C. Eisenbach, et al. [36] demonstrated that the overall mobility of a polymer as well as its polarity can influence the stokes shift of fluorescence by studying the emission of a fluorescent dye in plasticized and un-plasticized polymers which also varied in polarity. The authors found that plasticized polymers favoured excitation and emission band separation, in addition plasticized and polar polymers produced the largest Stokes shift. This does not agree with the shift in emission based on polymer mobility alone however, as inline measurement was carried out above the polymer T_g and yet produced a lower wavelength of maximum emission for the same excitation source. The polarity may be the main contributor to the shift in fluorescence emission as emission tends to shift to longer wavelengths as the polarity of the solvent is increased [37]. Though the mechanism of this small shift is beyond the scope of this study, it is interesting to postulate that if this shift to shorter wavelengths was due to a change in polarity as a function of temperature

of the latex then it could be a very useful tool for future investigation of the solvent free mechanism. With respect to the potential impact of light scattering on the shift in fluorescent emission, the offline samples were also sampled undiluted so any scattering effects would not be a result of different particle concentrations. Regardless of the mechanism of the shift, it should be noted that both recorded wavelengths of emission produce the same residence time distribution.

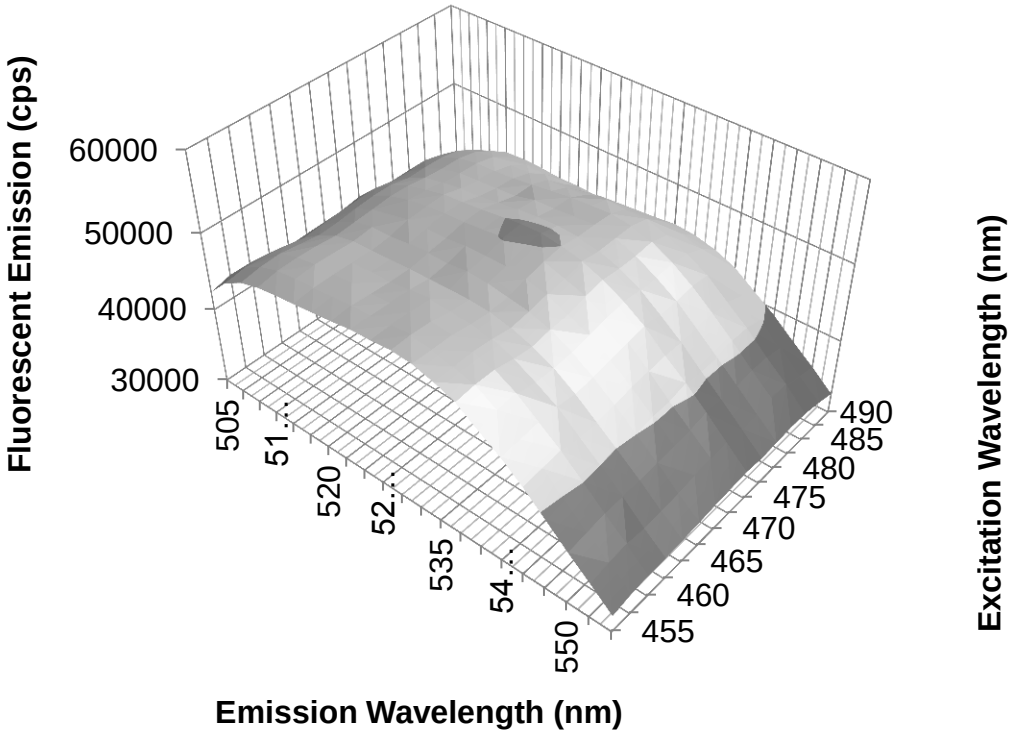

Figure 25 – Fluorescent Excitation vs. Emission in Counts Per Second of a Sample Corresponding to the Peak Residence Time in a Trial.

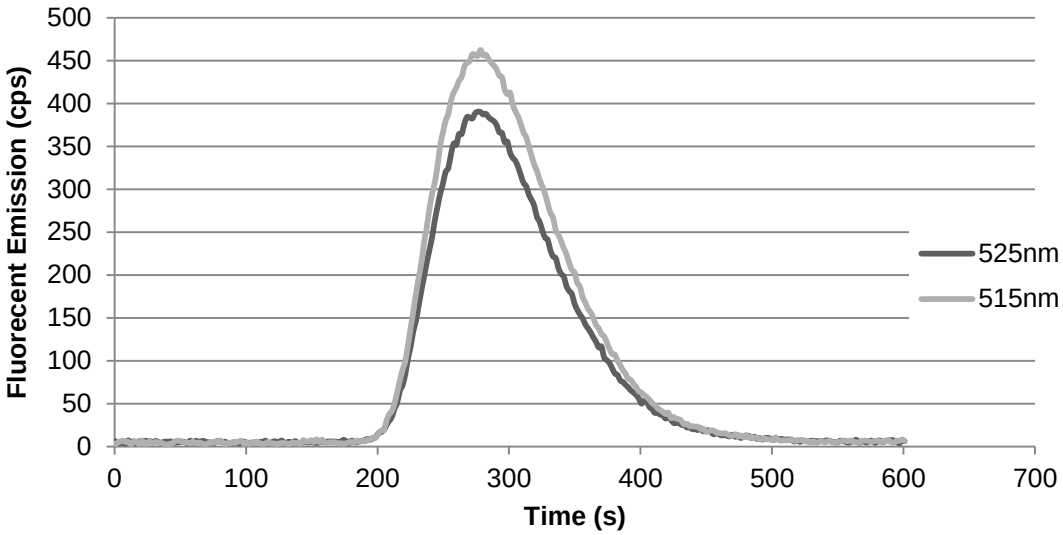

Figure 26 - Comparison Between Recorded Emission at 515nm and 525nm from an LED Excitation of 470nm.

3.3.7 Experimental Method of Determining In-line Residence Time Distribution

An important aspect of selecting a tracer for the residence time studies was confirming that there was a linear relationship between tracer mass and measured concentration. That is to say that the measured tracer concentration, fluorescent emission in counts per second, should be directly proportional to the actual concentration of tracer being measured (Beer-Lambert law) [29, 32]. Tracer concentrations were varied between 20 and 80 mg. The total tracer concentration, integrated from the fluorescent emission over the total run time as described in 3.3.8, was compared against the actual tracer masses used in the experiments; this is shown below in Figure 27. A good linear relationship was found to exist between the calculated tracer concentration and the actual mass of

tracer utilized in the pulse input. This confirms that the fluorescent emission of the tracer had a linear response to tracer concentration over the ranges of tracer masses used in this data. No saturation or plateau in response was observed at the highest tracer concentrations used. Deviation from the fitted linear relationship is likely mostly attributed to the error of the balance used to measure the tracer weight as the solid state detector in the mini spectrometer experiences very little drift once it has warmed up and the tracer weights were randomized within the runs.

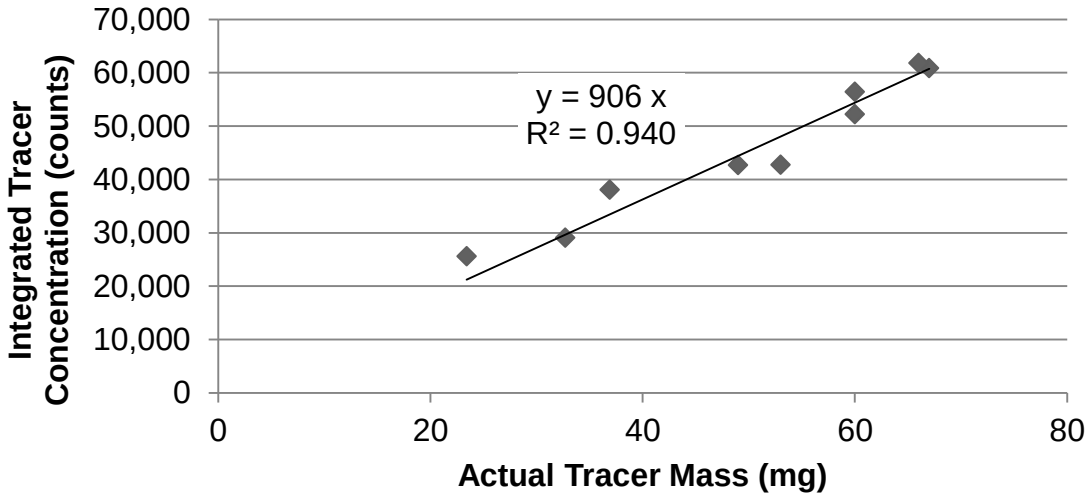

Figure 27 - Calculated Tracer Concentration vs. Actual Tracer Mass Used in (mg).

3.3.8 Twin Screw Extruder Operating Conditions

Two datasets were evaluated in this portion of the study and correspond to two different dispersion zone resin-to-water (R:W) ratios of 3.0 and 3.5 while the final diluted solids content stayed the same at the die-face. Screw speed was varied at 300 RPM, 400 RPM, and 500 RPM. The twin screw extruder was

operated with the following temperature profile in Table 2 for each zone with the feeding zone being cooled by domestic chilled water. The composition of the dry feed metered by the gravimetric feed into the feeding port of the extruder for the two datasets is given in Table 3.

Table 2 - Temperature profile of twin screw extruder for 033 and 035 datasets.

Zone	1	2	3	4	5	6	7	Die
Temperature (°C)	160	165	135	95	95	95	95	95

Table 3 – Dry feed composition for 033 and 035 datasets.

Feed	Parts	Percent of Dry Feed	Total (g/min)
Resin	100	92.17%	19.20
NaOH	0.85	0.78%	0.16
SDBS	10	9.22%	1.92
Total	110.85	102.17%	20.83

Experiments were conducted by first allowing the temperature of the extruder to reach the set points described in Table 2 before the extruder was started. The feeder would then be started along with the aqueous injection pumps; 30 minutes was given before experiments began after start-up. Ten minutes was given between the operating conditions given in Table 4. Tracer experiments would begin by collecting a sample of the latex for 3 minutes and starting the time acquisition of the mini-spectrometer and then dropping a pellet

of the fluorophore, described in 3.3.6, into the cooled feeding port (zone 0). Careful note of the actual start time was taken, corresponding to the time when the tracer was released into the feed. The tracer emission was recorded for a total of 10 minutes for each run, or until the emission as measured by the mini-spectrometer returned to baseline levels.

Table 4 - Operating conditions of the extruder for '3.0' and '3.5' data series.

Experiment	RPM	R:W	Dry Feed Rate (g/min)	Zone 2 DIW Injection Rate (mL/min)	Zone 6 DIW Injection Rate (mL/min)	Final Solids Concentration
300-3.5	300	3.5	20.83	5.37	36.93	33%
400-3.5	400	3.5	20.83	5.37	36.93	33%
500-3.5	500	3.5	20.83	5.37	36.93	33%
300-3.0	300	3	20.83	6.26	36.03	33%
400-3.0	400	3	20.83	6.26	36.03	33%
500-3.0	500	3	20.83	6.26	36.03	33%

3.3.8 Data Analysis and Processing

The data acquisition from the Ocean Optics SD2000 spectrometer was sent via USB to a computer with the ADC1000 analog to digital converter. Ocean Optics Spectrasuite software was utilized to configure the spectrometer and record the data which was then exported to excel for storage. *MathCad* version 15 (PTC, Needham, MA) was used for processing of the data before being sent back to Excel for graphing and presentation of the data.

A MathCad program was written to process the data for analysis, this program had the following main functions:

1. Read in time and concentration (recorded emission values [=] counts per second) into two vectors.
2. Calculate the baseline background emission values (noise) by averaging the recorded concentration over the first 100 seconds of the recorded values. This value of 100 seconds was below the minimum residence time of all samples which typically was >150 seconds.
3. Subtract the average background emission from the concentration vector to re-zero the concentration vector.
4. Calculate the heavyside function of the concentration vector and multiply by each element to set negative values to zero. This is required as the background noise produces oscillation in the data and as such the subtraction of the average background noise from the concentration values produced some negative values. Negative values of concentration are non-real and tend to skew the high moments of the distribution.
5. Fit a cubic spline to the discrete data to produce a continuous residence time distribution function. It should be noted that no smoothing was utilized in producing the fitted cubic spline.
6. Calculate total tracer concentration by integrating the splined concentration function over the total time the distribution was recorded (600 seconds).
7. Calculate the exit-age distribution function by dividing the concentration function by the total tracer concentration, shown in Equation 3.1.

8. Calculate the first and second moments of the exit-age distribution function corresponding to mean residence time and variance of the exit-age distribution, respectively, as shown in Equation 3.3 and 3.4.
9. Calculating discrete vectors of time and concentration from the continuous exit-age distribution function and returning them to excel for processing.
10. The dimensionless or normalized exit-age distribution function was then calculated in excel as shown in Equation 3.6 and 3.7.

3.4 Results and Discussion

The effect of screw speed on the resulting residence time distribution of polymer within the system was evaluated by comparing three screw speeds: 300, 400, and 500 RPM at two resin-to-water ratios: 3:1, and 3.5:1. This range was chosen to determine the incremental impact of increasing water content in the dispersion zone upon the variance of the residence time distribution. Optimization of the resin-to-water ratio is beyond the scope of this body of work, instead the purpose is simply to determine if an increase in water content leads to an appreciable impact on the mixing behaviour within the extruder.

A fluorescently-tagged polyester tracer was used to track the resin phase within the extruder. For illustration of the baseline subtraction method used, Figure 28 shows the recorded C(t) values for the first 100 seconds from the spectrometer to the baseline subtracted C(t) values. It should be noted that the baseline value, averaged over the first 100 seconds of the data, typically

corresponded to about 1% of the peak reading during an experiment and corresponded to a maximum of 3% during one of the experiments. It is assumed that subtraction of this minor value from the entire concentration data should have a negligible effect on the overall residence time distribution. It should be noted however that the influence of the baseline subtraction is larger for higher moments, or it would have a larger effect on the variance than it would on the mean residence time, for example.

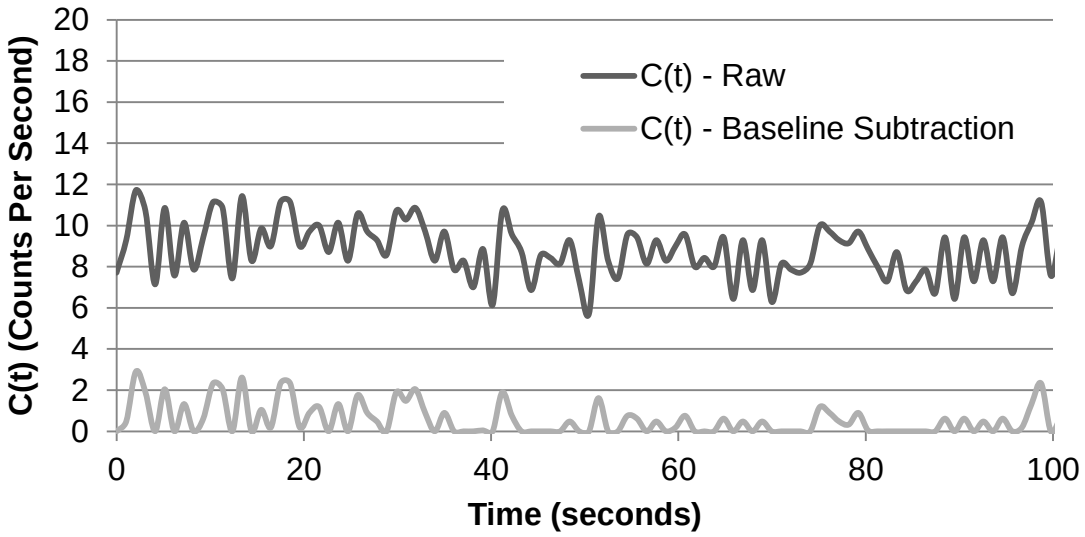

Figure 28 - Illustration of baseline subtraction method comparing the raw unadjusted C(t) vector to the baseline subtracted C(t) vector.

For illustrative purposes, Figure 29 compares the recorded C(t) data for two replicate runs with tracer weights of 60 mg and 53 mg at 400 RPM and a resin-to-water ratio of 3.5:1. Figure 30 shows the same two captured residence time distributions but displayed normalized as the dimensionless exit-age

distribution. By normalizing the distributions, direct comparisons of different tracer weights can be made readily.

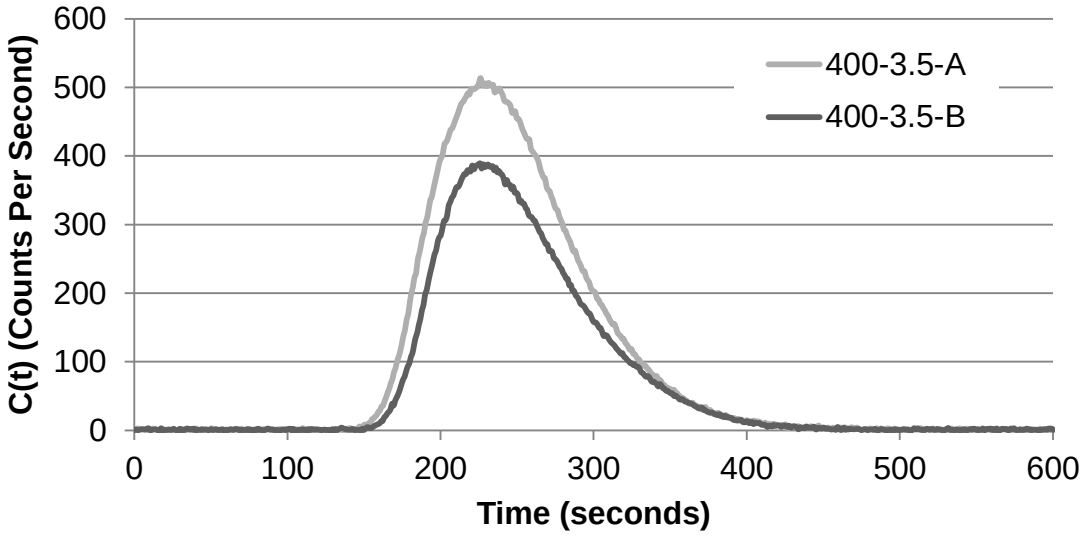

Figure 29 – Comparison of C(t) for replicate runs at 400 RPM and 3.5:1 resin-to-water ratio to illustrate influence of tracer weight (A=60mg, B=53mg).

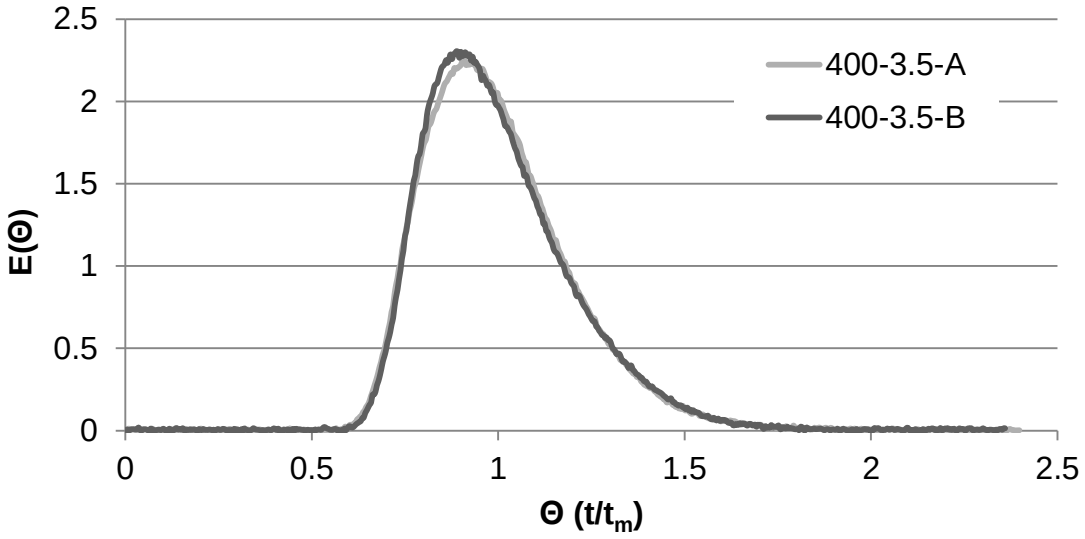

Figure 30 – Comparison of dimensionless exit-age distribution, E(Θ), for two replicate runs at 400 RPM and 3.5:1 resin-to-water ratio to illustrate normalization.

Figure 31 and Figure 32 compare the residence time and dimensionless variance among the residence time distributions, respectively, of the polymer tracer in the extruder for screw speeds of 300, 400, and 500 RPM, and resin-to-water ratios of 3 and 3.5. A summary of the experimental results are shown below in Table 5, including screw speed, resin-to-water ratios, mean residence times, dimensionless variance, feed rates, and water injection rates. Table 6 lists the D50 particle sizes obtained for the trials; samples in R:W = 3 were averaged.

Table 5 - Summary of results for screw speed, R:W vs. RTD experiment set.

Screw Speed	R:W	Feed (g/min)	Z2 DIW* (mL/min)	Z6 DIW* (mL/min)	Mean Residence Time (s)	Dimensionless Variance
300	3.5	20.8	5.37	36.9	266	0.039
400	3.5	20.8	5.37	36.9	269	0.038
500	3.5	20.8	5.37	36.9	267	0.041
300	3	20.8	6.26	36.0	244	0.042
400	3	20.8	6.26	36.0	251	0.041
500	3	20.8	6.26	36.0	250	0.042

** "Z2" = Zone 2; "Z6" = Zone 6; "DIW" = de-ionized water*

Table 6 – D50 Particle size data for residence time distribution trials.

Screw Speed	R:W	D50 (nm)
300	3.5	73
400	3.5	59
500	3.5	69
300	3	61
400	3	56
500	3	57

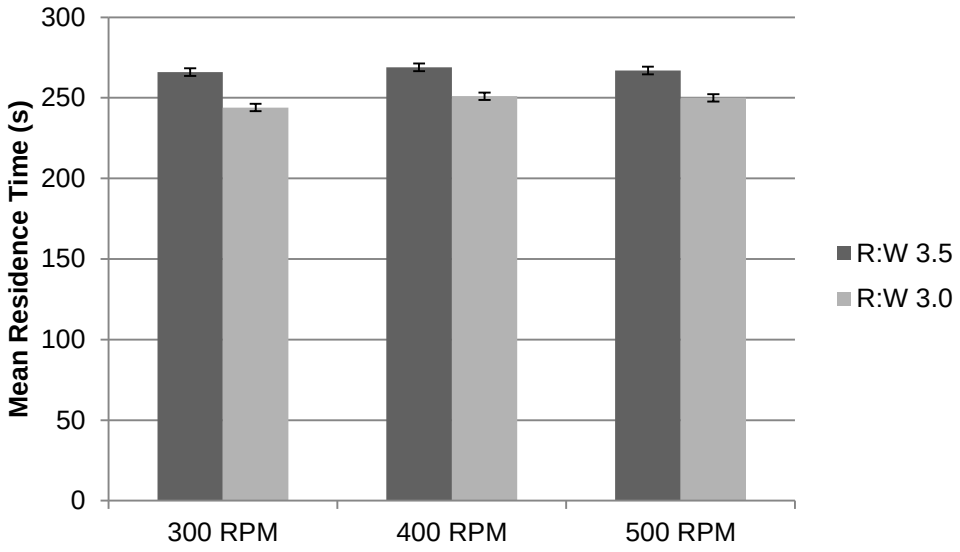

Figure 31 - Residence time of polymer in extruder at screw speeds of 300, 400, and 500 RPM and resin-to-water ratios of 3 and 3.5.

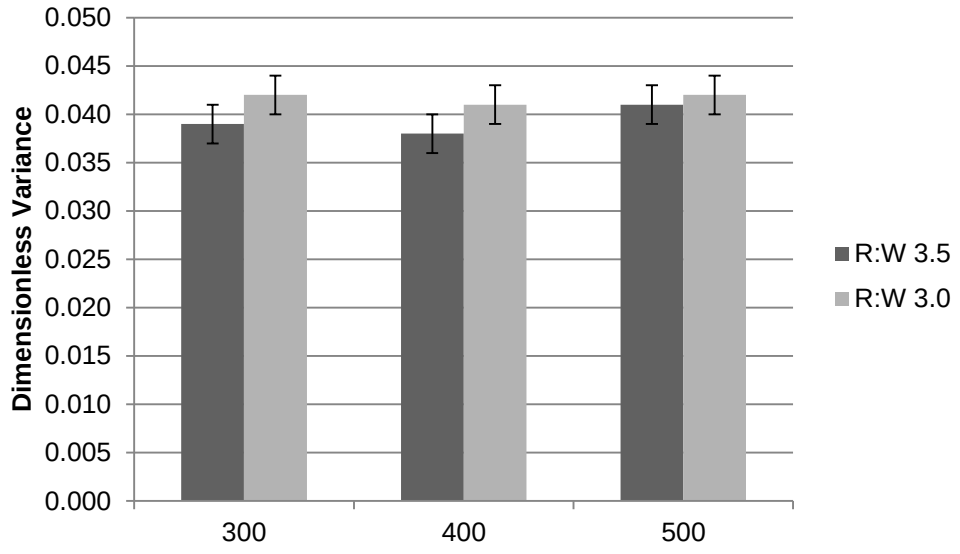

Figure 32 – Dimensionless variance in residence time distribution of polymer in extruder at screw speeds of 300, 400, and 500 RPM and resin-to-water ratios of 3 and 3.5.

The results of the experiment show that the mean residence time of the polymer tracer was not significantly impacted by varying screw speeds through the range observed. This is significant as it shows that, under the conditions of the experiment, any underlying time-dependant kinetics regarding the solvent free emulsification mechanism would not be dependent on screw speed. That is to say that screw speed and residence time, or reaction time, may be decoupled when describing the inversion mechanism in this operating region. It should be noted, however, that this does not preclude the possibility of interaction between the two factors of screw speed and residence time upon the resulting latex particle size distribution. A possible interaction between screw speed and residence time would be the strain distribution function, which would be dependent on both the shear rate – determined by the screw speed – and residence time distribution [6, 38, 39]. This interaction is to be evaluated in the following chapter by varying screw speed and feed rate and analyzing the response in particle size distribution. The determination of the strain distribution function was not within the scope of this work due to the difficulty in determining the complex viscosity of the resin/water mixture.

Decreasing the resin-to-water ratio in the dispersion zone led to a decrease in mean residence time distribution. This was to be expected as the volumetric flow-rate is increased downstream of the first water injection site though the total flow rate was identical after the second water injection site, as seen in Figure 33. This was significant since it showed that varying the resin-to-

water ratio in the dispersion zone effectively confounded its influence on latex particle size with the resultant change in residence time distribution. Although the total die-flow rate was held constant, the location of injection of the aqueous phase influences the residence time within the dispersion and dilution zone respectively. That is to say that changing the resin-to-water ratio affects the chemistry but also the physical time-dependent process. It means that making inferences regarding the dominant mechanism to the causes of particle size development will be unreliable by studying the resin-to-water ratio as a sole variable.

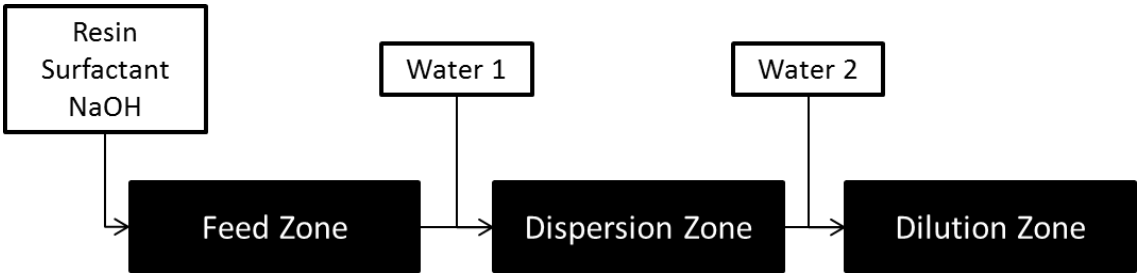

Figure 33 – Schematic model of system.

The dimensionless variance is a measure of mixing which can relate to axial dispersion (i.e. back-mixing), within a continuous flow reactor, such as an extruder [27]. The dimensionless variance is seemingly invariant with respect to screw speed and resin-to-water ratio within the data set observed, similar to the mean residence time. This is significant as it again decouples screw speed from back-mixing, within the dataset observed. It should be noted that the resin-to-water ratios here presented a limited set of the potential operational range and

that broader ranges of R:W ratios may induce viscosity changes that have a greater impact than on back-mixing than observed here.

Specific throughput or Q/N – where Q is the volumetric flow rate and N is the screw speed – is often used as an independent variable when analyzing residence time distributions in an extruder [40, 41]. In this study, Q/N varies by a factor of 1.6 (500/300 RPM) yet there is no impact upon the residence time or variance. This signifies that the degree of fill is 100% throughout the range of conditions analyzed. This finding is supported by the monitoring of the dispersion zone pressure by location of a pressure transducer in zone 3, immediately following the injection of water in zone 2. An overlay of data collected during the R:W = 3 trial is shown in Figure 34 for the six residence time trials. The dispersion zone pressure can be seen to vary between 1.38-2.07 mPa. This is well above the vapour pressure of water at the highest temperature in the extruder indicating that the screw is fully filled. The lack of change in the residence time distribution as a function of screw speed is consistent with fully-filled extruder as the degree-of-fill is no longer a function of screw speed.

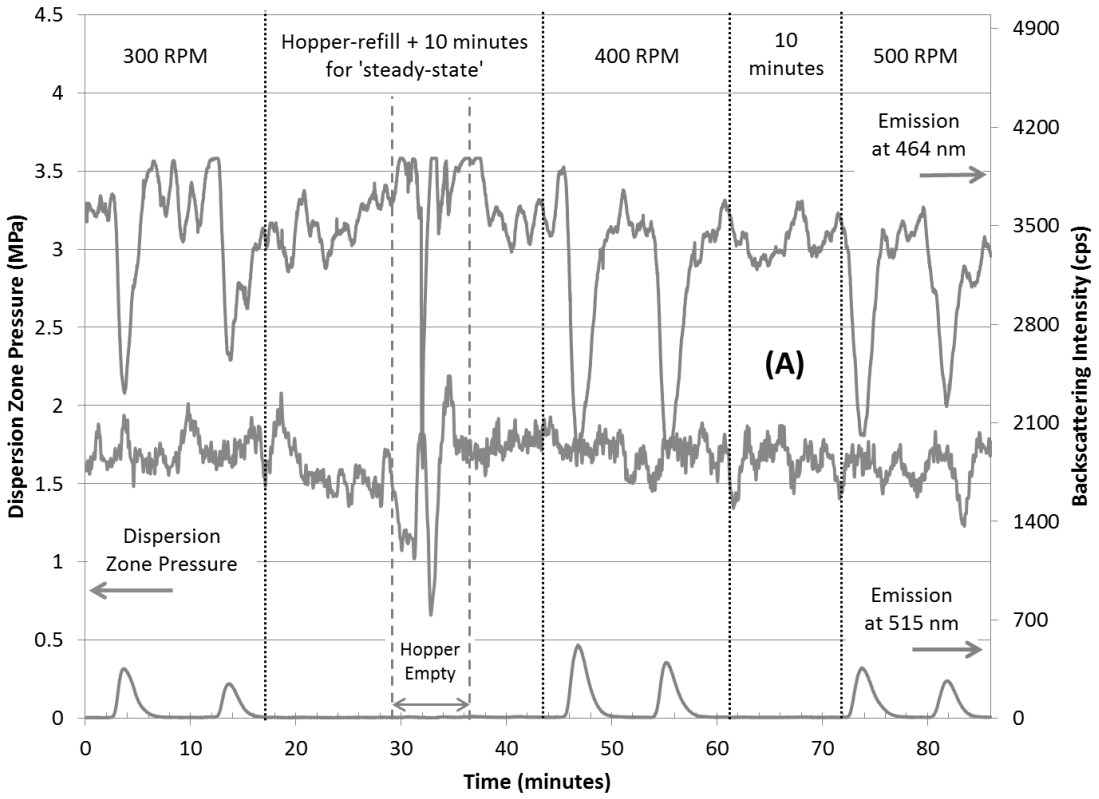

Figure 34 - Backscattering intensity at 464 nm, Fluorescent emission at 525 nm, and dispersion zone pressure during the R:W=3 trials.

Figure 34 display some interesting variation in the backscattering intensity at 464 nm (peak emission of blue LED light source) as a function of time. The peak minimum intensities correspond with the maximum emission of the fluorescent tracer due to absorption. The periodic fluctuations in between the peak residence time responses, however, are due to some sort of process instability which appears to be present in the dispersion zone pressure readings as well. These fluctuations in backscattering intensity in between the two tracers measured at 300 RPM, Figure 34 (A), spans from about 3400 to 3900 counts per second. It is possible that these fluctuations are a result of either variation in

particle size which alter the backscattering properties of the latex or that they related to variations in concentration of the latex, which would also influence the magnitude of backscattered light. Both explanations have interesting implications for the use of this system to monitor the production of continuous latex processes. With respect to process control, it is unclear to what extent a process may be controlled by monitoring these fluctuations but perhaps there would be some use in optimizing screw design parameters through minimization of these fluctuations. At the very least, it indicates some unstable behaviour within the extruder

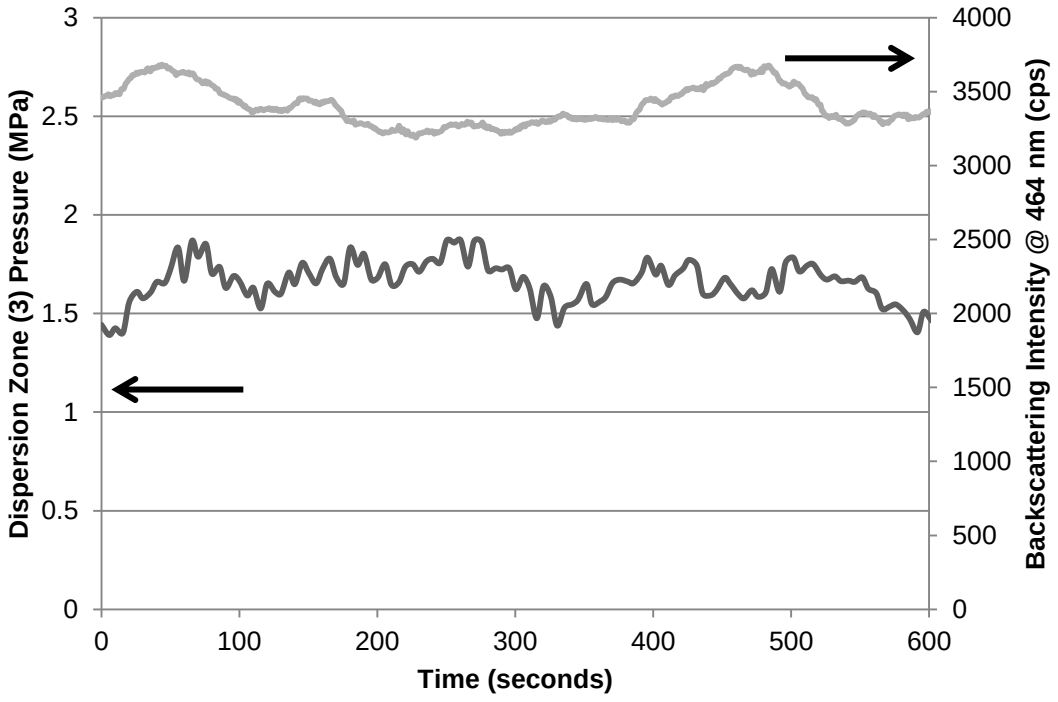

Figure 35 – Enlarged time span (A) from Figure 34: Dispersion zone pressure and backscattering intensity at 464nm as a function of time showing low levels of instability in the process.

3.5 Summary and Conclusion

To aide in the development of a mechanistic understanding of the dispersion process within the extruder, the time-scales of solvent-free emulsification have been established within the studied operating conditions. It was found that mean residence times of approximately 4 minutes were sufficient to allow for complete emulsification including: melting of the resin, dispersion of the water phase, and subsequent dilution to produce a latex continuously within an extruder. It was also shown that varying the water injection rate for a given dry feed rate also influences the mean residence time which has important implications when designing experiments. The two factors must be decoupled to analyze the individual responses, for example, when evaluating the specific response of resin-to-water ratio for a given residence time, the dry feed rate must also be adjusted to account for the change in volumetric throughput.

The dependence of the residence time distribution of solvent free emulsification upon the screw speed and water content within an extruder was studied. It was found that the flow pattern had a very low degree of variance, or back-mixing, regardless of the water content or screw speed. This is significant as it shows that the low viscosity aqueous component is being incorporated into a high viscosity resin component in a similar manner, independent of the magnitude of shear rate imposed.

CHAPTER 4 – EXPERIMENTAL RESULTS DOE

4.1 Objective and Scope

The purpose of this chapter is to determine the response of latex particle size distribution to the factors of screw speed and feed rate. The screw speed relates to the shear rate and strain rate, while the feed rate determines the residence time distribution in the solvent-free emulsification process.

4.2 Experimental

4.2.1 Experimental Setup

The same equipment was used in this chapter as described in section 3.3.2. A schematic layout of the locations of solids feed (*Z0*), and deionized water injection (*Z2*, *Z6*) is given again for reference, below, in Figure 18. The zone 2 DIW injection stream was first past through heated bath using a stainless steel coil for heat transfer before flowing into the injection nozzle mounted on the extruder. The bath temperature was set at 140°C

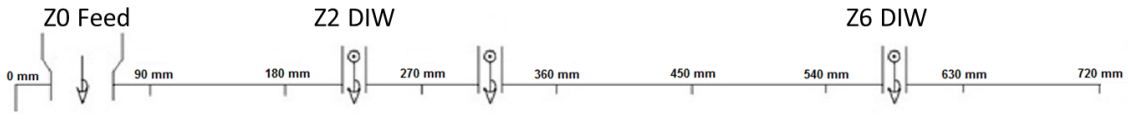

Figure 36 - Schematic layout of injection ports for screw speed, R:W vs. RTD experiment set.

4.2.2 Materials

The same material set was utilized as described in section 3.3.2 with the exception of surfactant, which was different in this chapter. DOWFAX 2A1 was purchased from Univar (Univar Canada Ltd., Tuxedo, MB, Canada). DOWFAX 2A1 is an Alkyldiphenyloxide Disulfonate anionic surfactant that is supplied as a liquid with 47 wt% active component with a water diluent.

4.2.3 Particle Size Measurement

A NANOTRAC NPA250 dynamic light scattering particle size measurement system was used to determine the particle size distribution of the latexes produced. The instrument was calibrated weekly using 100 nm polystyrene particles as a standard. Samples were measured in deionized water having an average resistivity of 18 M-Ohm.cm, and no less than 15 M-Ohm.cm

4.2.4 Sample Collection

The extruder was allowed to operate for 20 minutes after start-up and between different operating conditions. The extruder was started by first allowing the barrels to reactor the desired set-point temperature. The screws were then started at a rotational speed corresponding to the first operating condition of that day. Shortly after starting the screws, the dry feeder was started and immediately after, the aqueous injections were also started. Once steady state was reached, 4 samples were collected in 5 minute intervals. Samples were collected from the

extruder in 4 Dram vials and sealed quickly to prevent evaporation while cooling to room temperature.

4.2.5 Design of Experiments

The levels of the factors were chosen as they spanned the extremes in operability of the screw design utilized in this chapter. Lower feed rates could have potentially been utilized but 750 g/hr was the approximate lower limit of the gravimetric feeder before gross deviations from set point occurred. The upper limit of feed rate was based on the maximum level of torque that the extruder could handle. The screw design in this chapter is an earlier design which utilizes an extremely short melt/mixing section close to the feed opening. Feed rates higher than 1.25 kg/hr tended to trip the load limit on the motor due to limited softening of the resin prior to the first set of kneading blocks. The upper limit of screw speed was also determined due to torque limitations based on the screw design utilized. The lowest level of screw speed was chosen to maintain the integrity of melt seals between the feeding port and the first aqueous injection zone.

The experiments were carried out for sufficient periods of time to collect at least 4 samples in order to gain an idea of the stability in the process. The order of the experiments, with respect to screw speed, was randomized within each feed rate level by sorting random numbers generated by Excel, the order of feed rates were randomized using the same method. The experiments were grouped

by feed rate as to minimize the time between experiments as reaching steady state after changing the feed rate takes considerably longer than changing the screw speed. The order that the experiments were carried out is given in the Appendix in Table 13.

The experiments were carried out with an NaOH concentration of 1pph based on the mass flow rate of the resin; resin and powdered NaOH were blended and co-fed. The NaOH was milled using an IKA A11 analytical mill (IKA A11 basic; IKA-Werke GmbH, Staufen, Germany). Aqueous DOWFAX 2A1 was used at 47wt% and was heated by flowing through a tube submersed in a heated bath set to 140°C. Due to heat loss, the temperature was approximately 65°C when the aqueous surfactant was measured using a K-type thermocouple inline prior to entering the injector at zone 2. The concentration of surfactant was fixed at 10 pph based on resin feed rate. DIW dilution water was heated in a similar manner –the higher flow rate reduced heat loss and the temperature was approximately 120°C when measured using a K-type thermocouple inline prior to entering the injector in zone 6. The experimental feed rates of all components are summarized below, in Table 7.

Table 7 - Summary of flow rates utilized in this section based on resin feed rate.

Feed Rate (kg/hr)	Feed Rate (g/min)	DF2A1 [47wt%] (Z2) [mL/min]	Resin:Aqeuous Surfactant Ratio	Dispersion Zone Aqueous Content	DIW (Z6) [mL/min]
0.75	12.50	2.31	5.36	15.6%	26.10
1.00	16.67	3.08	5.36	15.6%	34.78
1.25	20.83	3.85	5.36	15.6%	43.46

4.2.6 Data Analysis and Processing

Minitab (Minitab 16 Statistical Software (2010), Minitab, Inc.) was used for regression of the measured particle size data against the operating condition factors of screw speed and feed rate.

4.3 Results and Discussion

Fifteen operating conditions were evaluated spanning the range of 100 - 300 RPM and 0.75-1.25 kg/hr with generally four samples being collected at each condition ranging. Two of the experimental conditions were sampled more intensely collecting 10 and 8 samples, respectively, as they were taken following the start-up of the extruder and un-steady state variations in torque and dispersion zone pressure were noted. The result was a total of 70 particle size measurements throughout the study. The reason some conditions were sampling more than 4 times was due to perceived process instability indicated in Figure 37 (top) by the variation shown in the boxplot summary of the D50 particle size for the samples as a function of screw speed and grouped by feed rate. For comparison, Figure 37 (bottom) shows the same data but with D50 particle size as a function of feed rate and grouped by screw speed. A contour plot is shown Figure 40 illustrating that the combination of low screw speeds and feed rates produced the smallest particle sizes.

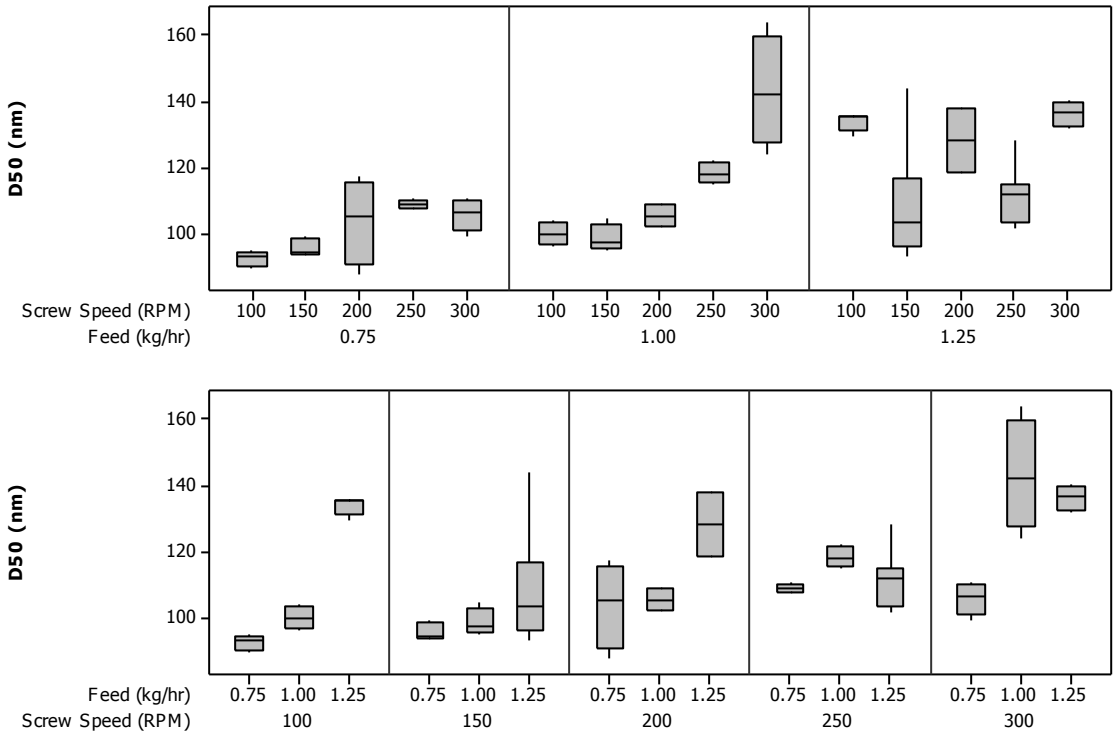

Figure 37 - Boxplot summary of D50 (nm) particle size for each operating point as a function of screw speed and grouped by feed rate (top) and feed rate grouped by screw speed (bottom).

The median values of the cumulative distribution are overlaid below, in Figure 38 and Figure 39, sorted by screw speed and feed rate, respectively.

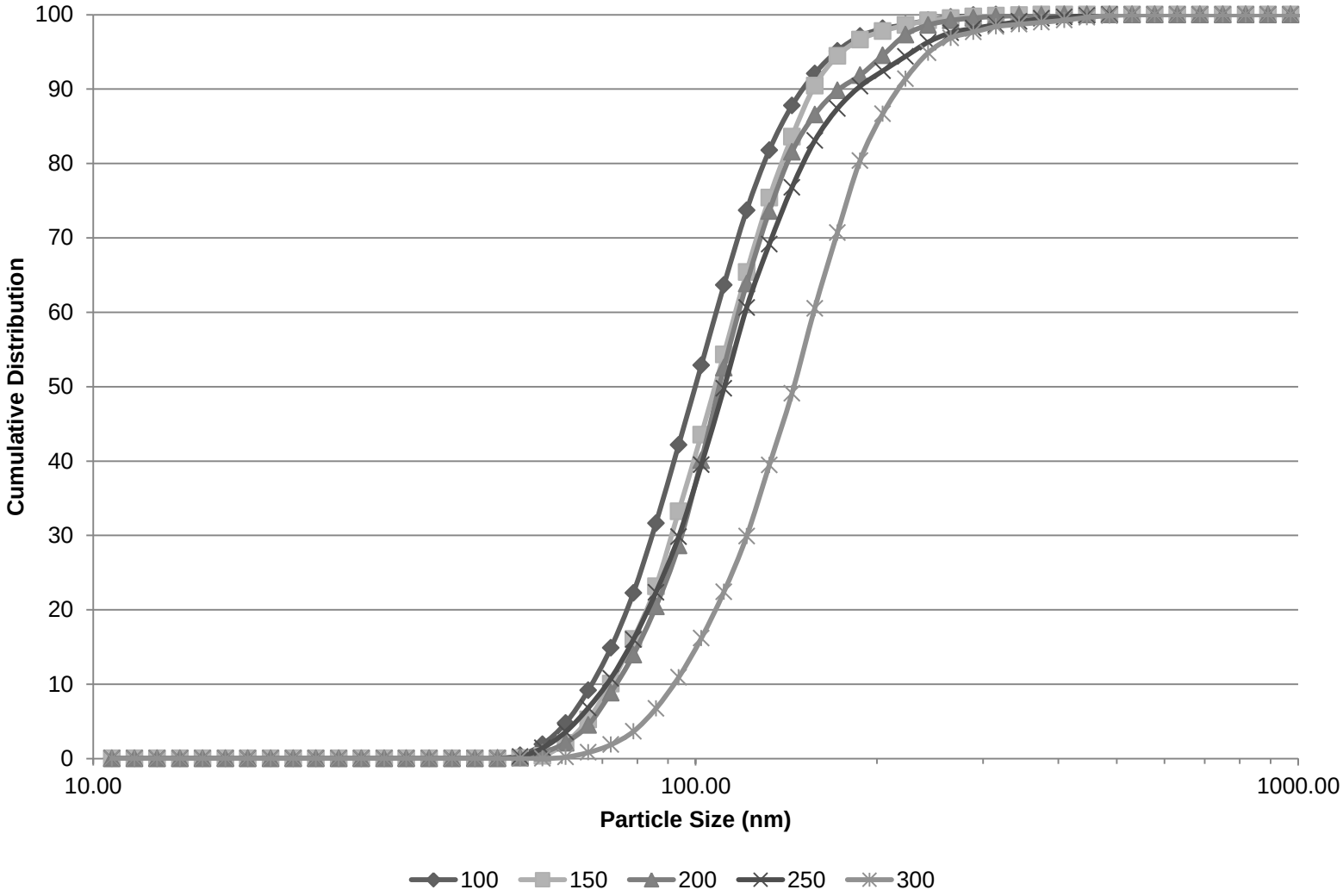

Figure 38 – Median cumulative particle size distribution sorted by screw speed (RPM).

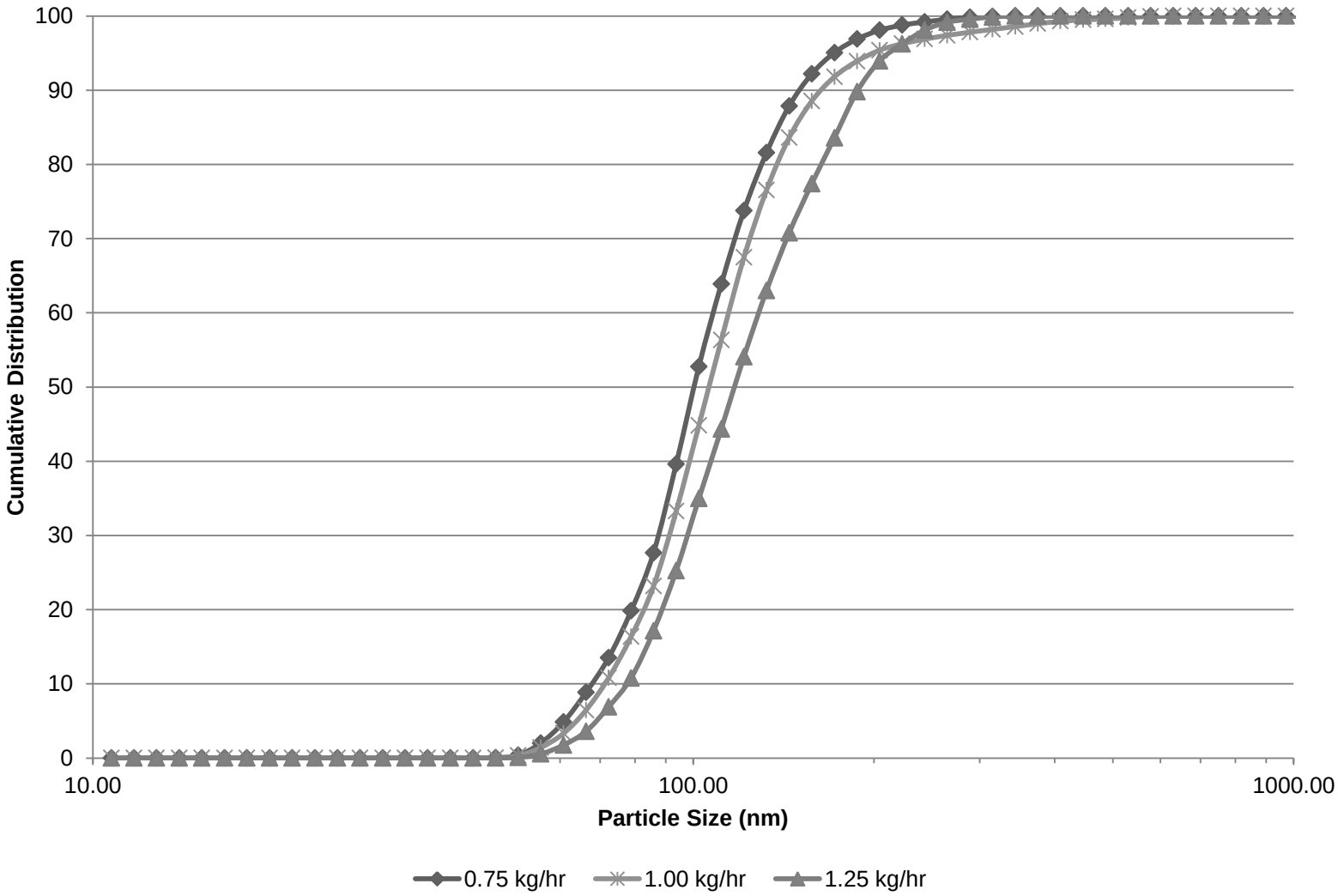

Figure 39 - Median cumulative particle size distribution sorted by feed rate (kg/hr).

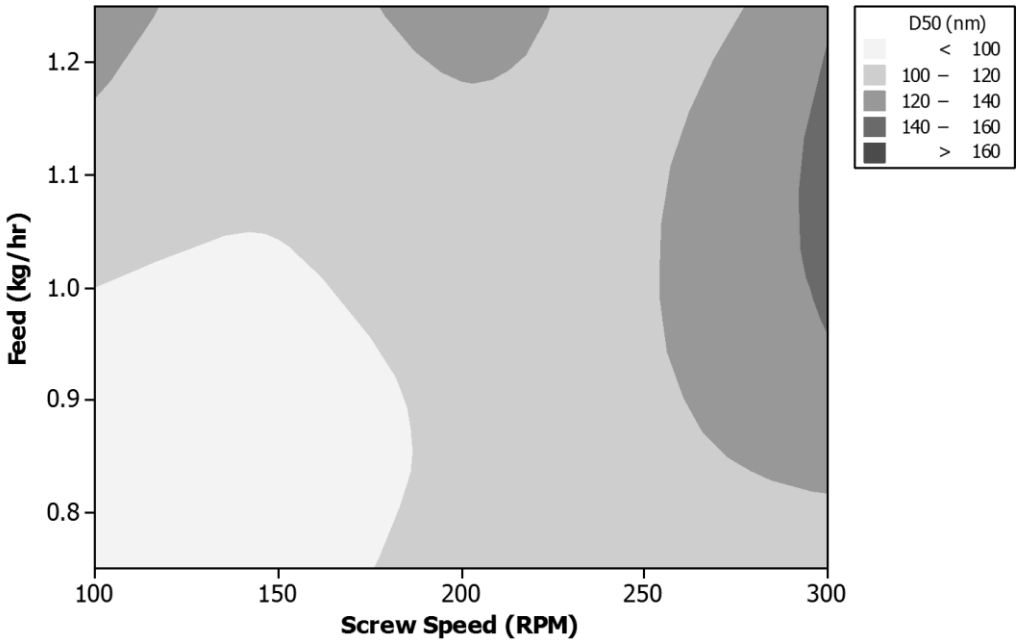

Figure 40 -Contour plot of D50 (nm) particle size as a function of screw speed (RPM) and resin feed rate (kg/hr).

The D50 particle size appears to be positively correlated with both screw speed and resin feed rate, as shown below in Figure 41 and Figure 42, respectively. It is an interesting observation that higher levels of shear rate lead to larger particle sizes. This relationship contrasts the mechanism of direct emulsification where the mean particle size is inversely proportional to the mechanical energy input into the system [42, 43]. The D50 particle size is also positively correlated with resin feed rate which determines the residence time distribution in the system. This relationship is more similar to phase inversion mechanisms in which there is a time-dependency attributed to morphology evolution of the minor aqueous phase dispersion through elongational mixing, prior to inversion by dilution.

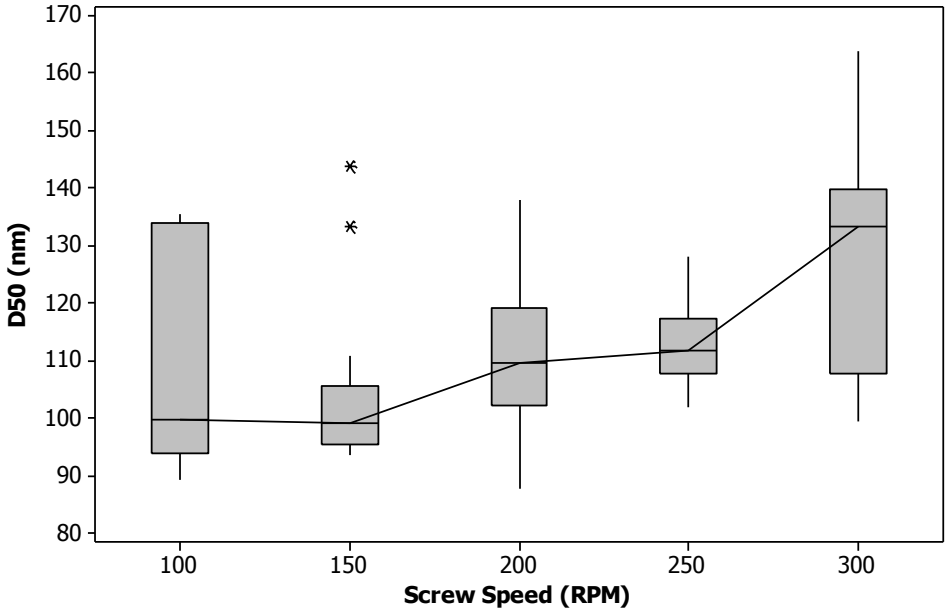

Figure 41 - Boxplot of the D50 particle size data showing a positive correlation between screw speed and D50 particle size.

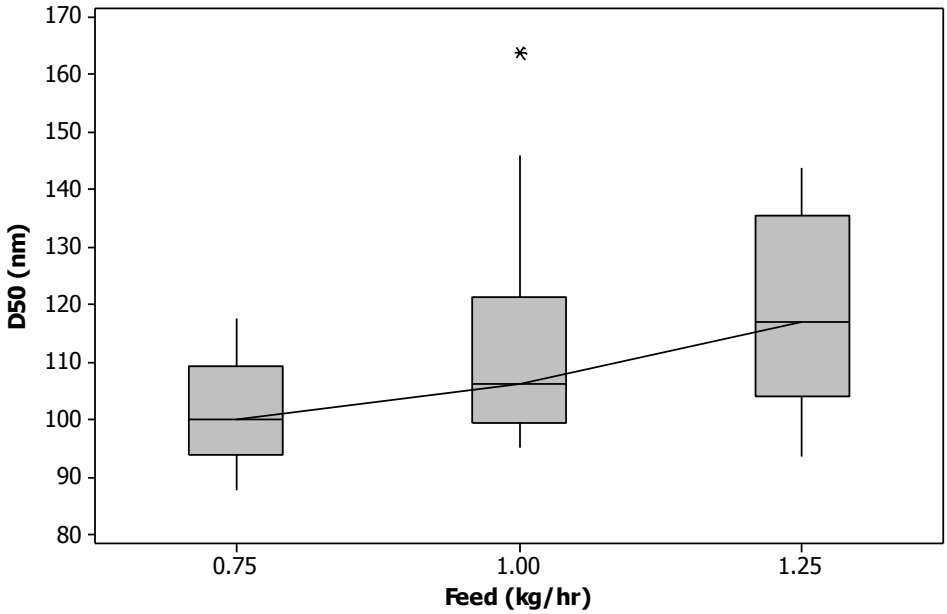

Figure 42 - Boxplot of the D50 particle size data showing a positive correlation between feed rate and D50 particle size.

An analogy to the SFE process would be for the water in a batch to be added as usual up to a point less than the critical PIP value then stopping the addition for some amount of time before adding the rest (dilution). The critical volume fraction for phase inversion has been semi-empirically modeled at length in the literature for both polymer-polymer systems and polymer-water systems, notable examples include Utracki [44], Willemse et al. [45], Avgeropoulos et al. [46], Metelkin and Blight [47], Jordhamo et al. [48], and Miles and Zurek [49], though many more exist. The important distinction to the system studied here is that, based on results shown in the next chapter, the volume fraction of water prior to dilution is below the critical phase inversion value yet above the critical co-continuous fraction. This means that the pre-inversion bicontinuous morphology develops at dispersed phase volumes below the critical values for inversion and may continue to develop until the dilution zone. This is significant with respect to the influence of feed rate as it directly influences the time at which the dispersed zone bicontinuous morphology can develop prior to dilution and inversion. The results of this study seem to show that longer dispersion times of the initial W/O emulsion of the dispersion zone lead to smaller particle sizes.

The positive correlation between resin feed rate and particle size is in good agreement with data based on the phase inversion of both polymer blends and aqueous emulsions. Charoensirisomboona et al. [50, 51] studied the emulsification of reactive polysulfone/polyamide blends through phase inversion and found the size of the discrete phase after inversion was reduced as a

function of mixing time to an asymptotic value define by emulsifier concentration. The same authors also found that preparation of a phase inversion within a mini twin-screw extruder (16mm) produced finer particle sizes than batch mixers [52]. Chuai et al. [53] studied the phase inversion of a polystyrene/poly(methyl methacrylate) (PS/PMMA) system and found that longer mixing times produced finer bicontinuous microstructures. In addition, they also noted that the range of volume fractions of PMMA in which phase co-continuity can exist, shrinks as a function of mixing time.

Regarding the interaction of screw speed and resin feed rate – the previous chapter showed that the screw speed had a negligible impact on residence time. This means that the effect of screw speed can be viewed as strictly a mechanical influence and not a temporal one. In polymer blending, droplet coalescence of the dispersed phase is based upon collision frequency which scales with shear rate [54]. Based on particle volume, the coalescence of two 100 nm droplets would lead to a single droplet having a diameter of approximately 125 nm. This means that the size increase due to coalescence of discrete latex particles would also be on a similar order as the span in D50 observed as a function of screw speed. Due to the relatively high surfactant loadings (low interfacial tension) and high melt viscosity of the resin, droplet coalescence of discrete latex particles should be largely suppressed however [50, 54]. Moreover, the primary mechanism of aggregation for the size range of latex produced is perikinetic flocculation, which is independent of shear [55]. That

is not to say that coalescence of the initial W/O dispersion does not occur. It is possible that there is coalescence of the water domains, due to the shear flows at higher screw speeds, that slows the reduction in domain size from affine deformation prior to co-continuity [6].

The increase in particle size with increasing shear rate is consistent with the findings by Li and Sundararaj [56] who studied the evolution in morphology during phase inversion for both compatibilized and un-compatibilized polymer blend systems in a twin screw extruder. The authors showed that the dispersed domain size distribution at the end of the extruder was higher at higher screw speeds and the difference was more pronounced for un-compatibilized blends. For both cases, using a sliding barrel extruder, the authors found that the morphology evolved along the length of the extruder and that the lower screw speed produced a faster evolution. This was attributed to a high degree of interfacial slip with the higher shear stresses from high screw speeds. The compatibilization between phases is thought to reduce the magnitude of the interfacial slip and hence provide a less pronounced sensitivity to shear stress. If this relationship were to apply to the current phase inversion system then perhaps the higher screw speed led to increased interfacial slip between the polymer and aqueous domains. This slip would delay the development of the water dispersion prior to inversion and hence coarsen the morphology of the pre-inversion mixture.

The increased screw speed will also have an influence on the viscosity of the system due to shear thinning behaviour. Niedzwiedz et al. [57] also showed that concentrated W/O emulsions show extensional shear thinning behaviour. The authors utilized capillary breakup elongational rheology (CaBER) to probe the elongational flow behaviour of a W/O emulsion having a Newtonian continuous oil. It was shown that shear thinning behaviour becomes prevalent above a critical dispersed phase volume fraction. In addition, the authors noted yield-stress behaviour at high dispersed phase fractions which was described by a Herschel-Bulkey model. The yield stress was correlated with the Lapalce pressure of the dispersed aqueous phase but no mention was made as to the possible cause of the shear-thinning behaviour observed. It is likely that this non-Newtonian response is due to the hydrogen bonding at the interface. This bonding would provide a sort of weak-entanglement at the interface, similar to the chain entanglement for which the shear-thinning behaviour arises in polymers. Although the dispersed phase concentration in the dispersion zone is much lower than the work by Niedzwiedz, the deformation is much higher in the current system which would greatly increase the interfacial area, similar to a concentrated static W/O emulsion. If the material in the dispersion zone did in fact exhibit shear-thinning behaviour, then the increased screw speeds (shear rate) would presumably reduce the capillary number and hence lead to larger water domains.

The viscosity of the polymer phase is known to be dependent upon both temperature and shear rate within the system. The screw speed has a known influence on the shear rate within the system with higher screw speeds yielding higher shear rates. The screw speed also relates to the heat generated through viscous dissipation, thereby also influencing the temperature of the melt and further reducing the viscosity of the polymer [58]. The sum of these two influences is that increasing screw speed both decreases viscosity and increases temperature. Sarazin and Favis [59] showed that increased temperatures during the blending of a poly(caprolactone)/Polystyrene system led to larger domain sizes in the bicontinuous state compared to lower temperatures. The impact of temperature upon the morphology evolution and microstructure within the dispersion zone will be discussed in chapter 5.

The screw speed will also then affect the viscosity ratio between the dispersed and continuous phases. The viscosity ratio of the system during the initial dispersion of water into the resin (W/O emulsion) has the polymer viscosity in the denominator. This means that as the viscosity of the polymer is reduced – by temperature and shear – the viscosity ratio increases as the water will be largely unaffected. Favis and Therrien showed that the domain size of a minor polycarbonate phase, prior to phase inversion in a polypropylene matrix, increased as a function of viscosity ratio [60]. In this system, decreasing the matrix viscosity also decreases the capillary number during the dispersion of

water into polymer which would limit the minimum domain size the aqueous phase could reach prior to phase inversion.

There was a marked increase in sample variance at the extremes of screw speed indicating a potential unsteady operation of the extruder. There was also a pronounced increase in the interquartile range of D90/D10 for samples taken after start up, as shown in Figure 43. The variable ‘set order’ corresponds to the order in which the operating conditions were carried out. As discussed in the experimental section above, all experimental sets were given the same 20 minutes to reach steady state after a change in operating conditions. The median value for D90/D10 after start-up was also somewhat higher than subsequent, non-start-up values. This indicates that the start-up procedure had likely not yielded a steady-state operation within the extruder for the initial subsequent experiments.

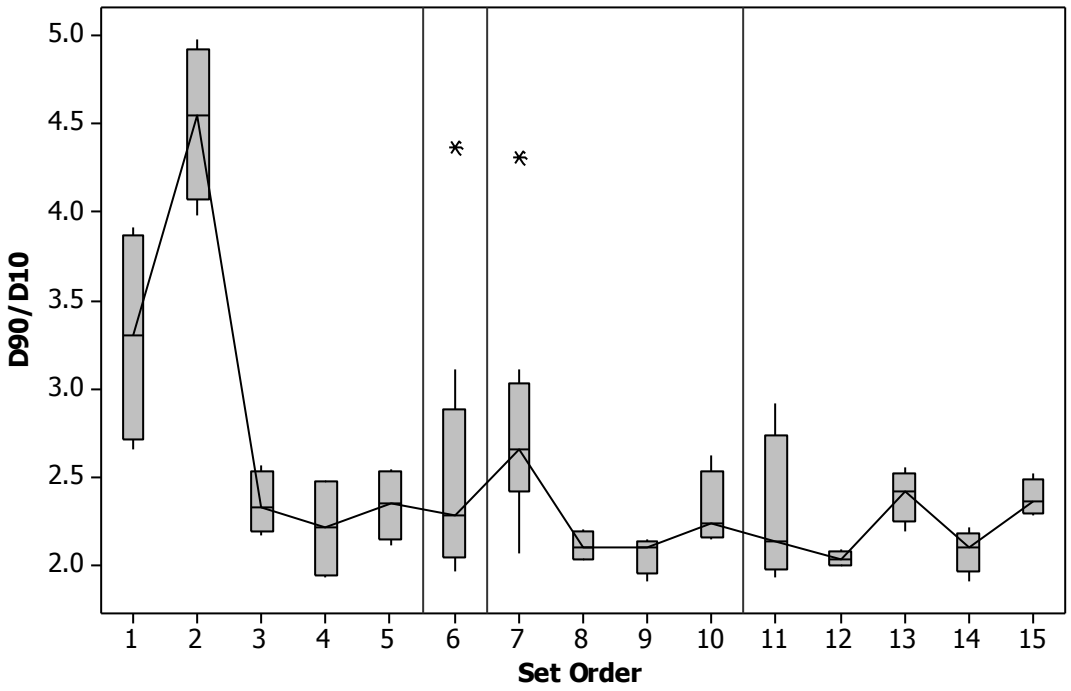

Figure 43- Boxplot of D90/D10 at each operating point as a function of set order of experiment; extruder start-up times shown as vertical reference lines in plot between experiments. Asterisks denote outliers.

The width of the particle size distribution, as characterized by the ratio of the 90th percentile and 10th percentile (D90/D10) shows a weak positive correlation to screw speed. The interquartile range of the samples taken at 300 RPM is much larger than at lower screw speeds. This effect appears to be real as samples carried out at 300 RPM never followed directly after start up. The median values of D90/D10 vary little throughout the data set. Only 6 samples out of 70 produced bimodal particle size distributions and half of them were produced at 300 RPM and a feed rate of 1 kg/hr, corresponding to set order '2' in Figure 43. The effect upon the particle size distribution can be clearly seen in Figure 44,

below, where the interquartile range of D90/D10 is the largest at 300 RPM. The D90/D10 interquartile range is smallest for the lowest screw speed of 100 RPM.

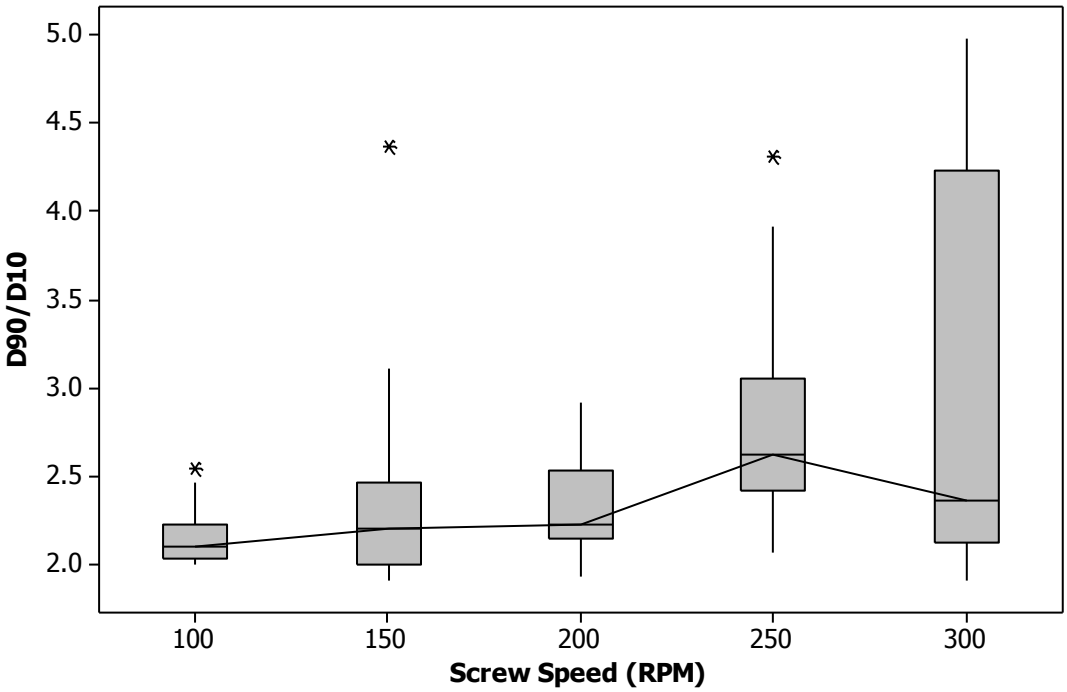

Figure 44- Boxplot of D90/D10 as a function of screw speed indicating increased levels of coarse particles at high screw speeds; asterisk denotes outliers.

Figure 45 shows the relationship between feed rate and D90/D10 within the second experiment condition where the screw speed was increased to 300 RPM (set order '2' by run-order) following the first experiment (set order '1') where the screw speed was 250 RPM. This bimodal particle size upon the increase in screw speed between the first and second experiments will have a significant impact on the interquartile range for a feed rate of 1 kg/hr. The median value of D90/D10 is also highest for the feed rate of 1 kg/hr. This is believed to be mainly an artifact of the start-up instability which occurred in the first data set (set

order 1-5, feed = 1 kg/hr) shown in Figure 43. Moreover, this sample was operated at the highest screw speed level (300 RPM), higher than the screw speed utilized during start-up (250 RPM), which may have loosened material adhered to the screw. Three out of four samples within the set order '2' experiment produced a bimodal particle size distribution. Figure 46 shows the effect of sample order (order within operating condition set) after the operating condition was changed to 300 RPM upon the relative volume fractions of the bimodal peaks. There is clearly an artifact of improper start-up procedures as the extruder was started at the screw speed corresponding to the first operating condition (250 RPM, set order '1').

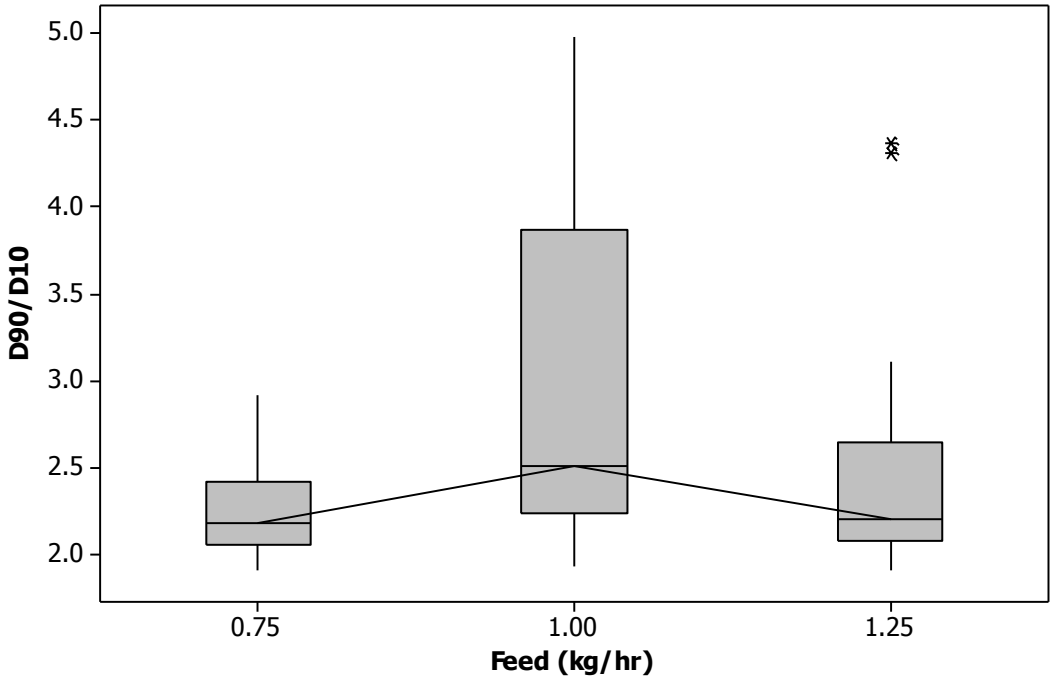

Figure 45 – Boxplot of D90/D10 as a function of feed rate indicating no real dependence on coarse particle generation.

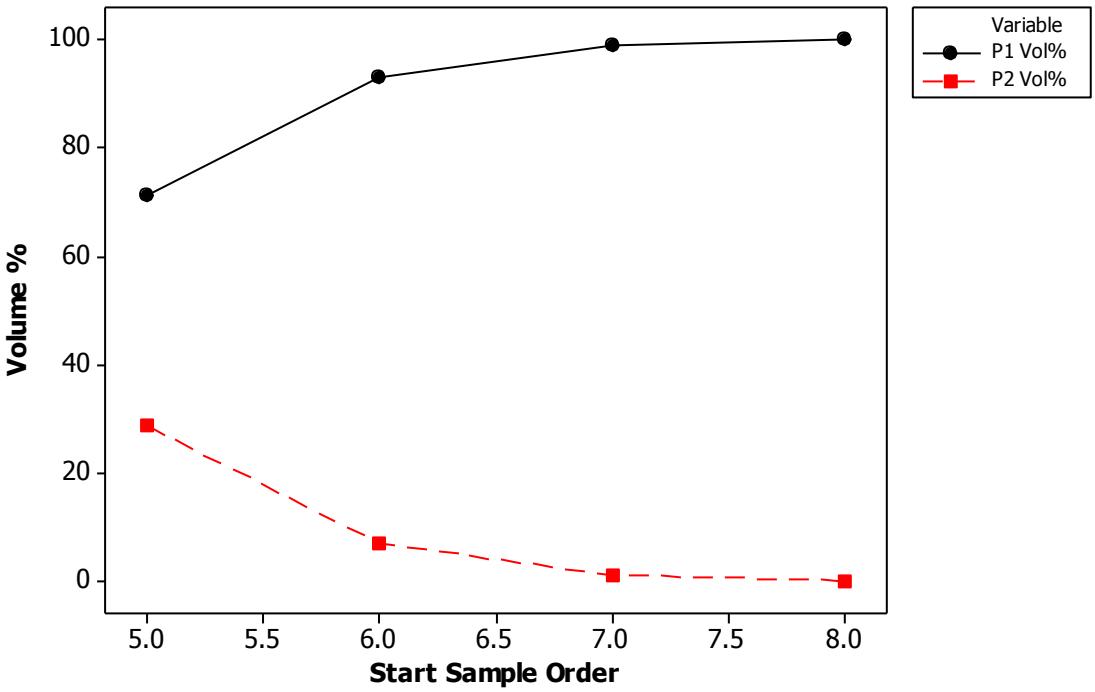

Figure 46 - Relative size of bimodal peaks as a function of order after changing operating condition.

4.4 Summary and Conclusion

A two factor, multi-level experimental design was carried out to analyze the response of particle size from screw speed and feed rate. The smallest particle sizes were found to be obtained at combination of lowest screw speed and throughput rate. In addition, the largest particle sizes were found to occur at the highest feed rates and screw speeds.

The D50 particle size was found to be positively correlated with both screw speed and feed rate. The relationship between feed rate and particle size is

largely believed to be due to the time-dependent evolution in morphology of the water phase and polymer within the dispersion zone. This behaviour could potentially be exploited as a process control output to vary the particle size based on product requirements. The D50 particle size was also found to be positively correlated with screw speed, which was somewhat counterintuitive in that higher shear rates yielded larger particles. The most likely explanation for this is shear induced coalescence of water domains prior to phase inversion. This overall rate of water domain size reduction (prior to phase inversion) is then believed to be a balance between affine deformation (size reduction) and domain coalescence (size increase). The potential effects of screw speed on temperature and viscosity were also discussed as possible contributions to increased particle size.

Repeated sampling at each operating condition yielded information about process stability. It was found that operating conditions which were carried out after start-up of the extruder showed a larger breadth of distribution in particle size quantified by D90/D10 as well as coarse particle generation. It was concluded that the start-up procedure was non-optimal and that longer times and higher screw speeds are required in order to reach steady state in this dynamic process.

Potential future work should include the following experiments:

1. Different resin-to-water ratios (water volume fractions) to understand the mechanism of the increase in particle size with screw speed. If a

coalescence mechanism is the cause of this relationship, higher water volume fractions should increase the shear-dependent coalescence prior to inversion and validate this theory.

2. Different surfactant concentrations and longer residence times to understand the mechanism of particle size decrease with increasing residence time. If there exists an asymptotic response in bicontinuous domain size as a function of mixing time prior to inversion, this should become prevalent at longer residence times. In addition, varying the surfactant concentration should shift the asymptotic value of the minimum microstructure size prior to inversion resulting in a finer particle size after phase inversion with increased surfactant.
3. Different dispersion zone temperatures to vary the viscosity ratio between the dispersed water phase and continuous polymer phase prior to inversion. This will allow for quantitative modeling of the influence of viscosity ratio upon the time dependent size reduction of the bicontinuous matrix prior to inversion. This will also allow for comparison to the wealth of data for polymer-polymer systems and help extend the understanding of the influence of viscosity ratio upon phase inversion at values $<<1$.
4. Coupling the residence time method described in the previous chapter to quantify the effects of (1), (2), and (3) to build a quantitative semi-empirical model of phase inversion.

CHAPTER 5 – SEM MORPHOLOGY STUDY

5.1 Objective and Scope

The purpose of this chapter was to evaluate the morphology of poorly-emulsified and pre-emulsifed resin. These ‘failure-mode’ materials are of specific interest as they yield insight to the physical mechanism of phase inversion as successful emulsification yields only uniform latex particles. This study was done to test the hypothesis put forth that the mechanism of latex formation was a phase-inversion type of emulsification. That phase inversion mechanism would first exist as water dispersed into the resin (or ‘oil’ phase) before forming a bi-continuous W-O phase and subsequently inverting to form an oil-in-water emulsion.

The hypothesized progression of morphology is as follows: (1) the water is injected into the extruder and is mixed to the macroscale level within the molten resin (W+O); (2) the water is further mixed to the microscale into the resin and discrete water domains are formed within the continuous resin phase (W/O); (3) the water domains begin to coalesce forming a bi-continuous morphology where both the resin and water phases extend out and no discrete phase is present (O-W); (4) the resin phase forms discrete domains within a continuous water phase (O/W).

To evaluate the proposed mechanism, two material sets were characterized by scanning electron microscope (SEM). First, poorly-emulsified material was prepared at temperatures and surfactant concentrations which yield poor emulsions. These ‘poor-emulsions’ typically have large amounts of coarse particles and a significant portion of the resin remains unemulsified. The resin-to-water ratio was varied over a range with two different dispersion-zone temperature profiles. The resin-to-water ratio is believed to affect the viscosity, temperature, and has already been shown to affect the residence time of the pre-dispersed material in the extruder. The temperature will affect the viscosity of the resin and hence should alter the mixing behaviour of the two phases. Second, the morphology of pre-dispersed material (i.e. undiluted, non-emulsified) was analyzed. This material was prepared without dilution as to analyze the morphology of the material within the dispersion zone of the extruder.

The scope of this chapter is limited to a single surfactant and NaOH concentration. The results in this chapter are by no means a definitive description of the solvent-free emulsification mechanism; instead they are simply a glimpse into the potential morphologies that may exist in the pre-dispersed state. Due to the nature of the SEM microscopy and the limited sampling possible within an extruder, the results will be discussed in mostly qualitative fashion with some references to the quantitative measurement of specific features commonly present in the images such as pore size. The location of the phase inversion will

also be evaluated in order to determine whether the latex particles are formed within the dispersion zone or in the dilution zone.

5.2 Experimental

5.2.1 Scanning Electron Microscopy

Images were analyzed using a Hitachi SU8000 scanning electron microscope (SEM). For all samples presented, the accelerating voltage utilized was 2.0 kV. Samples were prepared by drying the extrudate samples out in a fume hood before mounting on a stage and sputter coated with platinum/palladium. The samples from the extruder were diluted by a factor of approximately 100:1 prior to drying during sample preparation.

5.2.2 Image Analysis

Fiji (Is Just ImageJ) was used for image processing and analysis of morphological features which is based on *ImageJ* image processing program (v1.47t, National Institutes of Health, USA) [61]. The *Anisotropic Diffusion 2D* plugin was used to reduce noise in the SEM images using an algorithm based on Perona-Malik diffusion [62, 63]. The Enhance Local Contrast (CLAHE) plugin was used to increase the contrast of the SEM images using a contrast limited adaptive histogram equalization method [64, 65].

5.2.3 Experimental Setup

The same equipment was used in this chapter as described in section 3.3.2. For reference, a schematic layout of the locations of solids feed (*Z0*), and deionized water injection (*Z2*, *Z6*) is given, below, in Figure 47. The zone 2 DIW injection stream was first past through a heated bath using a stainless steel coil for heat transfer before flowing into the injection nozzle mounted on the extruder. The bath temperature was set at 140°C

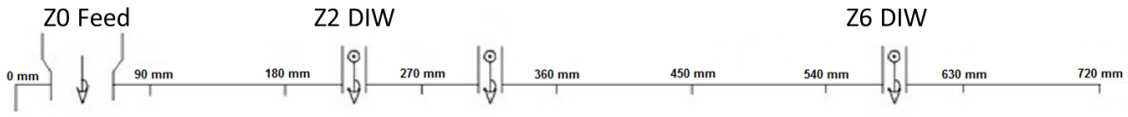

Figure 47 - Schematic layout of injection ports for SEM morphology study varying the resin-to-water ratio for two different temperature profiles.

5.2.4 Materials

The same materials as presented in section 3.3.2 were used.

5.2.5 Experimental Operating Conditions

Three data sets were evaluated to determine the morphology of un-dispersed resin in the solvent free emulsification process. The resin-to-water ratio was varied through several levels to qualitatively determine the influence of water volume fraction upon the resulting morphology. The first two data sets were evaluated at very high zone 6 injection rates in order to quench the morphology developed within the dispersion zone between zone 2 and zone 6. Samples were collected in a similar manner as presented in Chapters 3 and 4. The extruder was

allowed to reach steady state upon start-up at the initial operating condition. In between operating conditions 10 minutes was allowed for the system to fully transition to the new set point before sampling. Ten minutes was chosen based on the length of the tail section in the RTD curve presented in chapter 3 for this feed rate of 1.25 kg/hr.

The first data set was carried out at an elevated temperature profile, when compared to the profile used in Chapters 3 and 4. Moreover, the surfactant concentration was reduced and the sodium hydroxide concentration was increased to further promote the formation of poorly-emulsified material. The composition of the dry feed rate for the three data sets is presented below, in Table 8.

Table 8 - Composition of dry feed rate for the data sets 031A, 036A, 037A/B.

Feed	Parts	Percent of Dry Feed	Total (g/min)
Resin	100	90.21%	18.79
NaOH	1	0.90%	0.19
SDBS	7.5	6.77%	1.41
Total	108.5	97.88%	20.83

The experimental operating conditions for the first of the two data sets which utilized high injection rates at zone 6 to quench the dispersed zone morphology is shown below, in Table 9 (031A). The temperature profile of the 031A data set was much higher than what is typically used to prepare latex in the solvent free emulsification process. This high temperature leads to poorly-

emulsified latex wherein only a portion of the polymer is fully emulsified and the rest is formed of large particles which quickly settle out (micron to millimeter scale). The 036A data set utilizes lower temperatures which also facilitate the production of poorly-emulsified material. These 'failure-mode' materials are of interest because within the samples there is a gradient of morphologies of emulsification which is frozen upon diluted the matrix with large amounts of water in zone 6. These morphologies are those which yield good emulsions to those which yield coarse particles. The temperature profile is detailed in Table 12.

Table 9 - Experimental operating conditions studied with an extruder temperature profile of 160°C-165°C-135°C-135°C-135°C-95°C-95°C-95°C and 300 RPM.

Expt.	Feed Rate (g/min)	DIW (Z2) [mL/min]	Resin:Water	Dispersion Zone Water Content	DIW (Z6) [mL/min]
031A1	20.83	2.5	7.68	10.7%	62.5
031A4	20.83	3.5	5.49	14.4%	62.5
031A5	20.83	4	4.80	16.1%	62.5
031A6	20.83	4.5	4.27	17.8%	62.5
031A7	20.83	5	3.84	19.4%	62.5
031A8	20.83	5.5	3.49	20.9%	62.5

The experimental operating conditions for the second of the two data sets which utilized high zone 6 injection rates to quench the dispersed zone morphology is shown below, in Table 11 (036A). The temperature profile of the 036A data set was only by slightly higher than what is typically used to prepare latex in the solvent free emulsification process in order to subdue latex generation. The temperature profile is detailed in Table 12.

Table 10 - Experimental operating conditions studied with an extruder temperature profile of 160°C-160°C-115°C-115°C-115°C-95°C-95°C-95°C and 300 RPM.

Expt.	Feed Rate (g/min)	DIW (Z2) [mL/min]	Resin:Water	Dispersion Zone Water Content	DIW (Z6) [mL/min]
036A1	20.83	2.5	7.68	10.7%	62.5
036A2	20.83	3.5	5.49	14.4%	62.5
036A3	20.83	4	4.80	16.1%	62.5
036A4	20.83	4.5	4.27	17.8%	62.5
036A5	20.83	5	3.84	19.4%	62.5
036A6	20.83	5.5	3.49	20.9%	62.5

The experimental operating conditions for the last data set which utilized no zone 6 injection of DIW is shown below, in Table 11. The temperature profile of the 037 data set was varied by slightly and is detailed in Table 12.

The temperature was varied in this way to determine the relative impact on morphology of the resulting pre-dispersed latex. The temperatures are higher than those utilized in Chapters 3 and 4, most notably with higher temperatures in zones in the latter half of the extruder to compensate for the increased viscosity of the mixture in the absence of dilution water injection.

Table 11 - Experimental operating conditions studied without zone 6 dilution to determine morphology of pre-dispersed resin-water matrix.

Expt.	Feed Rate (g/min)	DIW (Z2) [mL/min]	Resin:Water	DIW (Z6) [mL/min]
037A1	20.83	4	4.80	0
037B	20.83	4	4.80	0

Table 12 - Zonal temperature profiles for data sets detailed in Table 9, Table 10, and Table 11 for the study of morphology by scanning electron microscopy.

	Zonal Temperatures (°C)							
Experiment Set	**1**	**2**	**3**	**4**	**5**	**6**	**7**	**Die**
031A*	160	165	135	135	135	95	95	95
036A*	160	160	115	115	115	95	95	95
037A1	160	165	135	125	115	115	115	100
037B	160	165	135	115	115	105	105	100

5.2.6 Sample Collection

It should be noted that the quality of dispersions produced in this chapter were purposely of very low quality, i.e. greater than 50% coarse fraction, as to study the intermediate stages during emulsification. No effort was made to quantify the particle size or coarse content in the samples collected as the size of particulates within the extruder ranged from several nanometers to several millimetres. Samples were collected in 4 dram vials at the die face and the entirety of the extrudate sample was obtained ranging from flowable emulsions to suspensions of coarse particulates with sizes on the order of millimeters. By collecting the un-diluted samples at the die face, it should be understood that this effectively increases the length of the dispersion zone by 2 barrel sections which increases the residence time within the dispersion zone.

5.3 Results and Discussion

Evidence of a phase inversion mechanism was found and is discussed below. The basis of this conclusion is the presence of morphologies which are indicative of both a water-in-resin dispersion, where the water forms the discrete phase within the resin, as well as a bi-continuous matrix wherein both the water and resin constitute the continuous phase. Conceptually, it is put forth that upon the injection of the DIW into zone 2 the water is first dispersed into the resin phase. The surfactant, being dry-blended with the resin feed, would presumably at this point be dispersed throughout the resin. In this way, it would serve to allow for easier incorporation of the aqueous phase into the resin by lowering the interfacial tension between the presently hydrophobic resin phase and water. The sodium hydroxide, also being dry-blended with the resin feed, should also be dispersed throughout the resin at this point. The neutralization of the terminal acid groups can be thought of as a type of reactive compatibilization within the extruder. This dispersion of base throughout the resin should allow for deprotonation of the terminal carboxyl groups on the polymer chains once in contact with the water. The hygroscopic nature of powdered sodium hydroxide does not preclude the possibility of sufficiently high adsorbed moisture content in the dry feed to allow for dissociation of the hydroxyl group within the polymer melt prior to the injection of the aqueous phase. Presumably, if the hydroxyl group dissociates within the polymer melt prior to addition of surfactant it is expected that significant hydrolysis of the resin would occur [66]. The influence of the

aqueous media on the resulting molecular weight of the polymer is; however, beyond the scope of this study.

The dispersion of the aqueous phase in the polymer melt with the aide of surfactant, followed by neutralization of the terminal acid groups with sodium hydroxide, should lead to a very low interfacial tension. Due to the dynamic nature of the interface and the high temperature, no offline measurements were made to quantify the interfacial tension.

5.3.1 High Temperature Dispersion Zone

The 031A data set was operated at a relatively high zonal temperature profile and hence the resin would be expected to have a lower viscosity than at lower temperatures. This higher temperature would then have a direct effect on the viscosity ratio between the water and resin.

Qualitatively, a clear transition in resin morphology upon the increase of water content within the dispersion zone does not seem to exist. There are however, some specific features which are more prevalent at either high or low water contents. Figure 48 shows a set of SEM images of the sampled extrudate for 031A1, having a high R:W of 7.7:1 and a dispersion zone water content of 10.7%. The presence of highly elongated fibrils is evident; moreover, these fibrils seem to be stratified by water as well. This is shown in Figure 49 and highlighted with white arrows oriented roughly perpendicular to long axis of striation.

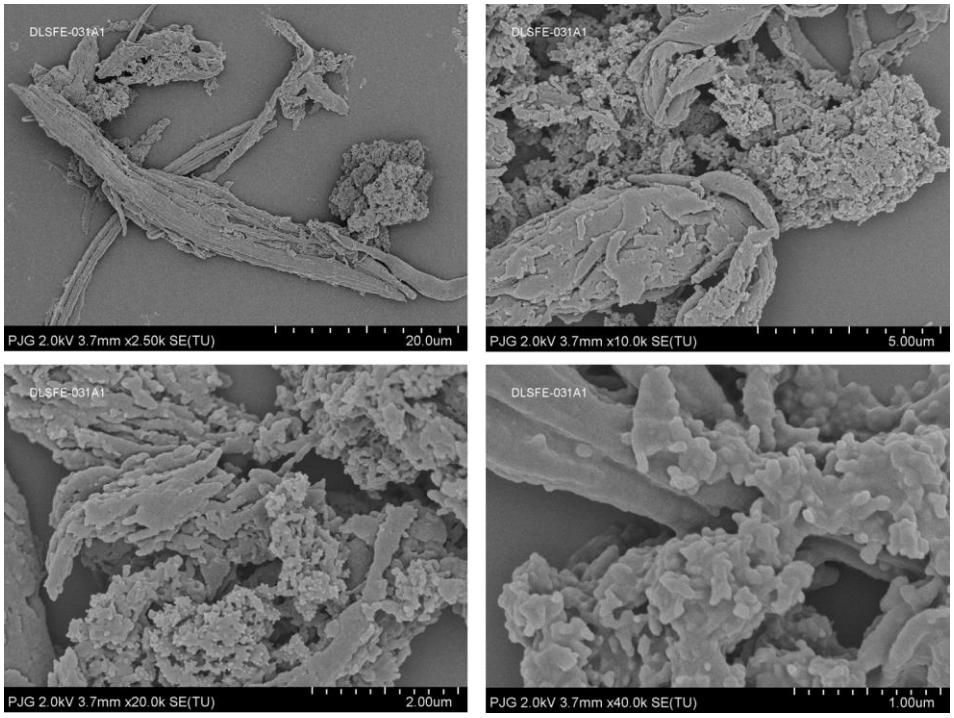

Figure 48 - SEM microscopy of sample 031A1 having a R:W of 7.7:1 and a corresponding dispersion zone water content of 10.7%.

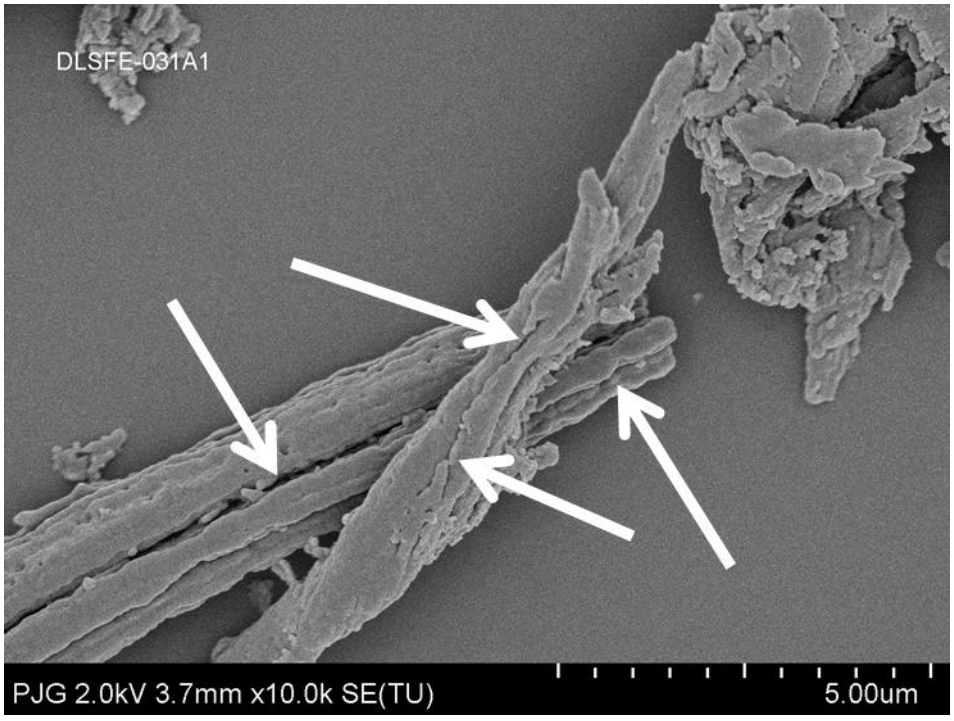

Figure 49 - Sample 031A1 with stratification of fibrils illustrated with white arrows.

This stratification of the fibrils by the striation of water is a sign of affine deformation during the incorporation of the aqueous phase within the polymer melt [67]. These fibrils would have been oriented in the shear field within the extruder and subjected to very high strain rates. Although the fibrils are separated in the SEM image in Figure 49, this separation was an intentional effect of the 100:1 dilution ration prior to drying. These fibrils would have existed in close packing with the rest of the resin phase observed in the various SEM images due to the overall low water content within the dispersion zone for this sample. The relatively high flow rate of water should have quenched and preserved most morphology from the dispersion zone, though it is difficult to determine dilution zone contributions (i.e. agglomeration and fragmentation). In section 5.5.3, two undiluted samples are presented which do not show this fibrillation or striated morphology indicating they are likely a result of dilution.

Figure 50, below, shows a separate region of sample 031A1 in a seemingly bicontinuous state wherein both the water phase and polymer phase extend through the matrix. The white arrows in Figure 50 point towards voids in the polyester matrix wherein it is assumed the water phase was located. The diameters of these voids range between 20-80nm and have non-uniform aspect ratios which is an indication of affine deformation.

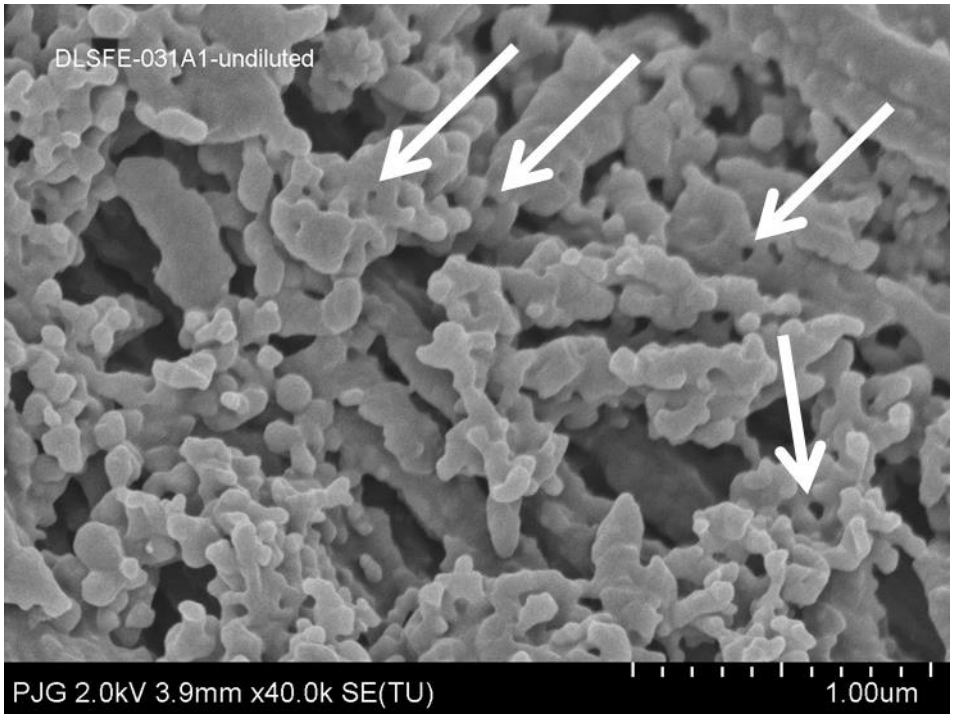

Figure 50 - Sample 031A1 with voids in polyester matrix illustrated with white arrows highlighting some of the voids for reference.

It is difficult to gauge the actual spacing between separated polyester nodules during dispersion at low water content since the quenching water would probably break up the a bicontinuous matrix into smaller pieces. This ‘nodular’ morphology could be interpreted as the retracted polymer struts which formed the bicontinuous matrix and were necked during dilution as the increase in water content increased phase separation.

Figure 51 shows a summary of the morphology observed upon moving to higher water injection rates with a R:W of 5.5 and a total dispersion zone water content of 14.4%. Overall, the morphology of 031A4 is similar to 031A1 except for a slight reduction in the appearance of fibrillated strands – though admittedly, the

nature of SEM microscopy makes for limited sampling of the entire population. Upon moving to higher water contents, the frequency of nano-scale striations seems to increase.

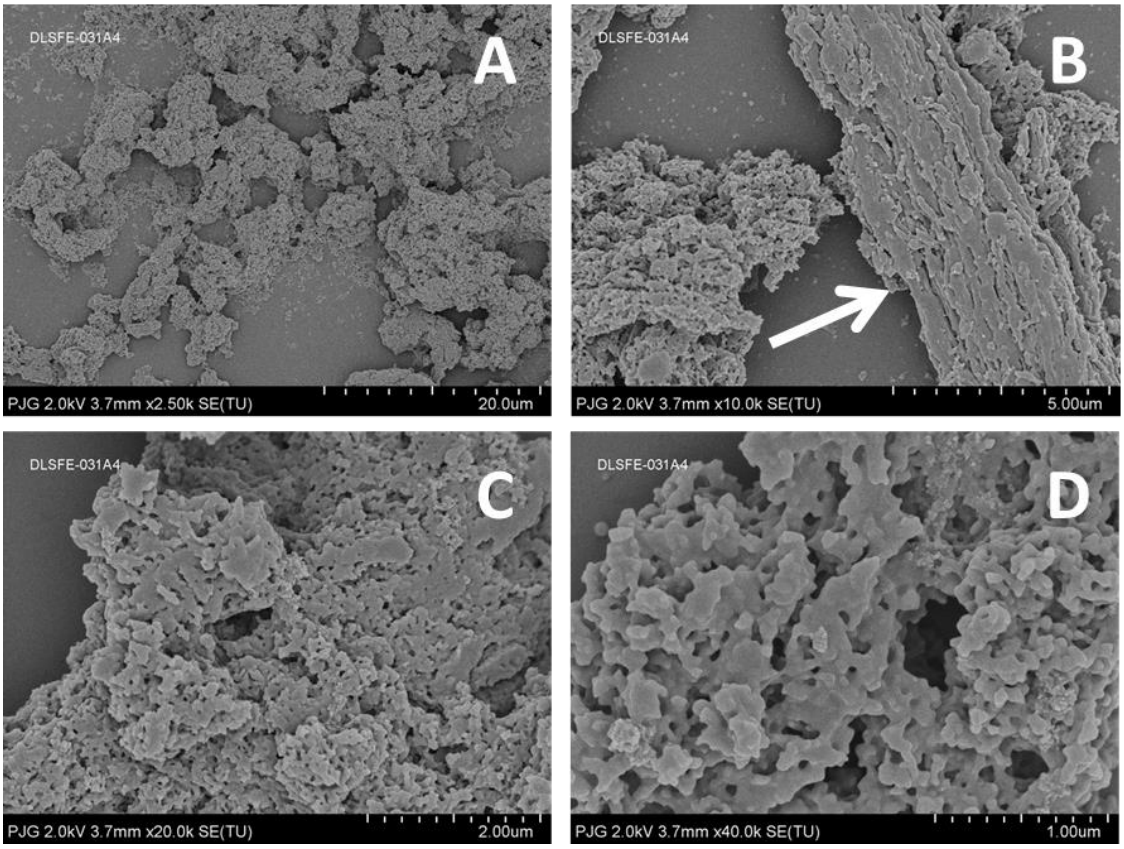

Figure 51 - SEM microscopy of sample 031A4 having a R:W of 5.5:1 and a corresponding dispersion zone water content of 14.4%.

Figure 51 (B) illustrates a macro-fibril, denoted by the white arrow, containing many aqueous derived-striations which are more prevalent than in sample 031A1. These striations seem to occur in two populations, nanometer scale and micron scale, in reference to their overall length. It is unclear whether these macro-scale fibrils are generated within the dilution zone or in the

dispersion zone. The relative size to the macro-fibrils would seemingly indicate they were formed in the dilution zone subsequent to the addition of large amounts of water. This increased water would reduce shear levels, from lubrication, leading to much larger-scale striations which would form these larger fibrils. Within the discrete macro-fibrils, many nano-scale striations exist which would seemingly have been formed at lower water volume fractions within the dispersion zone. These nano-striations appear to be the result of the affine deformation of the aqueous domains prior to dilution. Figure 52, below, shows Figure 51 (B) with increased contrast to enhance the definition of the nano-striations within the bulk macro-fibril, which is denoted by the white arrow.

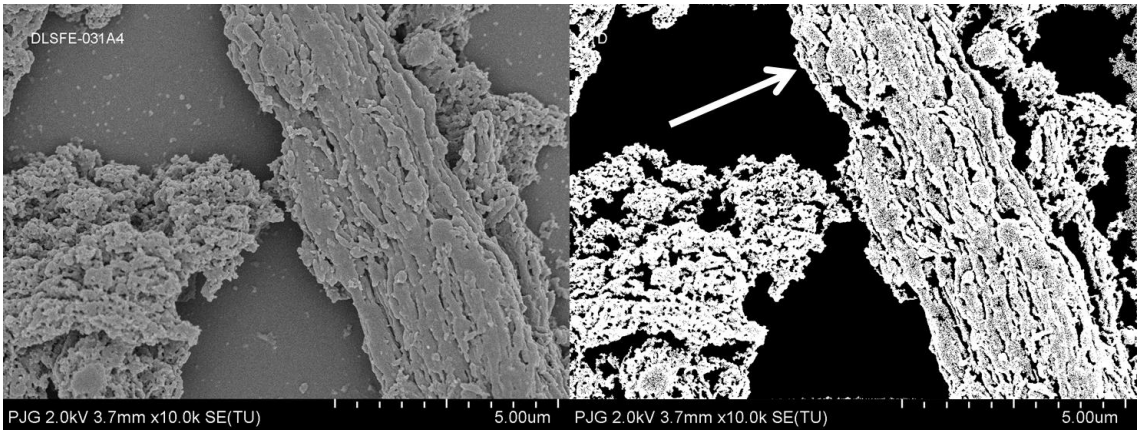

Figure 52 – Image from Figure 51 (B) shown larger (top) and then shown with increased contrast to enhance view of nano-striations within macro-fibril (arrow).

Figure 51 (B), above, includes another portion of the sample where the bi-continuous morphology as seen in 031A1, is evident. The size of the discrete water domains appear to be approximately the same magnitude as the voids found in 031A1 – they range in diameter from approximately 20-80nm. It should

be noted that these voids most likely represent only a cross-section of an interpenetrating water network throughout the polymer phase making their overall length difficult to determine. The size of the polymer nodules is also comparable to those observed in the bicontinuous matrix discussed above in 031A1.

Figure 53 below is a collection of images taken at different scales for the sample 031A5, having a R:W of 4.8:1 and a dispersion zone water content of 16.1% (i.e. more water added than the previous two samples). Figure 53 (B) shows the same macro-fibrils found at lower water contents marked by white arrows. These macro-fibrils could perhaps be formed during the dilution stage of the process where the high rate of water injection would allow for large micro-scale water phase striations leads to the isolation of discrete polyester fibrils. Figure 53 (C) shows evidence of tightly packed bicontinuous morphology, indicated by white arrows. Figure 53 (D) shows the presence of discrete micro-fibrils, denoted with a white arrow, presumably a result of nano-striation during the dispersion phase of the process. At sufficiently high strains or elongations, it is possible that these nano-fibrils begin to neck apart as neighbouring aqueous domains being to coalesce. This could potentially be at the heart of the phase inversion mechanism as the necking of highly elongated polymer fibrils would be expected to create sequentially smaller domains of discrete polymer phase. It is also possible that these fibrils are a result of the high temperature wherein the matrix viscosity (resin) was too low to allow for the deformation of the water domains to reach the critical capillary number for breakup. It will be shown in the

next section that the water volume fractions The micro-fibril denoted by the white arrow in Figure 53 (D) has a diameter of approximately 200 nm and the rest of the fibrils range in diameter from approximately 100 nm to 200 nm.

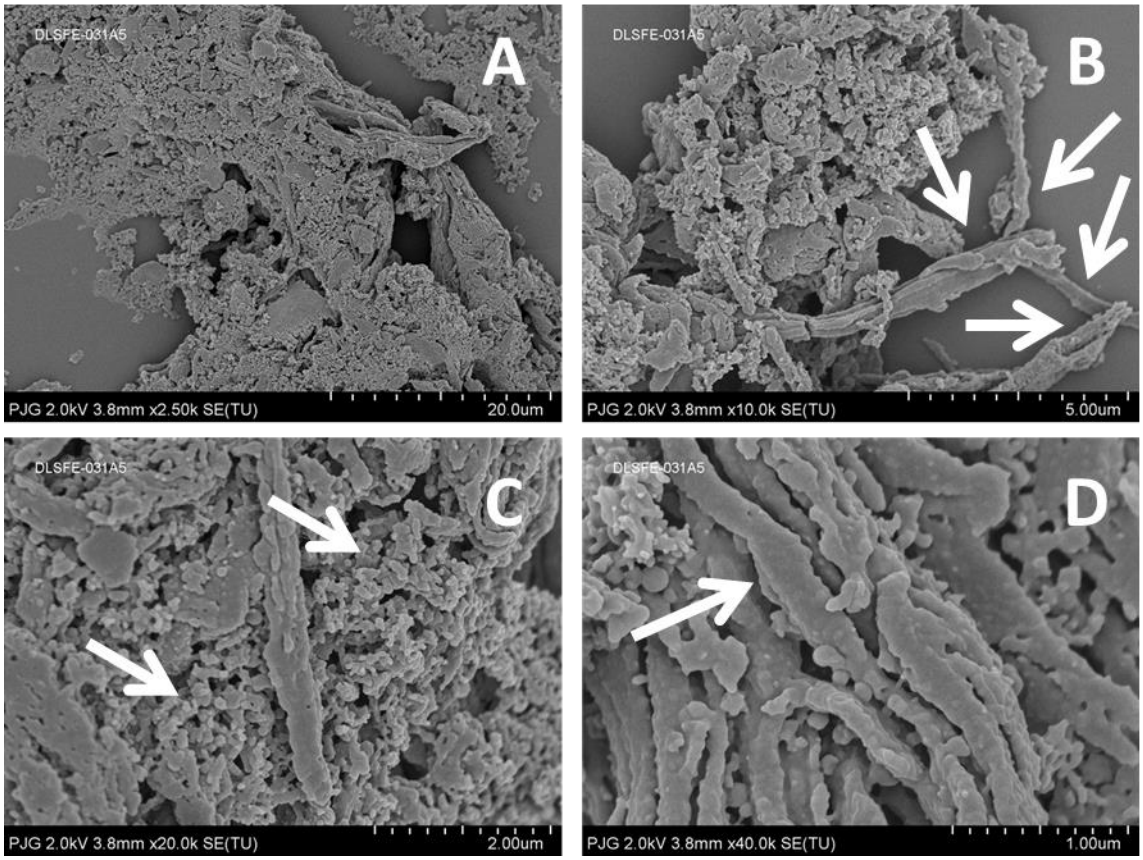

Figure 53 - SEM microscopy of sample 031A5 having a R:W of 4.8:1 and a corresponding dispersion zone water content of 16.1%.

Figure 54 shows a magnified area of a large macro-fibril which is permeated by a significant amount of nano-striations. These nano-striations all appear to be oriented in the same direction as the macro-fibril which contains them. This signifies that there is a significant physical component of the solvent free emulsification process which relies on elongational shearing. The

seemingly un-oriented domains seen in the bicontinuous matrices shown above are likely caused by relaxation of the affine deformation during dilution. It is possible that as a result of the quenching of the dispersion material in the dilution zone is non-uniform and that some morphology is frozen (oriented fibrils) while others (dis-oriented bicontinuous) is allowed to relax.

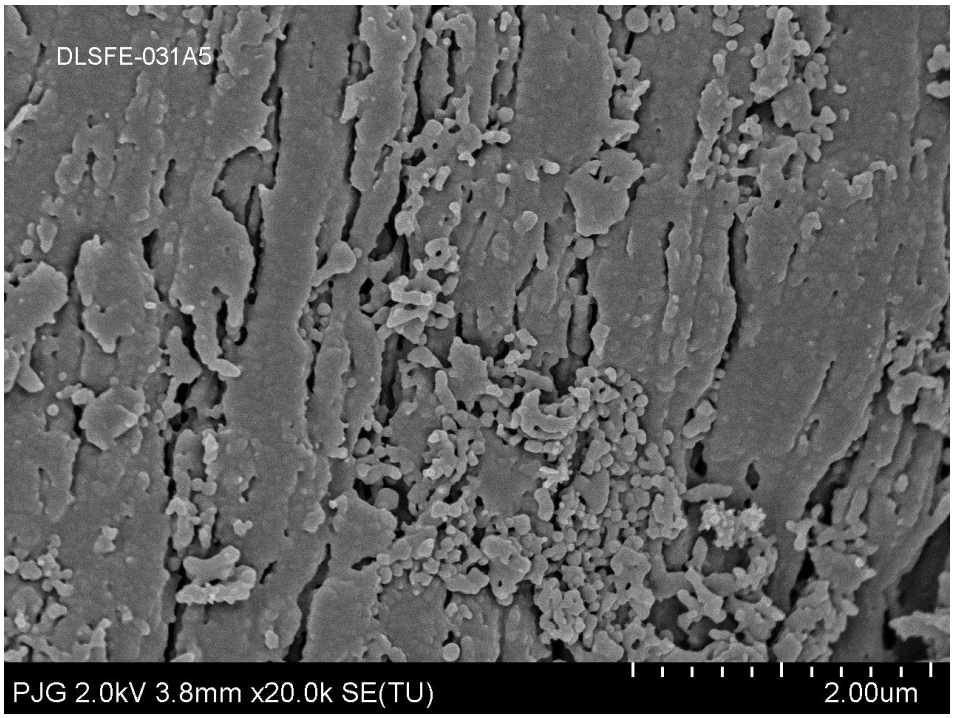

Figure 54 - Sample 031A5 showing a high degree of nano-striation within a discrete polyester macro-fibril domain.

Sample 031A6, with a R:W of 4.3:1 and dispersion zone water content of 17.8%, exhibits similar morphology as discussed above but with a seemingly more prevalent occurrence of voids and necked micro-fibrils. Figure 55 (A) shows a macro-fibril riddled with water voids (solid white arrow) connected to a fully-bicontinuous, disoriented lump of the matrix (dashed white arrow). This is

remarkable as both morphologies occur in such close proximity. Figure 55 (C) shows a enlarged section of (A) exhibiting nano-striations (solid white arrow) as well as the percolation of a bicontinuous matrix (dashed white arrow). Figure 55 (D) shows the remnants of a nano-striation (solid white arrow) surrounded by a fully percolated bicontinuous network.

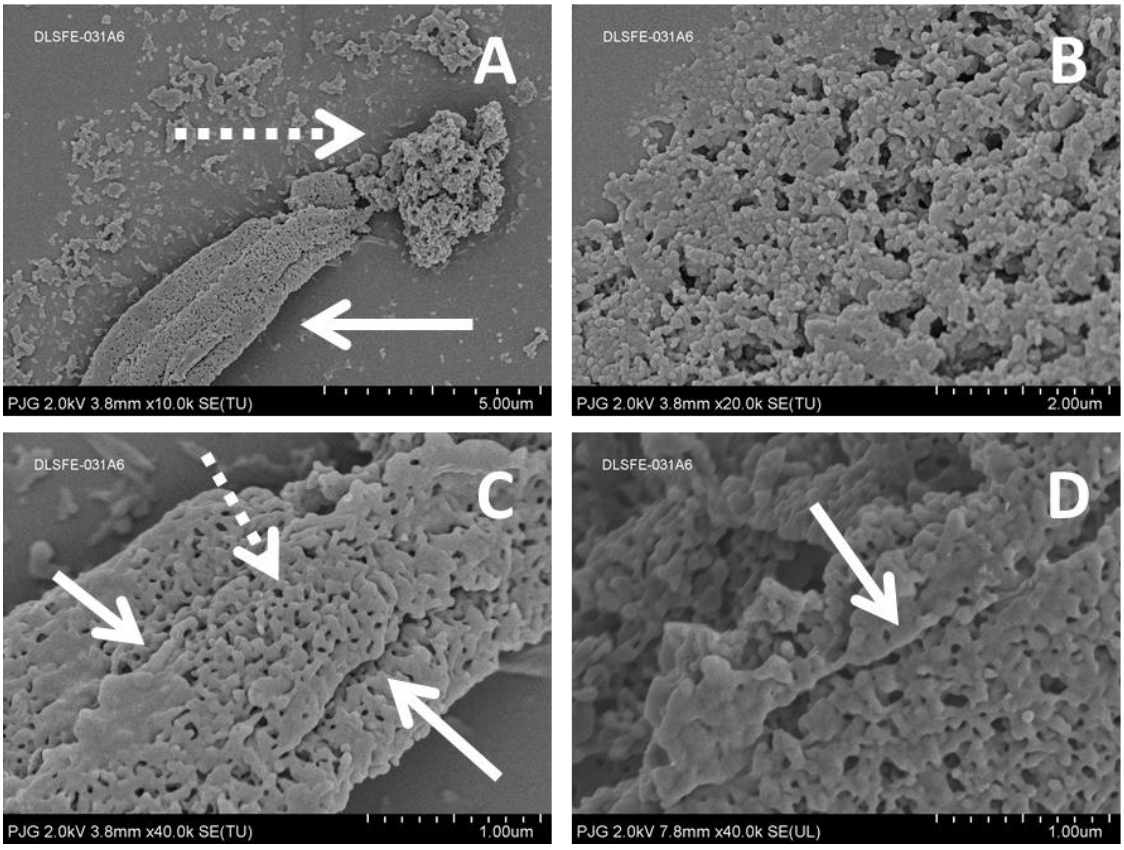

Figure 55 -SEM microscopy of sample 031A6 having a R:W of 4.3:1 and a corresponding dispersion zone water content of 17.8%.

Sample 031A7, with a R:W of 3.8:1 and dispersion zone water content of 19.4%, exhibited significant packing of both lamella and micro-fibrils. Figure 56 (A) shows tightly packed macro-fibril comprised of micro-fibrils ordered into tightly

packed lamella as well as exfoliated lamella (which is indicated by the white arrow). This exfoliation of some lamella is further seen in Figure 57 (A) and (B), with the white arrows directed towards the fibril bundles. Figure 56 (B) depicts a region comprised of tightly packed micro-fibrils perforated with voids corresponding to the placement of the aqueous phase. It is interesting to note that although the nano-fibrils in (B) maintain their orientation and elongated aspect ratio – the voids are nearly spherical. This signals that either the water phase has relaxed after dilution to a low energy state due to the high surface area to volume ratio, or that the strain rate within the micro-fibril was not sufficient to distort the voids which ranged from approximately 20-50nm. The size of these discrete water domains is of a similar magnitude to the aqueous nano-striations observed throughout, an example of which was shown in Figure 55 (D) and indicated by a white arrow, It is possible that these domains were then formed by the breakup of the affinely deformed aqueous domains by either Rayleigh disturbances or tip streaming, for example [5, 68]. This size range may represent a lower stain rate limit to the dispersed aqueous phase discrete size. The size of these domains also is similar to compatibilizer micelles in polymer blends [69].

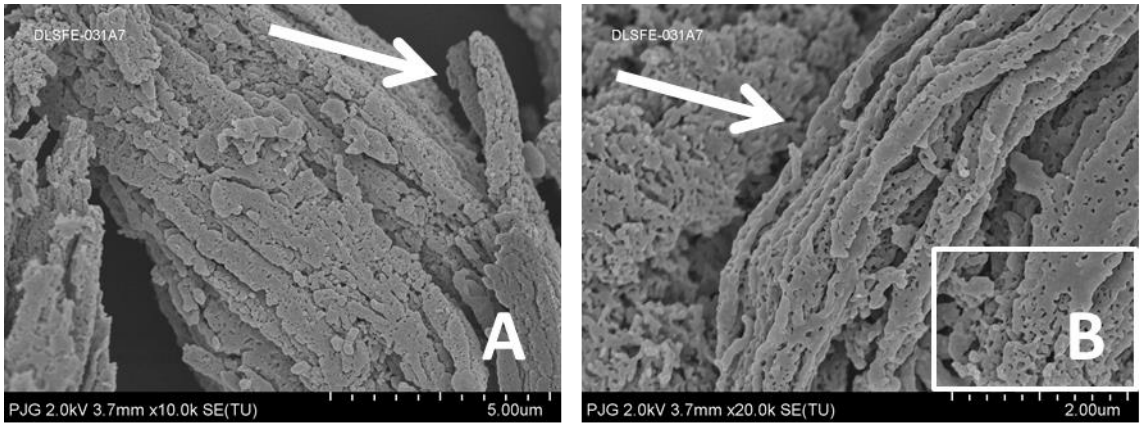

Figure 56 - SEM microscopy of sample 031A7 having a R:W of 3.8:1 and a corresponding dispersion zone water content of 19.4%.

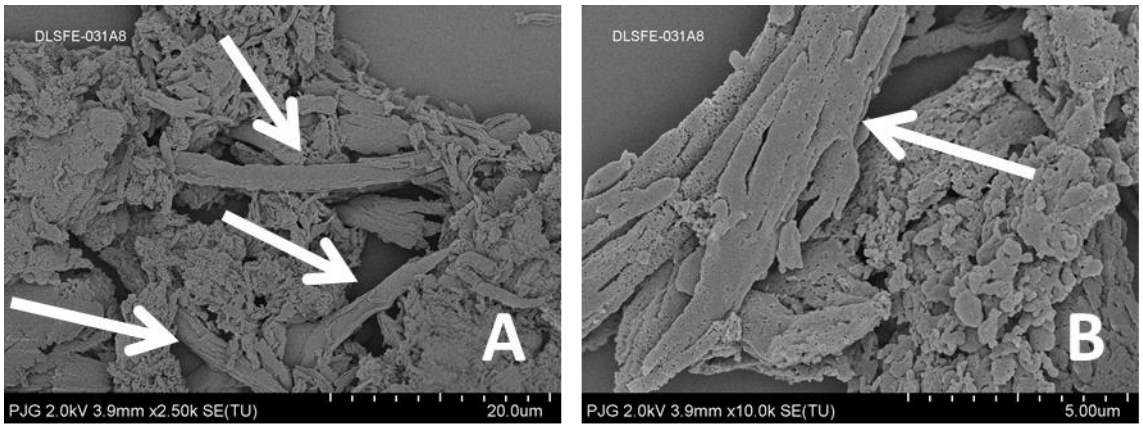

Figure 57 -SEM microscopy of sample 031A8 having a R:W of 3.5:1 and a corresponding dispersion zone water content of 20.9%.

Figure 58 shows a magnified section of Figure 56 (B) where the intercalation of water between adjacent fibrils or lamella can be seen (white arrows). The intercalation of water domains between sheets of bicontinuous polymer may be a result of the dilution step as the size domains is greater than the size of the bicontinuous aqueous domains. This size difference would make sense as the addition of large amounts of water in the dilution zone would effectively reduce the stress transfer (lubrication) to deform the water domains. At

the edge of these polymer sheets, evidence of the rupturing of bicontinuous morphology can be seen, as indicated by the white circle in Figure 58. The rupturing, presumably during dilution, has left dangling struts of polymer which appear to form nodules. Constant intercalation and rupturing of the bicontinuous polymer/water matrix with water during dilution might be the part of the mechanism of phase inversion.

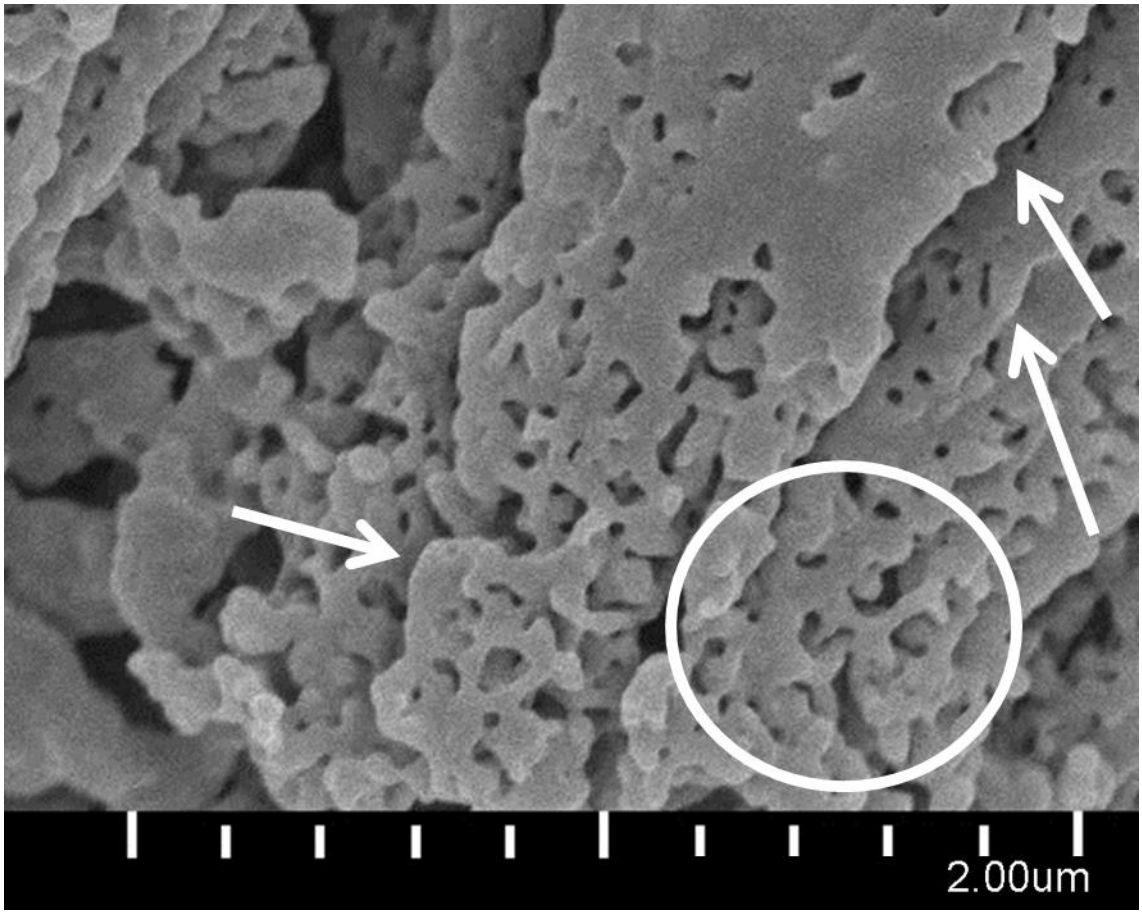

Figure 58 - Enlarged region (white box) from Figure 56 (B) of 031A6 showing signs of intercalation of adjacent fibrils/lamella (white arrows).

The last images are of the 031A8 data set shown in Figure 59, which displays a very interesting morphology. The white arrows direct towards droplets

that appear to be necking from the main body of the fibrils, the size of these droplets is approximately 80-100nm, as are the rest of the necking droplets. The white circle in Figure 59 also highlights a very interesting droplet which has been formed containing discrete voids attributed to the aqueous phase droplets. This is a very interesting find as it seems to depict a segment of micro-fibril which has relaxed towards a spherical shape while maintaining the voids within it. It is difficult to imagine how the surface tension might be high enough to cause relaxation in the fibril yet still low enough to preserve the voids which would increase the overall surface energy.

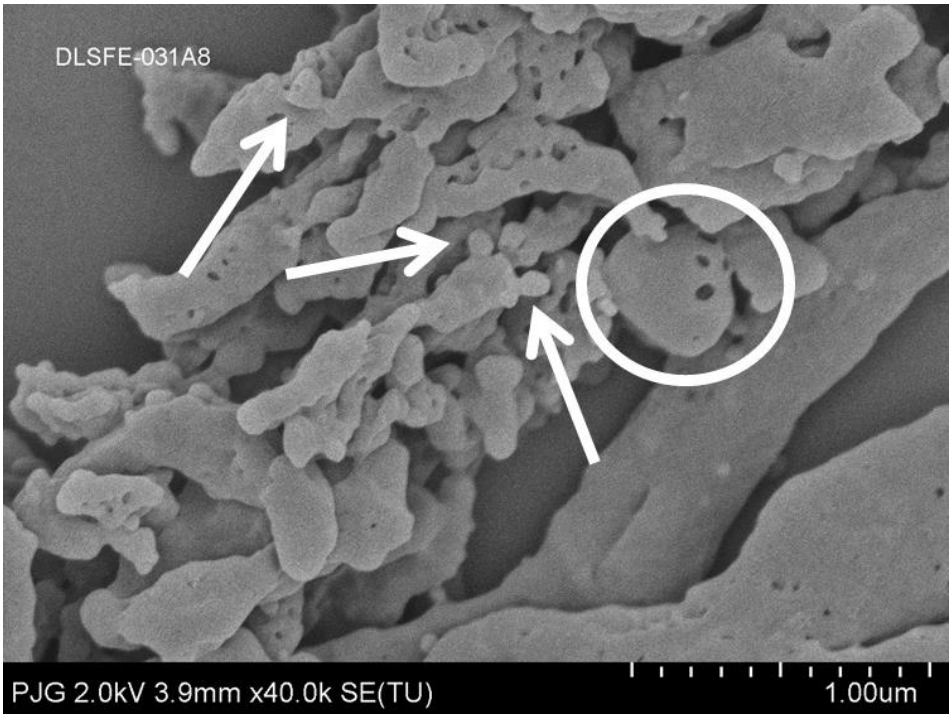

Figure 59 – Sample 031A8 showing the necking of droplets from the end of micro-fibrils (white arrows) and the appearance of a droplet with voids (white circle).

5.3.2 Low Temperature Dispersion Zone

The lower temperature dispersion zone produced a much greater fraction of latex particles than the high temperature study in the preceding section. This was evident during both the collection of samples from the extruder die face as well as the analysis of the samples by SEM. The increase in latex means that there is much less bulk morphology evolution to discuss – which is a significant result, showing that lower temperatures favour latex generation in solvent-free emulsification. Though there was an increase in latex generation, the particle size distribution was not analyzed as the scope of this chapter is focused upon the morphology evolution of undispersed resin.

Sample 036A1, having the lowest water volume in the dispersion zone of 10.7%, is shown below in Figure 60. Interestingly, Figure 60 (B) shows that there are voids present in both the discrete polymer particles and undispersed resin, as indicated by the white arrows, which range in size from 30nm to more than 300nm. These voids were also observed in the previous section in Figure 59 and were interpreted as a section of a micro-fibril, containing small water domains, which necked and subsequently relaxed to a lower aspect ratio.

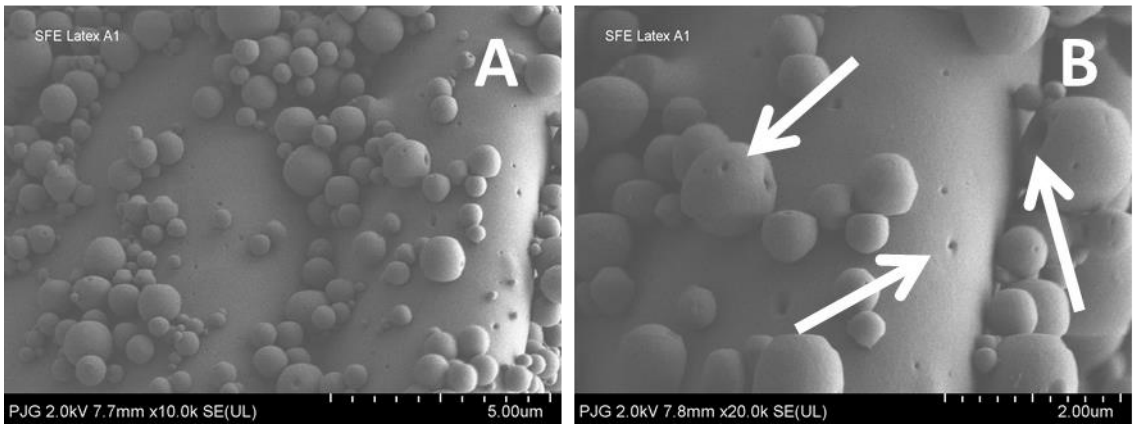

Figure 60 - Sample 036A1 showing a distinct increase in amount of latex generated on top of a large un-emulsified resin domain (A), and voids present in both discrete particles and un-emulsified resin (white arrows) (B).

At the macro-scale, very large voids left by water droplets are indicated by white arrows in Figure 61 (A) with a diameter ranging from approximately 0.4mm to larger than 0.7mm. The presence of these very large scale water domains indicate very low levels of strain within the melt. It is possible that due to the low water content in the dispersion zone, the distribution of water and surfactant was heterogeneous throughout the polymer phase until the dilution zone. Water dispersed into the resin within bulk resin in the dilution zone would have experienced very low strain rate due to the low matrix viscosity from the high water content. The dispersion of water into micron-scale domains within can also be seen in Figure 62 with domains ranging from approximately 50nm to upwards of 2.5µm. It is interesting to note that the sample in Figure 62 shows scales of water domains that are found in the dispersion zone, approximately 50nm-200nm, as well as much larger ones, upwards of several microns. This is a significant result as it shows that there is a significantly higher degree of strain

within the dispersion compared to the dilution zone. Beyond the onset of phase inversion (locally or globally) the addition of water results in larger aqueous phase domains within a continuous portion of the resin phase.

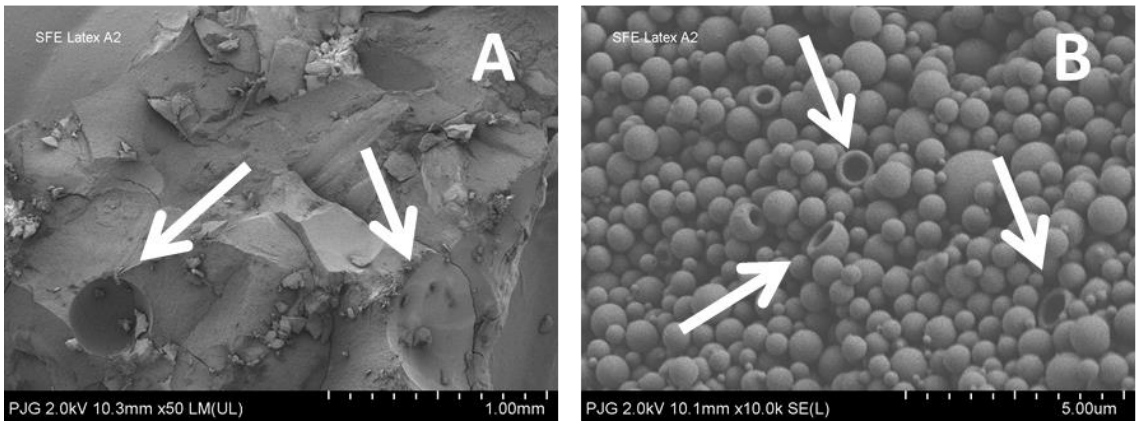

Figure 61 - Sample 036A2 showing the presence of voids left by large water droplets (white arrows) (A) as well as the formation of hollow discrete latex particles (white arrows) (B).

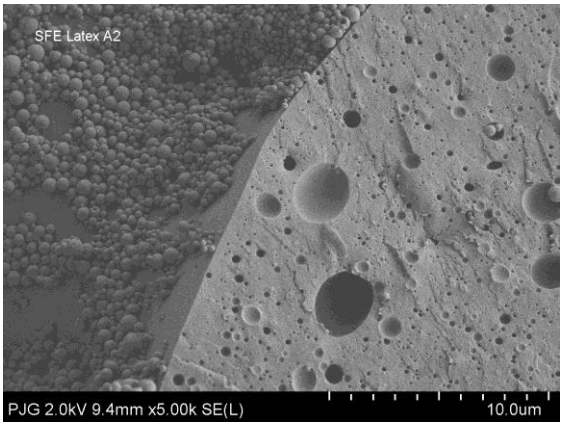

Figure 62 - Sample 036A2 showing a marked contrast between latex particles (left) and bulk resin with macro-scale water dispersion (right).

Samples 036A3-036A6 show similar morphology as discussed above and are show in sequence below, in Figure 63 (A-H). The left-column of images in Figure 63, (A, C, E, and G) depicts large regions of un-emulsified resin existing

on the millimetre scale. The frequency of these domains has not been determined but their occurrence is clearly prevalent throughout the entire 036A data series. The right-column of images in Figure 63, (B, D, F, and H) show that hollow latex particles have also been generated throughout this series (white arrows). The formation mechanism of these liposome-like particles is still unknown yet they did not appear in the samples processed at higher temperature profiles in 031A. The size distributions of the discrete latex particles are bimodal with sub-micron and micron particles. Figure 63 (F) and (H) show the same bimodal dispersion of water domains within un-emulsified resin domains, as discussed above.

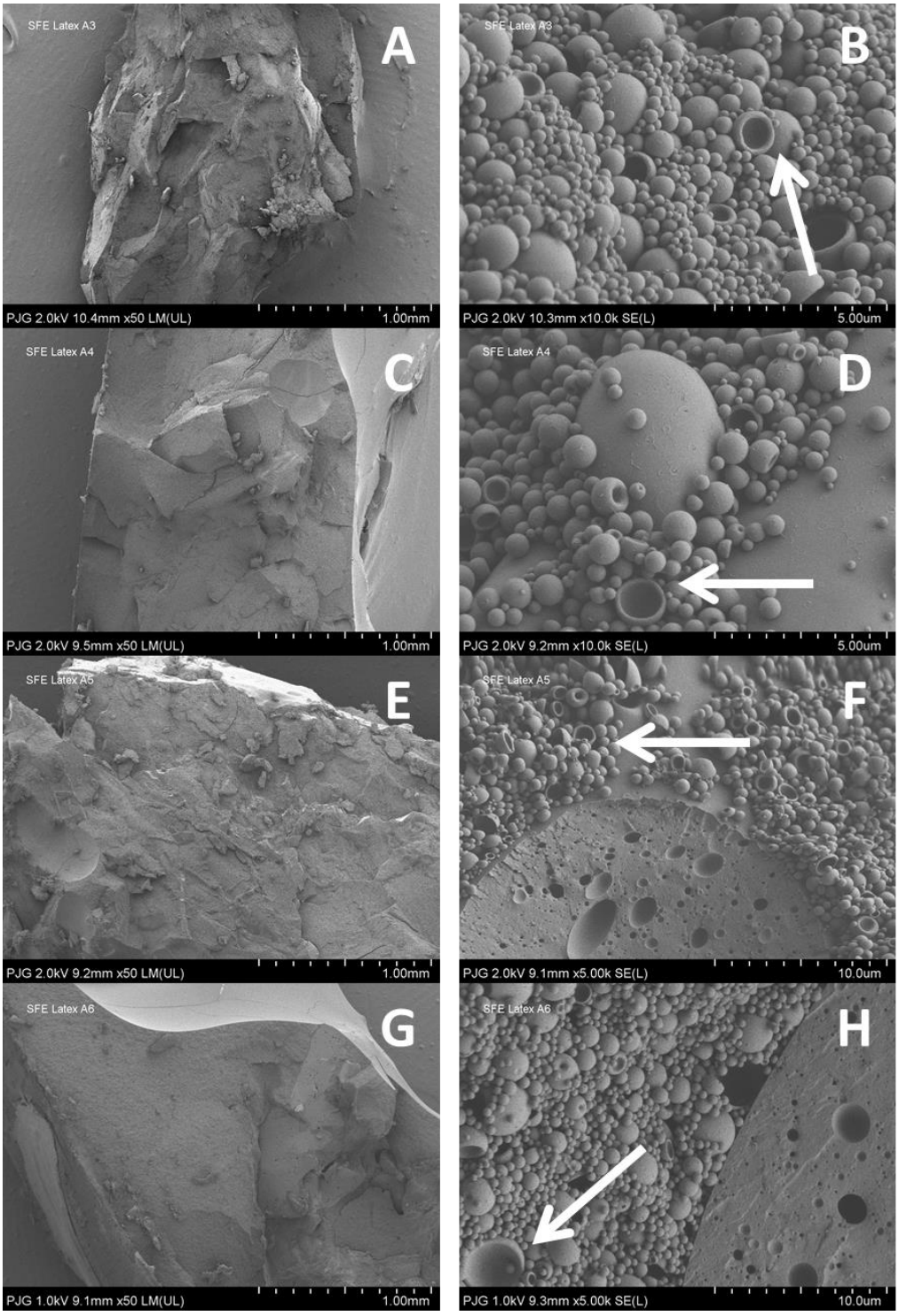

Figure 63 - Sample 036A3 (A,B), 036A4 (C,D), 036A5 (E,F), and 036A6 (G,H) showing similar morphological features of hollow latex formation (white arrows) as well as large regions of un-emulsified resin pitted with bimodal water domains.

5.3.3. High/Low Temperature with Dilution Summary

Overall, the morphology seems to be largely invariant of resin-to-water ratio, for the range of water volume fractions studied. This is not to say that there is no dependence, mechanistically, on water volume fraction within the dispersion zone as the distribution of morphologies was not quantified. Qualitatively, however, the specific macro and micro-structure features of the samples were present in all samples for a given temperature.

The transition from low to high water content within the dispersion zone yielded very little quantitative differences in morphology within the 031A data set. Qualitatively, local regions of bicontinuous networks appeared to be present at all of the water contents observed in the range of this data set, ~10-21 vol% water. It appears as though the relative fraction of the total sample which was bicontinuous increased with increasing water content. It is difficult, however, to distinguish the contribution of the dilution zone upon the morphology of the matrix in the evolution of the morphology. All of the samples in this high temperature series produced a relatively small total fraction of latex at these elevated temperatures. Moreover, the morphology throughout the samples was heterogeneous, exhibiting a mixture of both micro and macro-scale fibrillation and striation.

There was some evidence of the necking of droplets from micro-fibrils – this behaviour was most prevalent in regions with a uniform bicontinuous

morphology, such as in Figure 55 (B). This localized phase inversion may reflect the need for a homogenous distribution of bicontinuous morphology in order to obtain complete emulsification. This makes sense, qualitatively, as localized regions of phase inversion would have a significant impact on the local rheology of the matrix, thereby impacting the subsequent development of co-continuity adjacent to the region. This drop in matrix viscosity following phase inversion is a prevalent observation in the study of immiscible polymer blends; a notable example was by Chi-Kai Shih, who studied the torque profile of a batch mixing of a high-density polyethylene/rubber blend [70]. In regards to the morphological structure, high temperature samples showed a combination of bicontinuous morphology along with generation of fibrils at both the macro and micro-scales. The micro-scale morphology is believed to have developed in the dispersion zone whereas the macro-scale morphology is believed to have developed in the dilution zone. This is based on the relative water volume fractions present in each zone and the implications on the effective stress transfer throughout the matrix.

Song et al. ([22]) showed that the viscosity of the W/O emulsion prior to inversion was related to the resulting particle size of the final emulsion. The reduction in shear rate and stress transfer (based on the reduced viscosity from temperature) would limit the dispersion of water homogenously throughout the matrix prior to inversion. This effect would be compounded by the reduction in interfacial area caused by a larger dispersion of water. An additional result of the

reduction in interfacial area by a larger W/O dispersion would be the decreased neutralization of terminal carboxylic groups on the polymer chain.

In contrast, the morphology of the samples appears very different between the high and low temperature profiles of 031A and 036A data series, respectively. The amount of latex produced was far higher at lower temperatures than at higher ones which is consistent with the results by Song et al. [22] for a tackifier emulsion system. The low temperatures, however, also yielded much larger un-emulsified coarse particles as well as significant amounts of hollow latex particles. Low temperature samples also seemed devoid of fibular structures and existed as a combination of discrete latex particles and very large regions of un-emulsified resin. Within the latex particle population, there existed evidence of a complex emulsion formation as well, indicated by the presence of hollow droplets.

The bimodal distribution of features and presence of large resin domains at low temperatures is perplexing. The lubrication caused by phase inversion could produce a heterogeneous development of the water dispersion in the un-inverted portions of the resin. Salager et al. [8, 71] discussed the concept of local water-oil ratio (WOR) and described the implications it could have on the transition through the phase inversion locus, resulting in complex morphology including double emulsion formation. This could be a cause of the unemulsified resin at low temperature. Localized premature phase inversion produces the first peak of latex PSD and complex emulsion (hollow latex) while the subsequent, larger unemulsified particles are caused by the reduced strain rate from the prior

inversion. This reduced strain rate following the partial inversion of the matrix would lead to a heterogeneous W/O dispersion in the unemulsified material, thereby preventing bicontinuous morphology and subsequent inversion during dilution. Smaller, coarse particle development could also be a facet of this mechanism wherein a small portion of the resin has a delayed inversion, in relation to the rest, and thereby experiences lower strain, and a subsequently more coarse dispersion of water prior to inversion.

The reason the WOR would be influenced by the temperature is likely due to the rate at which the water is distributed into the resin upon injection. The balance of distributive mixing and dispersive mixing would seem a likely cause of local inversion. That is to say that a poor water distribution rate and high water dispersion rate could cause the local inversion at low temperatures. The difference in temperature, and ultimately viscosity, would support this as the dispersion rate would seemingly be much greater at low temperatures/high viscosities. The opposite scenario exists for the high temperature case wherein there would exist good distribution yet poor dispersion of water due to the reduced viscosity. This poor dispersion would seemingly explain the reduced fraction of resin which actually inverted upon dilution at higher temperatures.

5.3.3 Pre-dispersed Resin Without Dilution

Two samples were prepared in which the dilution water in zone 6 was absent and a corresponding dispersion zone resin-to-water ratio of 4.8:1 yielded

a dispersion zone water content of 16.1%. When the samples were taken from the extruder and measured in a moisture analyzer, the water content was on average 15.75%. These samples were prepared to determine the pre-diluted morphology in order to differentiate the influence of both the dispersion and dilution zones within the extruder; the caveat here being that these samples experienced higher shear stresses for a longer duration than the other series. Details of the experimental conditions can be found in Table 11 and Table 10. The two samples had temperature profiles in between the profiles presented in the previous section, 031A and 036A. This was done to evaluate the progression in morphology, as a function of temperature, within the dispersion zone.

Figure 64, below, shows the first sample 037A1 for which sheet-like lamellar structures are indicated by the white arrows in (A). Figure 64 (B), shows a similar water intercalation between adjacent lamella (white arrows), similar to the previous morphology observed in 031A series. The bicontinuous morphology appears to be homogenous throughout the matrix in the dispersion zone and would appear to precede the development of any macro-scale morphology including fibrils or striations. This is a significant finding as it shows that the bicontinuous network percolates prior to the dilution zone and at low overall water volume fraction.

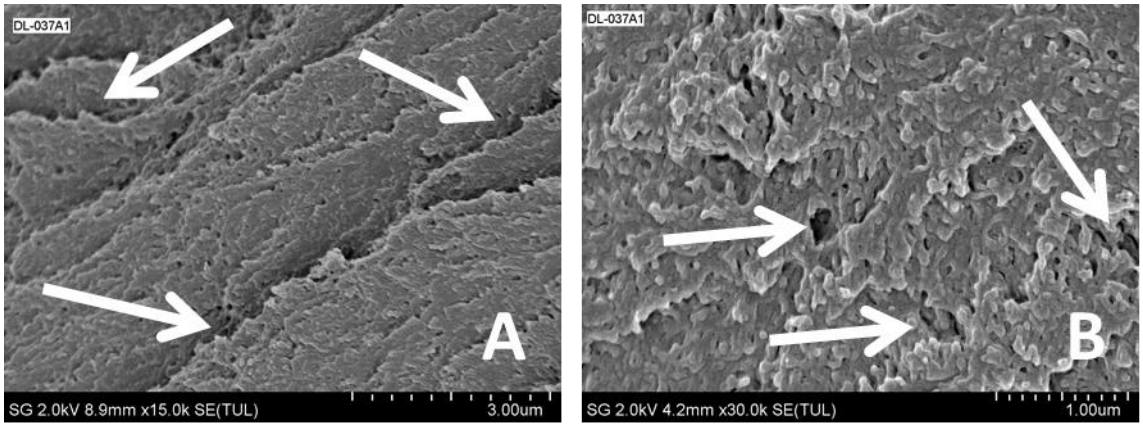

Figure 64 – Undiluted sample 037A1 showing evidence of lamella (white arrows) (A), and evidence of intercalation of lamella (white arrow) (B).

Figure 65 shows a magnified view of the bicontinuous network before (top) and after (bottom) contrast enhancement. The original image seems to show some film forming behaviour that makes the water-polymer interface difficult to determine. When the image was processed in Fiji with the Anisotropic Diffusion 2D and Enhance Local Contrast plugins, the interface becomes much more prevalent. Figure 66 shows the same image as in Figure 65 after processing with the *Bernsen* method of local image threshold binary processing [72]. All three images show progressively clearer indications of a bicontinuous network being formed with the polymer phase. The fibrils are present with varying diameters generally on the order of about 40-60nm.

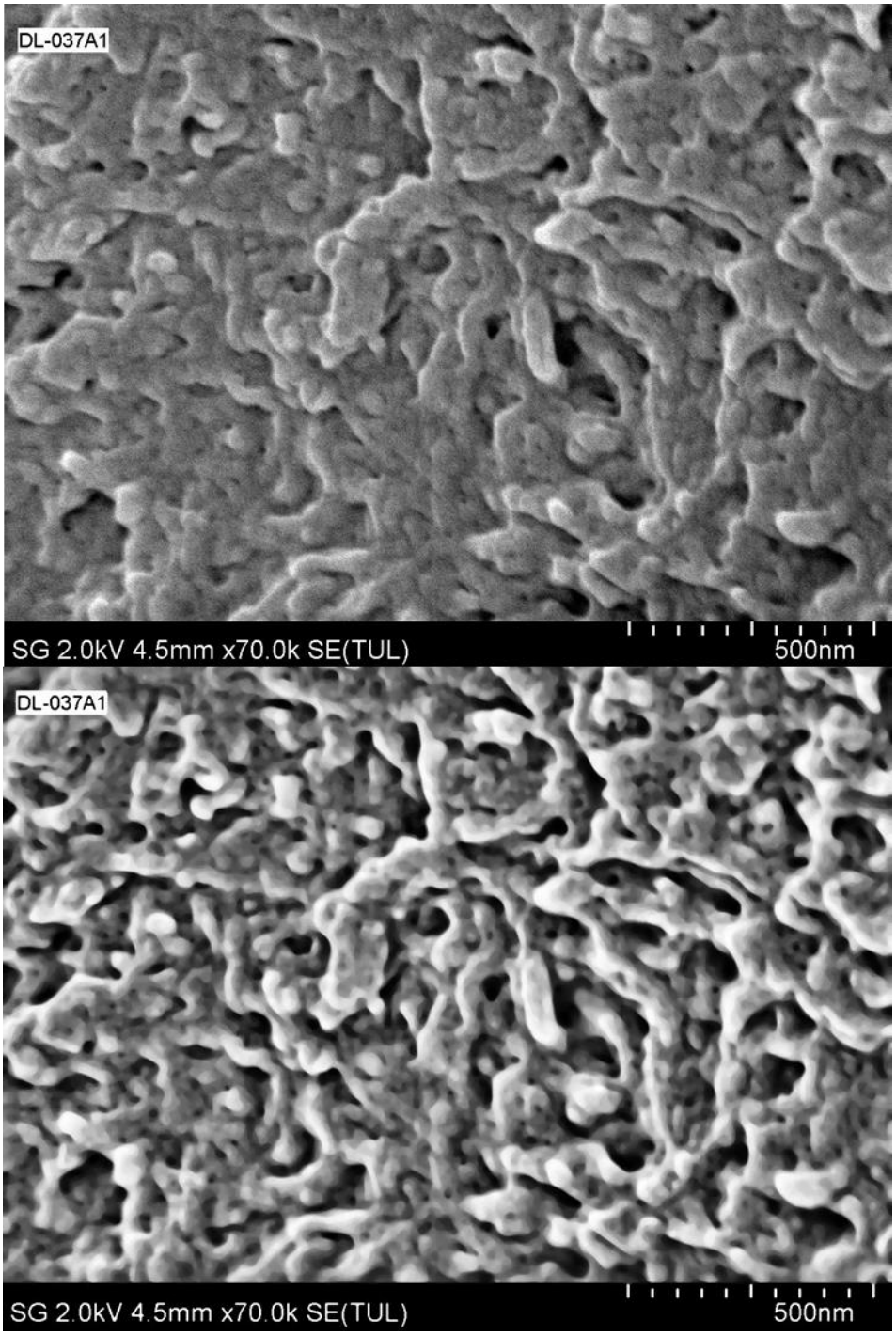

Figure 65 - Sample 037A1 with original image (top) compared to contrast enhanced image (bottom) which clearly shows a bicontinuous network.

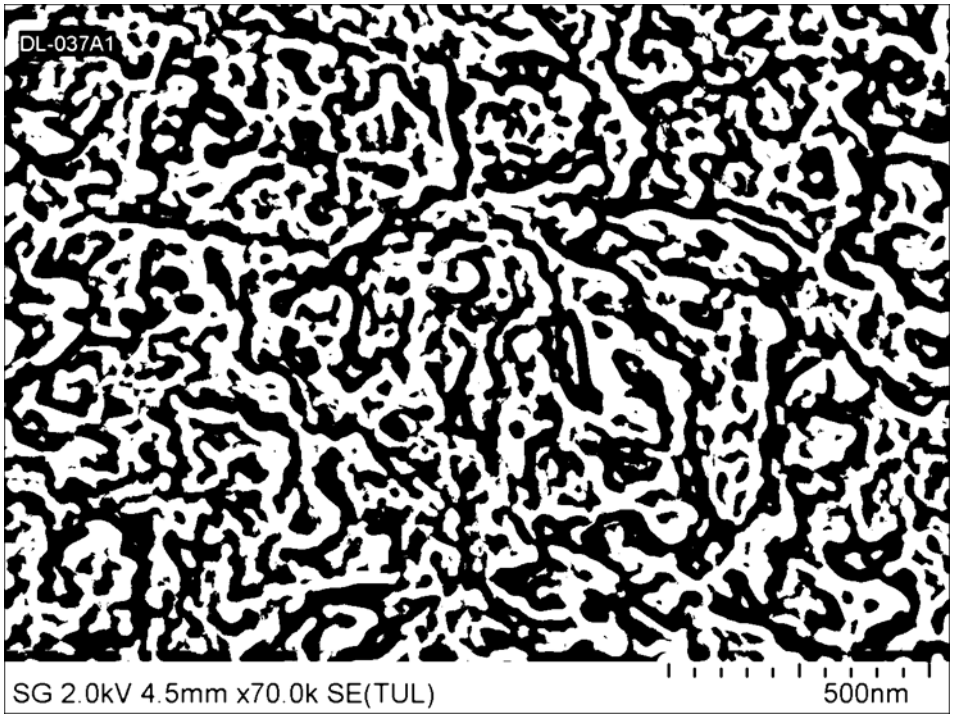

Figure 66 - Sample 037A1, as seen in Figure 65, after processing into binary 8-bit image using the *Bernsen* method of Automatic Local Image Threshold in Fiji; polymer phase is shown in black while water phase is shown in white.

Sample 037B was processed at a lower temperature profile than 037A1 yet still shows similar lamellar stacking as indicated by the white arrows in Figure 67 (A) and (B). The microstructure present in the morphology of sample 037B appears less distinct than 037A1 and the interface between the polymer and water phases is more difficult to see, Figure 68. The white arrows in Figure 68 highlight a few of the many voids left by the aqueous phase which appear on a similar scale of 10-30nm as seen in 037A1. Although the discrete water domains appear similar in size, the bicontinuous aqueous domains which lead to the definition of polymer fibrils are less frequent and smaller in 037B. The makes it appear as though there is a lower overall water volume fraction in 037B when in

fact it is equivalent to 037A1.There is still some visual indication of fibrillation of the polymer phase, though the length of the fibrils appears to extend to through shorter ranges than observed in 037A1.

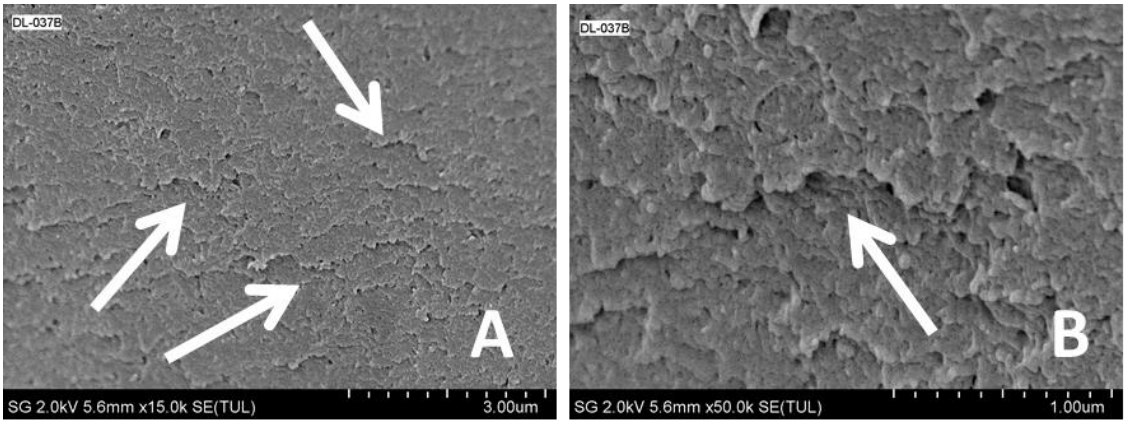

Figure 67 – Sample 037B exhibiting lamellar stacking similar to 037A1 (white arrows) in both (A) and (B).

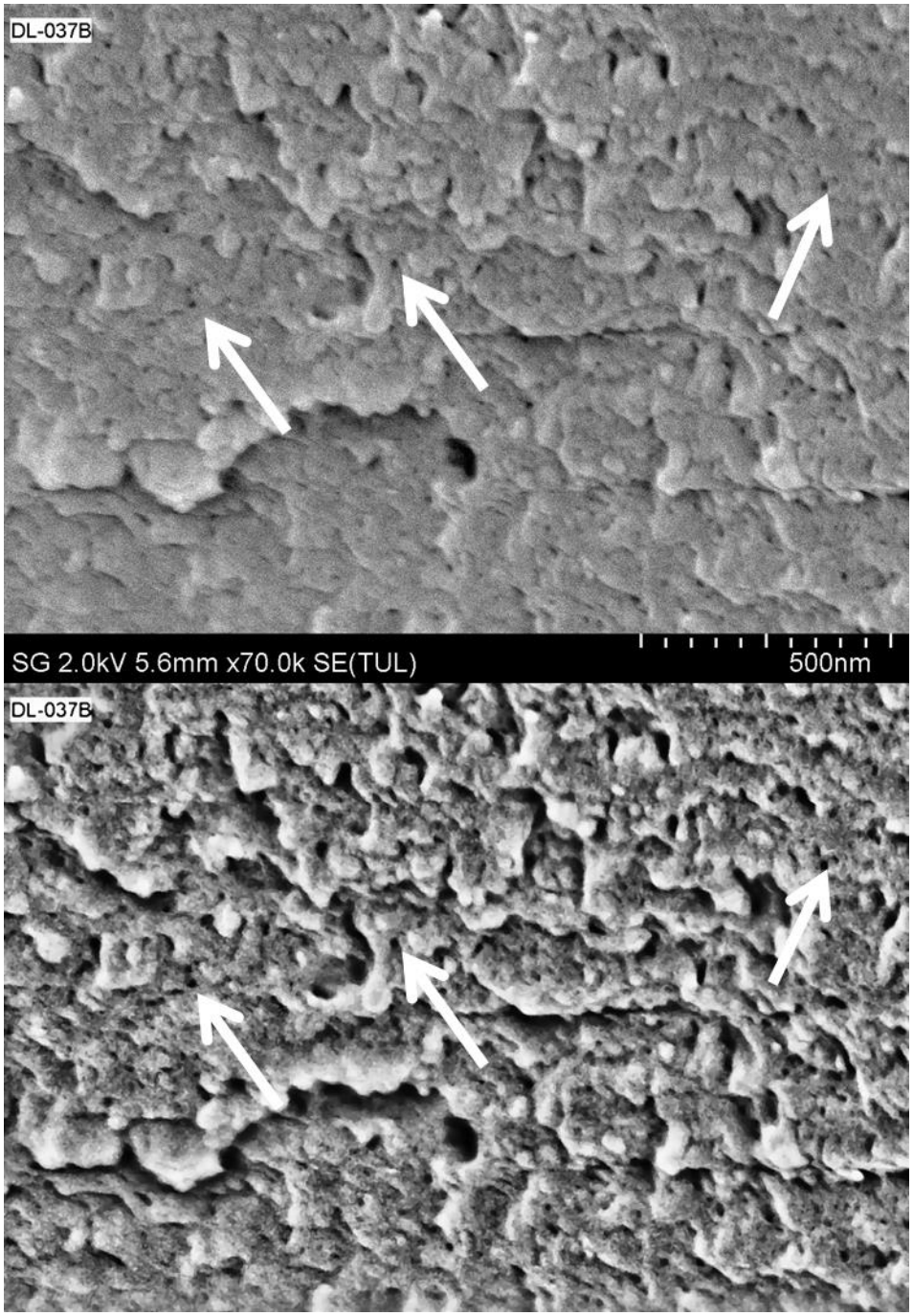

Figure 68 – Sample 037B showing a smaller microstructure than seen in 037A1 with some aqueous phase domains indicated by white arrows.

The evidence of a finer microstructure is more readily apparent upon application and comparison of the binary processed images between samples

037A1 and 037B in Figure 69. This method of processing is not the same as a true cross-section of the bicontinuous network yet still serves as a good method of comparison between the topologies of the fractured matrix. The binary images show that the relatively cooler temperature profile of 037B led to the development of smaller fibrillation and polymer domain sizes.

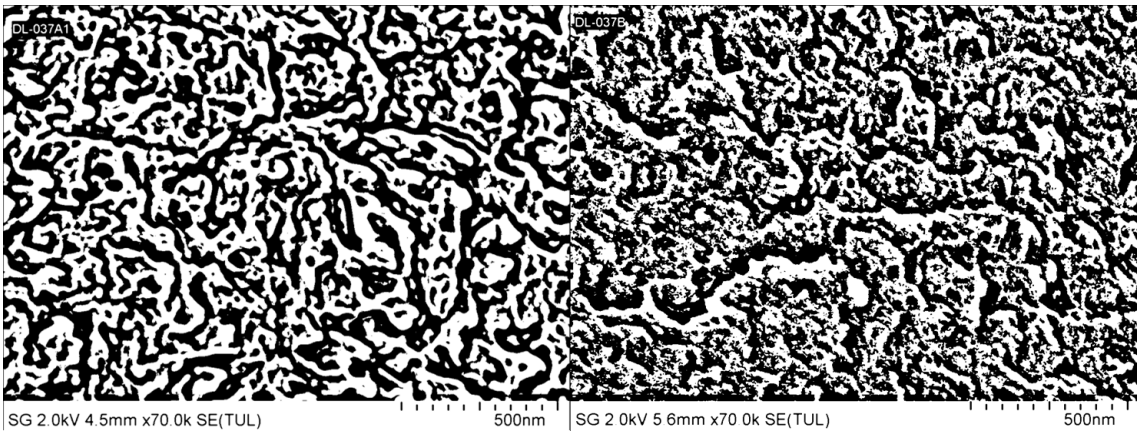

Figure 69 - Comparison of binary processed images of 037A1 (left) and 037B (right) showing the development of a finer microstructure in the morphology of 037B at lower processing temperatures.

This microstructure size reduction could be the result of the higher viscosity and hence higher shear rate of the polymer phase at lower temperatures. The deformation of the domains of an immiscible dispersed phase (water, prior to co-continuity) within a matrix (polymer) is dependent upon the local capillary number, which is given by [45]:

$$Ca = \frac{\eta_m \dot{\gamma} B}{2\sigma} \qquad (5.1)$$

Where η_m is the viscosity of the matrix; $\dot{\gamma}$, the shear rate; B, the diameter of the deformed dispersed phase; and σ, the interfacial tension. This relationship would seem to support the findings of smaller microstructure at lower temperatures given the resulting increase in shear rate by increase polymer phase viscosity.

During dilution, it is plausible that the water is initially dispersed into the bicontinuous morphology into discrete domains. The size of the aqueous domains created in dilution would be large (micron-scale) in comparison to the domains created at lower water volume fractions in the dispersion zone (nano-scale). This is due to both the short time scales in the dilution zone as well as the lower shear stress due to the lubrication of the aqueous phase. The injection of water in the dilution zone effectively shifts the water volume fraction through the locus of phase inversion in a similar manner as a catastrophic phase inversion. In addition, the overall salinity of the aqueous phase should also decrease upon dilution which would be similar to a transitional phase inversion process. With respect to the actual phase inversion event and its mechanism, it could then be a combination of CPI and TPI. The CPI mechanism would cause the newly formed micron-scale aqueous domains to begin coalescing with the aqueous portion of the bicontinuous matrix from the dispersion zone. The TPI mechanism would then tend to shift the surfactant affinity towards hydrophilic as the salinity of the aqueous phase decreases. It should be noted that the dilution would alter the affinity of both the anionic surfactant as well as the terminal anionic carboxylic salt group in the polymer. The combination of CPI and TPI inversion protocols

has been shown to produce some synergistic effects yielding extremely small particle size emulsions [8]

The main purpose of these two samples was to determine whether phase inversion occurred before or after the dilution second of the extruder. It was found that the inversion does not take place in the dispersion zone and that it occurs in the dilution zone. The function of the dispersion zone is then to produce a bicontinuous morphology wherein a smaller microstructure would promote inversion in the dilution zone.

5.4 Summary and Conclusion

In order to test the hypothesis of phase inversion being the mechanism of solvent-free emulsification, the morphology of pre-emulsified samples were evaluated. Discrete aqueous phase domains were found to occur within continuous matrices of resin, prior to latex generation. This is very significant as it shows that the mechanism of emulsification is not a direct dispersion of polymer within a continuous water phase. Instead the water is first mixed into the molten resin and dispersed into nanometer-scale domains. These domains are then drawn to high aspect ratios where they coalesce with adjacent water domains to form a percolative structure throughout the resin. This bicontinuous morphological development was found to occur in the dispersion zone and prior to subsequent inversion in the dilution zone. The transition between co-continuity and phase inversion is not well understood and requires further study.

As a result of the findings in this chapter, the evolution in morphology along the length of the extruder has been determined and is depicted schematically below, in Figure 70. The water is first injected into the extruder and distributed throughout the melt and dispersed to form a W/O emulsion. The water is then further dispersed into smaller domains as the interfacial tension drops due to the neutralization of the terminal carboxylic functional groups of the polymer chain. This drop in interfacial tension allows for very high deformations before the water phase eventually percolates to form a bicontinuous network with the polymer phase. The subsequent dilution of this bicontinuous network finally brings about the onset of phase inversion and discrete latex particles are formed. As the onset of phase inversion occurs in the dilution zone upon the addition of water (increase in water volume fraction) the SFE mechanism is thought to be a type of catastrophic phase inversion.

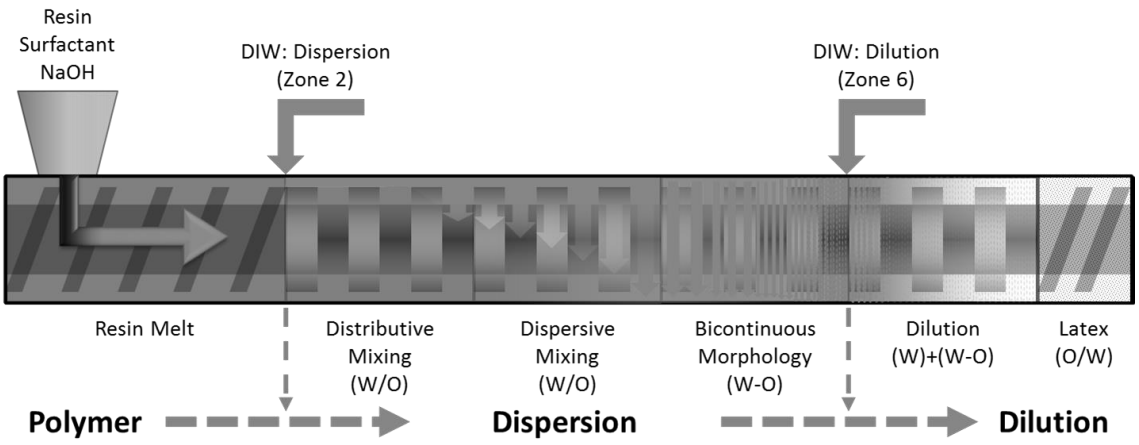

Figure 70 - Schematic depiction of the evolution in morphology along the length of the extruder in the solvent-free emulsification process.

A theory of localized phase inversion was also discussed which involved the inversion of a portion of the system prior to the homogenous development of bicontinuous structure throughout the mixture. This behaviour is a type of process instability which negatively influences the quality of the emulsion produced. The impact of temperature within the system appears to produce a finer microstructure at lower temperatures within the dispersion zone. Based on the local capillary number, lower temperatures are believed to increase the maximum deformation of the water domains as a result of the increase in matrix viscosity of the polymer melt.

CHAPTER 6 – SIGNIFICANT RESEARCH CONTRIBUTIONS AND RECOMMENDATION FOR FUTURE DEVELOPMENTS

6.1 Significant Research Contributions of Thesis Work

The purpose of this work was to study the solvent free emulsification mechanism for the production of nano-sized narrow particle size distribution polymer lattices in a twin screw extruder. Polymer lattices are of great interest industrially yet only certain polymers may be produced through emulsion polymerization. The remaining polymers much first be polymerized in bulk and subject to subsequent emulsification. Direct emulsification techniques are not suitable for the production of nano-scale polymer lattices and hence alternative methods are required. Solvent free emulsification, presents a novel method of creating these lattices yet without the use of costly and hazardous solvents. The use of a twin screw extruder is also of great interest as it allows for the continuous production of these lattices. Thus, the focus of this work was to understand the mechanism of this process in order to better understand the factors which influence latex production.

The SFE process was first studied by analyzing the time scales in which the mechanism takes place as well as analyzing the bulk mixing parameters associated with the residence time distribution within the extruder. A method to measure the residence time distribution was developed using a mini-spectrometer and an inline fiber optic probe which measured the concentration of

a fluorescent tracer from a pulse input. The flow pattern within the extruder was found to have a low degree of back-mixing, quantified by the dimensionless variance have values ranging from 0.038-0.046. The dimensionless variance was not found to vary significantly within the levels of screw speed or resin-to-water ratio; any variation was beyond the resolution of the method used. The mean residence time was not found to be dependent on the screw speed which signified that the extruder was fully filled, a result which supports the dispersion zone pressure measurements. The mean residence time for resin-to-water ratios of 3 and 3.5 were found to range between 244-251s and 261-269s, respectively, for equal die-flow rates. This is a significant result as it shows higher zone 1 aqueous injection rates effectively decrease the mean residence times within the dispersion zone. This means that the effect of resin-to-water ratio in the dispersion zone, with respect to time dependent evolution of morphology and volume fraction dependent evolution of morphology, cannot be analyzed independent of each other. The method presented therefore represents a suitable means of distinguishing the influence of these two effects.

The response in D50 particle size was evaluated based on factors of screw speed and feed rate, through five and three levels, respectively. A positive correlation between feed rate and D50 particle size was found to exist. This finding supports there being a time-dependent evolution in morphology within the dispersion zone which relates to the latex particle size obtained after dilution. A positive correlation between screw speed and D50 particle size was also found to

exist at the fixed surfactant concentration studied. The RTD chapter confirmed that the screw speed doesn't influence the residence time so the screw speed was treated as a strictly mechanical influence. This result was then somewhat counter intuitive from a high level as it appeared that higher levels of shear resulted in larger particles sizes. Two theories were put forth, (1) that interfacial slip is a significant factor which limits the elongational mixing and strain rate of the aqueous domains, and (2) that the screw speed also influenced the viscosity of the polymer through shear thinning behaviour as well as possibly by temperature increase through viscous heat dissipation. It is likely that both theories contribute to the increase in particle size upon increasing screw speed.

The morphology of coarse, micron-scale, particles was qualitatively analyzed through electron microscopic evaluation after processing at non-optimal temperature profiles and surfactant concentrations. The reason for this was to evaluate the morphology of samples in which there existed a range of morphological features from a W/O dispersion, co-continuity, and subsequent phase inversion to O/W latex. The water volume fraction, characterized by the resin-to-water ratio, was not found to significantly vary the types of morphology observed in the samples. Evidence was found of an initial W/O dispersion, affinely deformed aqueous domains, intercalated between lamella/fibrils of polymer that resulted in stratification of the polymer melt at the macro-scale. This spectrum of morphology was found to be consistent with those types of morphologies observed in the phase inversion of immiscible polymer blends. The

physical morphology of an extended dispersion zone configuration was also analyzed by at two different temperature profiles. It was found that lower temperature profiles favoured the development of a finer microstructure within the bicontinuous polymer-water matrix. This was believed to be due to the increased viscosity caused by the lower temperature which yielded lower viscosity ratios during the dispersion of water within the polymer melt.

6.2 Recommendations for Future Work

A method of determining the overall residence time within the extruder was provided in Chapter 3. This method should be expanded upon so that the residence time distribution within the dispersion and dilution zones may be evaluated, individually. This would involve placement of another inline fiber optic probe prior to the dilution zone so that the residence times at the die face and dispersion zone may be acquired simultaneously. In this way, the deformation time may be accurately determined within the dispersion zone. In addition, the time scales of dilution, wherein the inversion takes place, can also be accounted for. There are several other interesting facets of inline spectroscopy that may be prudent to investigate. For example, in-situ optimization of the stability of different extruder operating conditions, with respect to suppression of transient variation, may be realized by monitoring of the backscattering intensity of a semi-coherent light source (i.e. blue LED). Development of a process monitoring technique based on this backscattering would be of great industrial interest. Additionally,

there is a potential to use fluorophores as probes within the system to monitor the micro-polarity of domains. This could serve as a means of determining the time-scales of interface development as well as the neutralization of the carboxyl-terminated polyester.

Extension of the design of experiments work, detailed in Chapter 4, would also be of great interest towards the understanding of the solvent free emulsification mechanism. Specifically, the extension of the factors to include temperature and resin-to-water ratio in the dispersion zone, would be beneficial. Instrumenting the extruder with melt temperature sensors in the dispersion zone would also be useful for determining the effects of viscous heat dissipation upon the temperature of the polymer melt. This would help with the understanding of the effects of screw speed upon the initial water in polymer dispersion.

The morphology evolution within the dispersion zone was analyzed by SEM. The morphology analysis of the dispersion zone material should also be extended to the other factors mentioned above as surfactant concentration and resin-to-water ratio. The analysis by SEM has some benefits with respect to viewing the depth of sample, but also some limitations, with respect to determining the size of small domains. It is recommended that the extended dispersion zone experiments be repeated but with TEM analysis, and possible staining procedures to increase contrast. The use of image analysis software, such as Fiji used here, may also allow for quantification of the domain sizes such that a semi-empirical model may be developed.

REFERENCES

[1] G. Akay and L. Tong, "Preparation of Colloidal Low-Density Polyethylene Latexes by Flow-Induced Phase Inversion Emulsification of Polymer Melt in Water," *Journal of Colloid and Interface Science,* vol. 239, pp. 342-357, 7/15/ 2001.

[2] L. A. Utracki, *Polymer Blends Handbook* vol. I: Springer, 2002.

[3] L. A. Utracki, *Polymer Blends Handbook*: Springer, 2003.

[4] G. Taylor, "The Formation of Emulsions in Definable Fields of Flow," *Proceedings of the Royal Society of London. Series A, Containing Papers of a Mathematical and Physical Character,* vol. 146, pp. 501-523, 1934.

[5] H. P. Grace†, "DISPERSION PHENOMENA IN HIGH VISCOSITY IMMISCIBLE FLUID SYSTEMS AND APPLICATION OF STATIC MIXERS AS DISPERSION DEVICES IN SUCH SYSTEMS," *Chemical Engineering Communications,* vol. 14, pp. 225 - 277, 1982.

[6] Z. Tadmor and C. G. Gogos, *Principles of Polymer Processing*: Wiley, 2006.

[7] P. Fernandez, V. Andre, J. Rieger, and A. Kuhnle, "Nano-emulsion formation by emulsion phase inversion," *Colloids and Surfaces A: Physicochemical and Engineering Aspects,* vol. 251, pp. 53-58, 2004.

[8] J.-L. Salager, A. Forgiarini, L. Márquez, A. Peña, A. Pizzino, M. a. P. Rodriguez*, et al.*, "Using emulsion inversion in industrial processes," *Advances in Colloid and Interface Science,* vol. 108–109, pp. 259-272, 5/20/ 2004.

[9] F. Bouchama, G. A. van Aken, A. J. E. Autin, and G. J. M. Koper, "On the mechanism of catastrophic phase inversion in emulsions," *Colloids and Surfaces A: Physicochemical and Engineering Aspects,* vol. 231, pp. 11-17, 12/31/ 2003.

[10] W. D. Bancroft, "The theory of emulsification, V," *The Journal of Physical Chemistry,* vol. 17, pp. 501-519, 1913.

[11] K. Shinoda and H. Saito, "The effect of temperature on the phase equilibria and the types of dispersions of the ternary system composed of water, cyclohexane, and nonionic surfactant," *Journal of Colloid and Interface Science,* vol. 26, pp. 70-74, 1968.

[12] F. Leal-Calderon, V. Schmitt, and J. Bibette, *Emulsion science: basic principles*: Springer, 2007.

[13] P. Becher, *Encyclopedia of Emulsion Technology: Basic theory, measurement, applications*: M. Dekker, 1988.

[14] E. M. Herzig, K. A. White, A. B. Schofield, W. C. K. Poon, and P. S. Clegg, "Bicontinuous emulsions stabilized solely by colloidal particles," *Nat Mater,* vol. 6, pp. 966-971, 12//print 2007.

[15] G. Akay, "Flow-induced phase inversion in the intensive processing of concentrated emulsions," *Chemical Engineering Science,* vol. 53, pp. 203-223, 1998.

[16] G. Akay, "Stable oil in water emulsions and a process for preparing same," ed: EP Patent 0,649,867, 2001.

[17] G. Akay, L. Tong, H. Bakr, R. A. Choudhery, K. Murray, and J. Watkins, "Preparation of ethylene vinyl acetate copolymer latex by flow induced phase inversion emulsification," *Journal of Materials Science,* vol. 37, pp. 4811-4818, 2002/11/01 2002.

[18] J. I. Uriguen, L. Bremer, V. Mathot, and G. Groeninckx, "Preparation of water-borne dispersions of polyolefins: new systems for the study of homogeneous nucleation of polymers," *Polymer,* vol. 45, pp. 5961-5968, 8/5/ 2004.

[19] G. Akay, "Preparation of Colloidal Low-Density Polyethylene Latexes by Flow-Induced Phase Inversion Emulsification of Polymer Melt in Water," *Journal of Colloid and Interface Science,* vol. 239, pp. 342-357, 2001.

[20] Z. Z. Yang, Y. Z. Xu, D. L. Zhao, and M. Xu, "Preparation of waterborne dispersions of epoxy resin by the phase-inversion emulsification technique. 1. Experimental study on the phase-inversion process," *Colloid and Polymer Science,* vol. 278, pp. 1164-1171, 2000/12/01 2000.

[21] Z. Z. Yang, Y. Z. Xu, D. L. Zhao, and M. Xu, "Preparation of waterborne dispersions of epoxy resin by the phase-inversion emulsification technique. 2. Theoretical consideration of the phase-inversion process," *Colloid and Polymer Science,* vol. 278, pp. 1103-1108, 2000/11/01 2000.

[22] D. Song, W. Zhang, R. K. Gupta, and E. G. Melby, "Role of operating conditions in determining droplet size and viscosity of tackifier emulsions formed via phase inversion," *AIChE Journal,* vol. 57, pp. 96-106, 2011.

[23] S. Daoyun, Z. Wu, G. M. Earl, and K. G. Rakesh, "An instrumented mixer setup for making tackifier dispersions used to make pressure-sensitive adhesives," *Measurement Science and Technology,* vol. 19, p. 045801, 2008.

[24] D. Song, W. Zhang, R. K. Gupta, and E. G. Melby, "Droplet size and viscosity of tackifier emulsions formed via phase inversion," *The Canadian Journal of Chemical Engineering,* vol. 87, pp. 862-868, 2009.

[25] G. L. Warner and D. E. Leng, "Continuous Process for Preparing Aqueous Polymer Microsuspensions," United States Patent 4,123,403, 1978.

[26] K. Abe, M. Tsuruoka, S. Kiriyama, and K. Nakamori, "Aqueous Dispersion of Olefin Resins and Contiunuous Process for Preparing Thereof," United States Patent 4,320,041, 1982.

[27] H. S. Fogler, *Elements of Chemical Reaction Engineering*: Prentice-Hall International, Incorporated, 1999.

[28] E. B. Nauman, "Residence Time Distributions," in *Chemical Reactor Design, Optimization, and Scaleup*, ed: John Wiley & Sons, Inc., 2007, pp. 535-574.

[29] H. Fang, F. Mighri, A. Ajji, P. Cassagnau, and S. Elkoun, "Flow behavior in a corotating twin-screw extruder of pure polymers and blends: Characterization by fluorescence monitoring technique," *Journal of Applied Polymer Science,* vol. 120, pp. 2304-2312, 2010.

[30] R. E. Hayes and J. P. Mmbaga, *Introduction to Chemical Reactor Analysis*: CRC Press/Taylor & Francis Group, 2012.

[31] A. J. Bur and F. M. Gallant, "Fluorescence monitoring of twin screw extrusion," *Polymer Engineering & Science,* vol. 31, pp. 1365-1371, 1991.

[32] G.-H. Hu, I. Kadri, and C. Picot, "One-line measurement of the residence time distribution in screw extruders," *Polymer Engineering & Science,* vol. 39, pp. 930-939, 1999.

[33] O. S. Carneiro, J. A. Covas, J. A. Ferreira, and M. F. Cerqueira, "On-line monitoring of the residence time distribution along a kneading block of a twin-screw extruder," *Polymer Testing,* vol. 23, pp. 925-937, 2004.

[34] I. Ocean Optics. (2012, July 7th, 2013). *Reflection/Backscattering Probes for Expanded Wavelength Coverage*. Available: http://www.oceanoptics.com/Products/reflectionprobesexpanded.asp

[35] I. Ocean Optics. (2012, July 7th, 2013). *Light Sources: Absolute Spectral Output*. Available: http://www.oceanoptics.com/products/ls450.asp

[36] C. D. Eisenbach, R. E. Sah, and G. Baur, "Characteristic features of the matrix effect on the stokes shift of fluorescent dye molecules in pure and plasticized polymers," *Journal of Applied Polymer Science,* vol. 28, pp. 1819-1827, 1983.

[37] J. R. Lakowicz, *Principles of Fluorescence Spectroscopy*: Springer London, Limited, 2006.

[38] W. Lertwimolnun and B. Vergnes, "Effect of processing conditions on the formation of polypropylene/organoclay nanocomposites in a twin screw extruder," *Polymer Engineering & Science,* vol. 46, pp. 314-323, 2006.

[39] G. Pinto and Z. Tadmor, "Mixing and residence time distribution in melt screw extruders," *Polymer Engineering & Science,* vol. 10, pp. 279-288, 1970.

[40] J. Gao, G. C. Walsh, D. Bigio, R. M. Briber, and M. D. Wetzel, "Residence-time distribution model for twin-screw extruders," *AIChE Journal,* vol. 45, pp. 2541-2549, 1999.

[41] J. Gao, G. C. Walsh, D. Bigio, R. M. Briber, and M. D. Wetzel, "Mean residence time analysis for twin screw extruders," *Polymer Engineering & Science,* vol. 40, pp. 227-237, 2000.

[42] A. Boudenne, L. Ibos, Y. Candau, and S. Thomas, *Handbook of Multiphase Polymer Systems*: Wiley, 2011.

[43] E. L. Paul, V. Atiemo-Obeng, and S. M. Kresta, *Handbook of Industrial Mixing: Science and Practice*: Wiley, 2004.

[44] L. A. Utracki, "On the viscosity-concentration dependence of immiscible polymer blends," *Journal of Rheology,* vol. 35, pp. 1615-1637, 11/00/ 1991.

[45] R. C. Willemse, A. Posthuma de Boer, J. van Dam, and A. D. Gotsis, "Co-continuous morphologies in polymer blends: a new model," *Polymer,* vol. 39, pp. 5879-5887, 11// 1998.

[46] G. N. Avgeropoulos, F. C. Weissert, P. H. Biddison, and G. G. A. Böhm, "Heterogeneous Blends of Polymers. Rheology and Morphology," *Rubber Chemistry and Technology,* vol. 49, pp. 93-104, 1976/03/01 1976.

[47] V. Metelkin and V. Blekht, "Formation of a continuous phase in heterogeneous polymer mixtures," *Colloid J USSR,* vol. 46, pp. 425-429, 1984.

[48] G. M. Jordhamo, J. A. Manson, and L. H. Sperling, "Phase continuity and inversion in polymer blends and simultaneous interpenetrating networks," *Polymer Engineering & Science,* vol. 26, pp. 517-524, 1986.

[49] I. S. Miles and A. Zurek, "Preparation, structure, and properties of two-phase co-continuous polymer blends," *Polymer Engineering & Science,* vol. 28, pp. 796-805, 1988.

[50] P. Charoensirisomboon, T. Chiba, T. Inoue, and M. Weber, "In situ formed copolymers as emulsifier and phase-inversion-aid in reactive polysulfone/polyamide blends," *Polymer,* vol. 41, pp. 5977-5984, 7// 2000.

[51] P. Charoensirisomboon, T. Inoue, S. I. Solomko, G. M. Sigalov, and M. Weber, "Morphology of compatibilized polymer blends in terms of particle size–asphericity map," *Polymer,* vol. 41, pp. 7033-7042, 9// 2000.

[52] P. Charoensirisomboon and M. Weber, "Reactive PSU/PA blends: comparison of materials prepared by mini-twin screw extruder and batch mixer," *Polymer,* vol. 42, pp. 7009-7016, 7// 2001.

[53] C. Z. Chuai, K. Almdal, and J. Lyngaae-Jørgensen, "Phase continuity and inversion in polystyrene/poly(methyl methacrylate) blends," *Polymer,* vol. 44, pp. 481-493, 1// 2003.

[54] L. A. Utracki and Z. H. Shi, "Development of polymer blend morphology during compounding in a twin-screw extruder. Part I: Droplet dispersion and coalescence—a review," *Polymer Engineering & Science,* vol. 32, pp. 1824-1833, 1992.

[55] X. Jia, J. Gregory, and R. Williams, *Particle Deposition & Aggregation: Measurement, Modelling and Simulation*: Elsevier Science, 1998.

[56] H. Li and U. Sundararaj, "Morphology Development of Polymer Blends in Extruder: The Effects of Compatibilization and Rotation Rate," *Macromolecular Chemistry and Physics,* vol. 210, pp. 852-863, 2009.

[57] K. Niedzwiedz, H. Buggisch, and N. Willenbacher, "Extensional rheology of concentrated emulsions as probed by capillary breakup elongational rheometry (CaBER)," *Rheologica Acta,* vol. 49, pp. 1103-1116, 2010/12/01 2010.

[58] C. Rauwendaal, *Polymer Extrusion*: Hanser Publishers, 1986.

[59] P. Sarazin and B. D. Favis, "Stability of the co-continuous morphology during melt mixing for poly(ε-caprolactone)/polystyrene blends," *Journal of Polymer Science Part B: Polymer Physics,* vol. 45, pp. 864-872, 2007.

[60] B. D. Favis and D. Therrien, "Factors influencing structure formation and phase size in an immiscible polymer blend of polycarbonate and polypropylene prepared by twin-screw extrusion," *Polymer,* vol. 32, pp. 1474-1481, // 1991.

[61] J. Schindelin, I. Arganda-Carreras, E. Frise, V. Kaynig, M. Longair, T. Pietzsch*, et al.*, "Fiji: an open-source platform for biological-image analysis," *Nat Meth,* vol. 9, pp. 676-682, 07//print 2012.

[62] D. Tschumperle and R. Deriche, "Vector-valued image regularization with PDEs: a common framework for different applications," *IEEE Trans Pattern Anal Mach Intell,* vol. 27, pp. 506-17, Apr 2005.

[63] V. J. Pilny, Jiri. (2006). *Anisotropic Diffusion 2D - Fiji* [Fiji Plugin]. Available: http://fiji.sc/Anisotropic_Diffusion_2D

[64] S. Saalfeld. (2010). *Enhance Local Contrast (CLAHE) - Fiji* [Fiji Plugin]. Available: http://fiji.sc/Enhance_Local_Contrast_(CLAHE)

[65] K. Zuiderveld, "Contrast limited adaptive histogram equalization," in *Graphics gems IV*, S. H. Paul, Ed., ed: Academic Press Professional, Inc., 1994, pp. 474-485.

[66] A. M. Grancarić and N. Kallay, "Kinetics of polyester fiber alkaline hydrolysis: Effect of temperature and cationic surfactants," *Journal of Applied Polymer Science,* vol. 49, pp. 175-181, 1993.

[67] N. Grizzuti, G. Buonocore, and G. Iorio, "Viscous behavior and mixing rules for an immiscible model polymer blend," *Journal of Rheology,* vol. 44, pp. 149-164, 01/00/ 2000.

[68] C. Rauwendaal, *Polymer Extrusion*: Hansler Verlag, 2001.

[69] A. Adedeji, S. Lyu, and C. W. Macosko, "Block Copolymers in Homopolymer Blends: Interface vs Micelles," *Macromolecules,* vol. 34, pp. 8663-8668, 2001/12/01 2001.

[70] C.-K. Shih, "Mixing and morphological transformations in the compounding process for polymer blends: The phase inversion mechanism," *Polymer Engineering & Science,* vol. 35, pp. 1688-1694, 1995.

[71] S. E. Salager, E. C. Tyrode, M.-T. Celis, and J.-L. Salager, "Influence of the Stirrer Initial Position on Emulsion Morphology. Making Use of the Local Water-to-Oil Ratio Concept for Formulation Engineering Purpose," *Industrial & Engineering Chemistry Research,* vol. 40, pp. 4808-4814, 2001/10/01 2001.

[72] J. Bernsen, "Dynamic thresholding of gray-level images," presented at the International Conference on Pattern Recognition, 1986.

APPENDIX

Table 13 - Experiment ordering and replicate sampling for Chapter 4 experiments.

Order	ID	Resin	Screw Speed
1	010E1	1.00	250
2	010E2	1.00	250
3	010E3	1.00	250
4	010E4	1.00	250
5	010H1	1.00	300
6	010H2	1.00	300
7	010H3	1.00	300
8	010H4	1.00	300
9	010B1	1.00	200
10	010B2	1.00	200
11	010B3	1.00	200
12	010B4	1.00	200
13	010K1	1.00	150
14	010K2	1.00	150
15	010K3	1.00	150
16	010K4	1.00	150
17	010N1	1.00	100
18	010N2	1.00	100
19	010N3	1.00	100
20	010N4	1.00	100
21	010L1	1.25	150
22	010L2	1.25	150
23	010L3	1.25	150
24	010L4	1.25	150
25	010L5	1.25	150
26	010L6	1.25	150
27	010L7	1.25	150
28	010L8	1.25	150
29	010L9	1.25	150
30	010L10	1.25	150
31	010F1	1.25	250
32	010F2	1.25	250
33	010F3	1.25	250
34	010F4	1.25	250
35	010F5	1.25	250
36	010F6	1.25	250
37	010F7	1.25	250
38	010F8	1.25	250
39	010P1	1.25	100
40	010P2	1.25	100
41	010P3	1.25	100
42	010P4	1.25	100
43	010I1	1.25	300
44	010I2	1.25	300
45	010I3	1.25	300
46	010I4	1.25	300
47	010C1	1.25	200
48	010C2	1.25	200
49	010C3	1.25	200
50	010C4	1.25	200
51	010A1	0.75	200
52	010A2	0.75	200
53	010A3	0.75	200
54	010A4	0.75	200
55	010M1	0.75	100
56	010M2	0.75	100
57	010M3	0.75	100
58	010M4	0.75	100
59	010D1	0.75	250
60	010D2	0.75	250
61	010D3	0.75	250
62	010D4	0.75	250
63	010J1	0.75	150
64	010J2	0.75	150
65	010J3	0.75	150
66	010J4	0.75	150
67	010G1	0.75	300
68	010G2	0.75	300
69	010G3	0.75	300
70	010G4	0.75	300